Available online at www.sciencedirect.com
ScienceDirect
Journal of Computational Physics 219 (2006) 322–390
JOURNAL OF COMPUTATIONAL PHYSICS
www.elsevier.com/locate/jcp

A steady state capturing and preserving method for computing hyperbolic systems with geometrical source terms having concentrations

Xin Wen *

Institute of Computational Mathematics, Academy of Mathematics and Systems Science, Chinese Academy of Sciences, P.O. Box 2719, Beijing 100080, China

Received 10 August 2005; received in revised form 19 March 2006; accepted 22 March 2006
Available online 8 May 2006

Abstract

We propose a simple well-balanced method named *the slope selecting method* which is efficient in both steady state capturing and preserving for hyperbolic system with geometrical source terms having concentrations. Physical problems under consideration include the shallow water equations with discontinuous topography, and the quasi-one-dimensional nozzle flows with discontinuous cross-sectional area. This method is an extension from the interface type method developed in [S. Jin, X. Wen, An efficient method for computing hyperbolic systems with geometrical source terms having concentrations, J. Comput. Math. 22 (2004) 230–249]. The slope selecting method keeps two merits of the previous method. It can be applied when the homogeneous system solver is available and has efficient steady state capturing property. Compared with the previous method, the slope selecting method has two improvements. One is this method also has satisfactory steady state preserving property. The other is this method can be applied to any conservative scheme for the homogeneous system. Numerical examples provide strong evidence on the effectiveness of this slope selecting method for various unsteady, steady and quasi-steady state solutions calculations as well as the flexibility of this method of being applicable to any conservative scheme for the homogeneous system.

MSC: 65M06; 35L60; 76B15; 76M20

Keywords: Shallow water equations; Nozzle flow equations; Discontinuous topography; Well-balanced scheme; Surface gradient method; Shock capturing

1. Introduction

Hyperbolic systems with geometric source terms arise in many physical applications, including the shallow water equations with bottom topography and the quasi-one-dimensional nozzle flow equations with variable

* Tel.: +86 10 62623711; fax: +86 10 62542285.
E-mail address: wenxin@amss.ac.cn.

0021-9991/$ - see front matter
doi:10.1016/j.jcp.2006.03.019

cross-sectional area. In this paper, we are concerned with the situation when the source terms in the system have concentrations, corresponding to a δ function in the source, which is the case when the bottom is discontinuous for shallow water equations or cross-sectional area is discontinuous for nozzle flow equations. For such system with singular source term, conventional source term approximation methods usually fail to resolve two related numerical issues. The first is *steady state capturing*, namely given an unsteady state initial condition, a numerical method should be able to produce the numerical steady state solution satisfying the correct steady state conditions. The conventional numerical method may give poor approximations to the steady state equations due to the first order numerical viscosity used at discontinuities [16]. It is shown in [21,23] the conventional cell average method fails in steady state capturing for such problems. The second is *steady state preserving*, namely given an exact steady state solution as initial condition, a numerical method should be able to efficiently keep this initial condition as numerical steady state solution. This property is important for a numerical method to be able to correctly calculate quasi-steady state solutions [30]. This issue needs to be carefully studied even when the source terms for the hyperbolic system do not have concentrations. For example, fractional step methods and the pointwise source discretization method are shown to be improper in steady state preserving for shallow water equations when the bottom is continuously variable [19,30]. We will show in this paper that a method which is efficient in steady state preserving when the source terms for the hyperbolic system do not have concentrations does not necessarily work well for hyperbolic system with source terms having concentrations.

A well accepted strategy for dealing with hyperbolic system with source term is to design so-called *well-balanced* scheme that balances the numerical flux with the source term such that the steady state solution is captured or preserved numerically exactly or with at least a second order accuracy. Many well-balanced schemes have been proposed by many authors in recent years, including well-balanced scheme based on non-conservative product [16] and its extensions [5,10,13–15,17], LeVeque's quasi-steady computing scheme [30], kinetic schemes [2,4,31,38], relaxation schemes [8,32], central schemes [26], HLLE scheme [7] and schemes based on SGM (surface gradient method) [39,40]. Nonlinear extension of Roe's linear idea [34] was made in [3,19,21,36]. Many of these methods require the modification of the numerical flux in order to achieve well-balance property of the schemes.

We investigate in this paper a simple well-balanced scheme which has satisfactory roles in both steady state capturing and steady state preserving for hyperbolic system with geometrical source terms having concentrations. Our scheme can effectively calculate the unsteady, steady and quasi-steady state solutions of considered equations. This scheme is an extension of the method in [23]. Based on the same principle of the *interface method* by Jin [21] and the methods in [23,24], this scheme uses interface values rather than cell averages in the source terms and can be applied when a black-box homogeneous equations solver is available. The main advantages of this type of methods are that they do not require the modification of the numerical fluxes for the nonlinear convection terms, and the added numerical effort is small compared with solving the homogeneous hyperbolic system. The present method has two improvements on the method in [23]. Firstly, the method in [23] is an efficient steady state capturing scheme while it does not deal with the steady state preserving issue. In this paper, our method keeps similar steady state capturing merit, and also has satisfactory steady state preserving role. Secondly, the method in [23] can only apply to Godunov type schemes for the homogeneous equations providing interface values of conserved variables, which are those values by substituting into the flux expression of the hyperbolic system yield the numerical fluxes for the schemes. This is because a key step to obtain the well-balance of the method in [23] is the use of interface values in the source term approximations. However, such Godunov type schemes providing interface values are limited nearly to Godunov [12] and Roe [33] method, and exclude many popularly used schemes such as central schemes [20,27], relaxation scheme [25] and HLLE scheme [9,18] in which numerical fluxes are directly given without aid of defining interface values of conserved variables. The method in the present paper gets rid of such restrictions and can apply to *any conservative scheme* for the homogeneous part of the considered hyperbolic system in which only numerical fluxes need to be provided.

We call the method proposed in this paper *the slope selecting method*. Our method hybridizes three important ingredients. Take shallow water equations with discontinuous bottom topography as example. Firstly, we start from the *surface gradient method* (SGM) [40]. SGM is a convenient method which achieves the

steady state preserving role for a continuous variable bottom function by incorporating into the conventional cell average method a simple data reconstruction procedure. It uses gradient of water surface level rather than that of water height to reconstruct conserved variables for obtaining numerical fluxes. Secondly, as SGM is no longer reliable for preserving (non-stationary) steady state solution for shallow water equations with discontinuous bottom, we propose a slope selecting strategy which modifies the slopes for water surface level or water height in cells near a bottom discontinuity. This process facilitates the achieving of steady state preserving role of our method, and also provides a suitable way to define the interface values of water height using the cell average values to be used in the source term approximation. Thirdly, we need to apply the same interface type source term approximation proposed in the method [23] in the cell containing a bottom discontinuity, which is indispensable for our method to be efficient in both steady state capturing and preserving for discontinuous bottom problem. Since the interface values of conserved variables needed by the interface type source term approximation are provided by the slope selecting strategy and numerical fluxes, our method is thus applicable to any conservative scheme providing numerical fluxes for the homogeneous shallow water equations. With the hybridization of these three ingredients, our method is able to achieve satisfactory steady state preserving role for shallow water equations with general discontinuous and variable bottom topography.

For nozzle flow equations, following the same design principle of SGM, we have designed similar data reconstruction strategies which are efficient steady state preserving method when the cross-sectional area in the problem is continuous variable. They are called the *density gradient method* (DGM) and the *energy gradient method* (EGM) for isothermal and non-isothermal nozzle flow equations, respectively. The hybridization in our slope selecting method for nozzle flow equations with discontinuous cross-sectional area is similar. We combine with the DGM or EGM, the slope selecting strategy and the interface type source term approximation to get a method having satisfactory role in steady state preserving for the nozzle flow equations with discontinuous and variable cross-sectional area.

Furthermore, the steady state capturing role of the method in [23] is preserved in our present method with the improvement that the present method is applicable to more general schemes for the homogeneous hyperbolic systems – any conservative scheme providing numerical fluxes. Similar to the method in [23], the slope selecting method can also correctly calculate both unsteady and steady state solution for the hyperbolic systems with concentration source terms. This slope selecting method can correctly deal with the sub- or super-critical flow case and when adding a transonic fix in the source term approximation can solve well the transonic flow over the concentration.

In Sections 2–4, we introduce our slope selecting method for shallow water equations, isothermal and non-isothermal nozzle flow equations, respectively. We give proof for each problem that our method is capable of preserving the steady state solution *with any desired accuracy* in the simple but important case when the bottom topography or the cross-sectional area is a step function. The fact that our method keeps similar efficiency in steady state capturing as in the method [23] for these problems are demonstrated numerically. Numerical examples show that our method, being widely applicable to conservative schemes for the homogeneous hyperbolic system, gives satisfactory unsteady, steady solutions and also efficiently preserve steady state solutions for these problems.

Similar to SGM, the well-balance of our slope selecting method is generally hold when using both uniform and nonuniform meshes. For simplicity, in this paper we discuss about the uniform meshes. In the following we will use $x_{j+1/2}$ to denote the grid point, $\Delta x = x_{j+1/2} - x_{j-1/2}$ the mesh size, $w_{j+1/2} = w(x_{j+1/2})$ the interface value of a general quantity w, and $w_j = \frac{1}{\Delta x}\int_{x_{j-1/2}}^{x_{j+1/2}} w(x)\,\mathrm{d}x$ the cell average of w over the cell $[x_{j-1/2}, x_{j+1/2}]$.

2. The shallow water equations

Consider the one-dimensional shallow water equations with topography

$$h_t + (hv)_x = 0, \tag{2.1}$$

$$(hv)_t + \left(hv^2 + \frac{1}{2}gh^2\right)_x = -ghB_x, \tag{2.2}$$

where h is the depth of the water, v is the mean velocity, g is the gravitational constant, and $B(x)$ is the bottom topography. It is known that the steady state solutions on continuous bottom part is either smooth solutions satisfying

$$hv = C_1, \tag{2.3}$$

$$\frac{1}{2}v^2 + gh + gB = C_2 \tag{2.4}$$

or the stationary shock.

In [1] the authors studied the shallow water Riemann problem with a bottom step. Since the solution to Riemann problem has self-similarity, the solution reaches steady state across the bottom step immediately after initial time. The analytic solution constructed in [1] is guided by seeking classical solution to the homogeneous shallow water Riemann problem away from the bottom step, which can be connected by proper steady state conditions across the bottom step. These steady state conditions can be interpreted as regarding the bottom step as a steep continuous bottom topography and assuming a smooth flow over the bottom step. Thus the flow at two sides of the bottom step satisfy the momentum and energy conservation, namely the conditions (2.3), (2.4) are satisfied across the bottom step. Moreover, in a smooth steady state transition across the bottom step, the states i.e. subcritical when $\frac{|v|}{\sqrt{gh}} < 1$, transcritical when $\frac{|v|}{\sqrt{gh}} = 1$ or supercritical when $\frac{|v|}{\sqrt{gh}} > 1$ at two sides of the bottom step are limited. They can be both subcritical or be both supercritical, but a direct transition between subcritical and supercritical states across the bottom step is not allowed. This is because in a *smooth* steady state shallow water flow the transcritical point connecting subcritical and supercritical flow can only be attained at the maximum bottom point. In the same reason, the subcritical or supercritical state can be connected with a transcritical state to compose the smooth steady state flow across the bottom step with the condition that the transcritical state is reached at the higher bottom step side.

With the aid of the above steady state conditions across the bottom discontinuity, we can give the definition of the corresponding steady state solutions to shallow water equations (2.1), (2.2) with discontinuous bottom as follows

Definition 2.1. Steady state solutions to shallow water equations with discontinuous bottom: for a given initial condition to shallow water equations (2.1), (2.2) with discontinuous bottom, the solution will remain unchanged, i.e. the initial condition is the steady state solution for shallow water equations with discontinuous bottom, if the initial condition is steady state solution on continuous bottom part, and across the bottom discontinuity the conditions (2.3), (2.4) hold, namely

$$h_l v_l = h_r v_r, \tag{2.5}$$

$$\frac{1}{2}v_l^2 + gh_l + gB_l = \frac{1}{2}v_r^2 + gh_r + gB_r, \tag{2.6}$$

where h_l, v_l, B_l and h_r, v_r, B_r are the water height, velocity in the initial condition and the bottom function value at two sides of the bottom discontinuity, and one of the following situations occurs

$$\text{(i)} \qquad \frac{|v_l|}{\sqrt{gh_l}} < 1, \quad \frac{|v_r|}{\sqrt{gh_r}} < 1, \tag{2.7}$$

$$\text{(ii)} \qquad \frac{|v_l|}{\sqrt{gh_l}} > 1, \quad \frac{|v_r|}{\sqrt{gh_r}} > 1, \tag{2.8}$$

$$\text{(iii)} \qquad \begin{cases} \frac{|v_l|}{\sqrt{gh_l}} = 1 & \text{if } B_l > B_r, \\ \frac{|v_r|}{\sqrt{gh_r}} = 1 & \text{if } B_l < B_r. \end{cases} \tag{2.9}$$

Notice when the momentum and energy are conserved across the bottom discontinuity, but the two sides states are subcritical and supercritical, respectively, the solution is not in steady state, and will evolve to a physically permissible steady state solution.

The smooth transition across the bottom discontinuity described in Definition 2.1 are not all the possible steady state conditions across the bottom discontinuity. In [6] the authors investigate the resonance phenomenon which is the situation that a stationary shock superposes with the bottom discontinuity. Thus it is possible that a subcritical state being connected with a supercritical state with *energy not conserved* to compose a steady state flow across the bottom discontinuity. Such a steady state transition across the bottom discontinuity is essentially non-smooth. Nevertheless, it is shown in [1] that the solutions constructed under the smooth steady state conditions across the bottom step described in Definition 2.1 form rich solution patterns. Therefore, such problems are commonly encountered in which the solutions evolve to the steady state solutions belonging to Definition 2.1.

In this section, we are concerned with the steady state capturing and preserving for such steady state solutions belonging to Definition 2.1. We design a well-balanced scheme for (2.1), (2.2) which is proved or numerically demonstrated to be efficient in both steady state capturing and preserving. The investigation of numerical scheme suitable for those steady state solutions related to the non-smooth steady state conditions across the bottom discontinuity is of interest in the future study. We notice that the well-balanced scheme built in [6] based on solution of shallow water Riemann problem with a bottom step is generally efficient for computing solution with smooth or non-smooth transition across the bottom discontinuity. But solving the shallow water Riemann problem with a bottom step is a much more complex task than solving the homogeneous Riemann problem. The merits of the interface type methods [23,24] and the present method, as mentioned before, are that they only use the conventional scheme for homogeneous shallow water equations. By implementing the well-balanced source term approximation, these methods automatically correctly compute the solutions for shallow water equations with discontinuous bottom topography (for smooth transition across the bottom discontinuity) without involving the complication of recognizing different solution structures corresponding to different initial conditions in the system with singular source term. As demonstrated in Sections 2–4, the slope selecting method can be easily applied to different hyperbolic system with geometrical source terms having concentrations with the knowledge of the homogeneous system conservative solver.

2.1. The cell average method

We first present the conventional *cell average method* for the shallow water equations,

$$\partial_t h_j + \frac{m_{j+\frac{1}{2}} - m_{j-\frac{1}{2}}}{\Delta x} = 0, \tag{2.10}$$

$$\partial_t (hv)_j + \frac{e_{j+\frac{1}{2}} - e_{j-\frac{1}{2}}}{\Delta x} = -gh_j \frac{B_{j+\frac{1}{2}} - B_{j-\frac{1}{2}}}{\Delta x}, \tag{2.11}$$

where $B_{j\pm\frac{1}{2}} = B(x_{j\pm\frac{1}{2}})$ and $m_{j-\frac{1}{2}}$, $m_{j+\frac{1}{2}}$, $e_{j-\frac{1}{2}}$, $e_{j+\frac{1}{2}}$ denote, respectively, numerical fluxes for water height and momentum at interfaces $j-\frac{1}{2}$, $j+\frac{1}{2}$ obtained by solving the homogeneous part of Eqs. (2.1), (2.2).

As is well known, when the bottom function $B(x)$ is continuous, the cell average method is suitable for steady state capturing but not for steady state preserving. For the purpose of steady state preserving in the context of a continuous bottom function, the SGM [40] is a convenient choice. When $B(x)$ contains a discontinuity, the cell average method even loses the function of steady state capturing due to the first order numerical viscosity added at discontinuities. This matches with the fact that the shallow water equations in the form (2.1), (2.2), which are referred as mass-momentum formulation in [1], no longer hold valid when the bottom slope becomes infinite.

2.2. An interface type method

We next present our method in [23] using interface values. This method is a hybrid scheme that *uses the cell average method everywhere* except at cells that contain a discontinuity of $B(x)$. In this method we always locate the discontinuity of $B(x)$ in a cell center. In the following we assume that a discontinuity of $B(x)$ is contained in the center of a cell $[x_{j-\frac{1}{2}}, x_{j+\frac{1}{2}}]$. We use $B_{j\pm\frac{1}{2}}$ to denote the interface values of B at $x_{j\pm\frac{1}{2}}$.

At the interfaces of the cell $[x_{j-\frac{1}{2}}, x_{j+\frac{1}{2}}]$, we use a Godunov type solver providing the interface values of water height and velocity which give the numerical fluxes by substituting into the flux expression to solve the homogeneous shallow water equations. Denote the interface values of h, v at $x_{j\pm\frac{1}{2}}$ by such Godunov type solver to be $h_{j-\frac{1}{2}}$, $h_{j+\frac{1}{2}}$, $v_{j-\frac{1}{2}}$, $v_{j+\frac{1}{2}}$ and denote the numerical fluxes for water height and momentum at interfaces $x_{j\pm\frac{1}{2}}$ by such Godunov type solver to be $m_{j-\frac{1}{2}}$, $m_{j+\frac{1}{2}}$, $e_{j-\frac{1}{2}}$, $e_{j+\frac{1}{2}}$, respectively. Then it holds that

$$m_{j-\frac{1}{2}} = h_{j-\frac{1}{2}} v_{j-\frac{1}{2}}, \quad m_{j+\frac{1}{2}} = h_{j+\frac{1}{2}} v_{j+\frac{1}{2}},$$
$$e_{j-\frac{1}{2}} = h_{j-\frac{1}{2}} v_{j-\frac{1}{2}}^2 + \frac{1}{2} g h_{j-\frac{1}{2}}^2, \quad e_{j+\frac{1}{2}} = h_{j+\frac{1}{2}} v_{j+\frac{1}{2}}^2 + \frac{1}{2} g h_{j+\frac{1}{2}}^2.$$

Our scheme in [23] in this cell takes the form

$$\partial_t h_j + \frac{\left(h_{j+\frac{1}{2}} v_{j+\frac{1}{2}}\right) - \left(h_{j-\frac{1}{2}} v_{j-\frac{1}{2}}\right)}{\Delta x} = 0, \tag{2.12}$$

$$\partial_t (hv)_j + \frac{\left(h_{j+\frac{1}{2}} v_{j+\frac{1}{2}}^2 + \frac{1}{2} g h_{j+\frac{1}{2}}^2\right) - \left(h_{j-\frac{1}{2}} v_{j-\frac{1}{2}}^2 + \frac{1}{2} g h_{j-\frac{1}{2}}^2\right)}{\Delta x} = -g \left(\frac{1}{\Delta x} \int_{x_{j-\frac{1}{2}}}^{x_{j+\frac{1}{2}}} \hat{h} \, \mathrm{d}x \right) \frac{B_{j+\frac{1}{2}} - B_{j-\frac{1}{2}}}{\Delta x}, \tag{2.13}$$

where a general hat-function $\hat{q}$ denotes a *smooth function* in the cell $[x_{j-\frac{1}{2}}, x_{j+\frac{1}{2}}]$ with endpoint values $q(x_i)$ at x_i $(i = j - \frac{1}{2}, j + \frac{1}{2})$.

It remains to explain how to define the function $\widehat{h}$ in the cell $[x_{j-\frac{1}{2}}, x_{j+\frac{1}{2}}]$. This function is appropriately chosen so that the well-balance of the scheme is achieved. Define function $H(x)$ in the cell $[x_{j-\frac{1}{2}}, x_{j+\frac{1}{2}}]$ to be the *linear interpolant* through interpolating points $(x_i, h_i v_i)$, $i = j - \frac{1}{2}, j + \frac{1}{2}$, $G(x)$ in $[x_{j-\frac{1}{2}}, x_{j+\frac{1}{2}}]$ to be the linear interpolant through $(x_i, \frac{1}{2} v_i^2 + g h_i + g B_i)$, $i = j - \frac{1}{2}, j + \frac{1}{2}$, $\widehat{B}(x)$ in $[x_{j-\frac{1}{2}}, x_{j+\frac{1}{2}}]$ to be the linear interpolant through (x_i, B_i), $i = j - \frac{1}{2}, j + \frac{1}{2}$. Namely,

$$H(x_i) = h_i v_i, \quad G(x_i) = \frac{1}{2} v_i^2 + g h_i + g B_i, \quad \widehat{B}(x_i) = B_i, \quad i = j \pm \frac{1}{2}. \tag{2.14}$$

We then determine $\hat{h}$, $\hat{v}$ from the identities

$$H = \hat{h}\hat{v}, \tag{2.15}$$

$$G = \frac{1}{2} \hat{v}^2 + g\hat{h} + g\widehat{B}, \tag{2.16}$$

or $\hat{h}$ can be determined by the relation

$$\frac{1}{2} \frac{H^2}{\hat{h}^2} + g\hat{h} + g\widehat{B} = G. \tag{2.17}$$

This equation generally has two positive roots, corresponding to subcritical and supercritical states, respectively.

The following theorem shows that above hybrid scheme is well-balanced. The proof is given in [23].

Theorem 2.1. *Our hybrid scheme (2.12), (2.13) can preserve the steady state conditions (2.3), (2.4) exactly at cell interfaces at two sides of bottom discontinuity in numerical steady state solution*:

$$h_{j-\frac{1}{2}} v_{j-\frac{1}{2}} = h_{j+\frac{1}{2}} v_{j+\frac{1}{2}}, \tag{2.18}$$

$$\frac{1}{2} v_{j-\frac{1}{2}}^2 + g h_{j-\frac{1}{2}} + g B_{j-\frac{1}{2}} = \frac{1}{2} v_{j+\frac{1}{2}}^2 + g h_{j+\frac{1}{2}} + g B_{j+\frac{1}{2}}. \tag{2.19}$$

The cell average of $\hat{h}$ in the source term approximation (2.13) was approximated by composite quadrature rules (e.g. the composite Simpson's rule), with the values of $\hat{h}$ at the quadrature points obtained by solving the algebraic equation (2.17) using Newton's iteration. The values of $\hat{h}$ are chosen according to sub- or supercritical states of the solution. In the transcritical solution case, a transcritical fix is used to help determining the values of $\hat{h}$. The details are given in [23].

2.3. The slope selecting method

We now describe our slope selecting method for shallow water equations (2.1) and (2.2).

In order to maintain steady state preserving property, our method starts from SGM [40]. In the similar way to the interface type method described in the above subsection, our slope selecting method is a hybrid scheme that *uses SGM everywhere* except modifying the slope definitions and source term approximation near or in the cell containing the bottom discontinuity. In our method we always locate the discontinuity of $B(x)$ in a cell center. Here we briefly describe the procedure of SGM.

(1) In the step of defining the slopes of conserved variables – water height and momentum in each cell. Instead of defining the slope of water height as usually adopted in solving the homogeneous shallow water equations, define the slope(denoted by S_k) for water surface level $\eta = h + B$

$$S_k = G(\eta_{k-1}, \eta_k, \eta_{k+1}),$$

where G is a standard slope limiter [29] such as minmod limiter or van Leer limiter. The slope of momentum is still defined since momentum is a constant in the steady state solution.

(2) The values of water height on the left and right of the cell interface $x_{k+\frac{1}{2}}$ are given by

$$h^{\mathrm{L}}_{k+\frac{1}{2}} = \left(\eta_k + \frac{1}{2}\Delta x S_k\right) - B_{k+\frac{1}{2}}, \quad h^{\mathrm{R}}_{k+\frac{1}{2}} = \left(\eta_{k+1} - \frac{1}{2}\Delta x S_{k+1}\right) - B_{k+\frac{1}{2}}.$$

The left and right values of momentum are still obtained by the momentum cell average values and slopes. These left and right values of conserved variables at interface $x_{k+\frac{1}{2}}$ are used by a homogeneous shallow water equations solver to get the numerical fluxes for water height and momentum $m_{k+\frac{1}{2}}$, $e_{k+\frac{1}{2}}$.

(3) Once the numerical fluxes for conserved variables are obtained, one can use the cell average formula (2.10), (2.11) as the numerical scheme.

It is proved in [40] that SGM satisfies the Z-property defined as follows

Definition 2.2. Z-property: (i) a numerical scheme provides the exact values of a variable in the flow domain to the stationary case that η being a constant, $v \equiv 0$; (ii) the scheme exactly preserves this stationary flow when a centered discretization is used for source terms.

While SGM is efficient in preserving steady state solutions for shallow water equations with continuous bottom, in the following we will show that SGM fails to preserve non-stationary steady state solutions for shallow water equations with discontinuous bottom. Assume that a discontinuity of $B(x)$ is contained in the center of a cell $[x_{j-\frac{1}{2}}, x_{j+\frac{1}{2}}]$, and $B(x)$ is continuous in the neighborhood on each side of x_j. Consider the situation that a non-stationary steady state solution, i.e. the steady state solution in which water velocity v is non-zero, is reached, and there is no stationary shock existing in the neighborhood of x_j. Denote water height in the steady state solution to be $h^{\mathrm{s}}(x)$, and water surface level to be $\eta^{\mathrm{s}}(x) = h^{\mathrm{s}}(x) + B(x)$. In a non-stationary steady state, $h^{\mathrm{s}}(x)$ and $\eta^{\mathrm{s}}(x)$ both are discontinuous across the bottom discontinuity at x_j in order to satisfy the steady state conditions (2.3) and (2.4). Since no stationary shock exists in the neighborhood, $h^{\mathrm{s}}(x)$ and $\eta^{\mathrm{s}}(x)$ are continuous on each side of x_j locally. Remember the notations specified at the end of Section 1. Since $\eta^{\mathrm{s}}(x)$ is discontinuous across x_j, one has that $\eta^{\mathrm{s}}_{j+\frac{1}{2}} - \eta^{\mathrm{s}}_{j-\frac{1}{2}}$ is a O(1) quantity with regard to decreasing Δx. Due to the continuity of $\eta^{\mathrm{s}}(x)$ on each side of x_j, it holds that

$$\eta^{\mathrm{s}}_{j+1} = \eta^{\mathrm{s}}_{j+\frac{1}{2}} + \mathrm{o}(1), \quad \eta^{\mathrm{s}}_{j-1} = \eta^{\mathrm{s}}_{j-\frac{1}{2}} + \mathrm{o}(1), \quad \eta^{\mathrm{s}}_j = \frac{\eta^{\mathrm{s}}_{j+\frac{1}{2}} + \eta^{\mathrm{s}}_{j-\frac{1}{2}}}{2} + \mathrm{o}(1) \tag{2.20}$$

with regard to decreasing Δx. In SGM, the slope of water surface level in the cell $[x_{j-\frac{1}{2}}, x_{j+\frac{1}{2}}]$ is defined by applying a standard slope limiter $G(\eta^{\mathrm{s}}_{j-1}, \eta^{\mathrm{s}}_j, \eta^{\mathrm{s}}_{j+1})$. Then the predicted water surface level value on the left of interface $x_{j+\frac{1}{2}}$ is given by

$$\eta^{s,L}_{j+\frac{1}{2}} = \eta^s_j + \frac{1}{2}\Delta x G(\eta^s_{j-1}, \eta^s_j, \eta^s_{j+1}). \tag{2.21}$$

Denote $\widehat{G}(\eta^s_{j-1}, \eta^s_j, \eta^s_{j+1}) = \Delta x G(\eta^s_{j-1}, \eta^s_j, \eta^s_{j+1})$, then $\widehat{G}(\eta^s_{j-1}, \eta^s_j, \eta^s_{j+1})$ is of the form

$$\widehat{G}(\eta^s_{j-1}, \eta^s_j, \eta^s_{j+1}) = (\eta^s_{j+1} - \eta^s_j)\phi\left(\frac{\eta^s_j - \eta^s_{j-1}}{\eta^s_{j+1} - \eta^s_j}\right), \tag{2.22}$$

where function ϕ is continuous and $\phi(1) = 1$.

Together with (2.20), (2.21) and (2.22) gives

$$\eta^{s,L}_{j+\frac{1}{2}} = \frac{\eta^s_{j+\frac{1}{2}} + \eta^s_{j-\frac{1}{2}}}{2} + o(1) + \frac{1}{2}\left(\frac{\eta^s_{j+\frac{1}{2}} - \eta^s_{j-\frac{1}{2}}}{2} + o(1)\right)\phi(1 + o(1)) = \frac{3\eta^s_{j+\frac{1}{2}} + \eta^s_{j-\frac{1}{2}}}{4} + o(1).$$

The error between this predicted water surface level value by SGM on the left of $x_{j+\frac{1}{2}}$ and the exact value is

$$\eta^{s,L}_{j+\frac{1}{2}} - \eta^s_{j+\frac{1}{2}} = \frac{\eta^s_{j-\frac{1}{2}} - \eta^s_{j+\frac{1}{2}}}{4} + o(1),$$

which is a O(1) quantity with regard to decreasing Δx since $\eta^s_{j-\frac{1}{2}} - \eta^s_{j+\frac{1}{2}}$ is.

Thus SGM fails to correctly predict one side water surface level value on the interface near the bottom discontinuity for non-stationary steady state solution, in comparison with that it exactly predicts such value for stationary steady state solutions cases. In fact, the principle allows SGM to be able to exactly predict water height value at interfaces for stationary steady state solutions cases is that water surface level is constant in those solutions. Thus it is not surprise that SGM fails in this role for non-stationary steady state solutions with discontinuous bottom function since here water surface level is discontinuous, and fundamentally different from a constant. Since SGM gives wrong one side water surface level value on the interface, it will also give wrong one side water height value on this interface by subtracting the correct bottom function value. Consequently, the resulting numerical flux calculated on this interface by SGM is also wrong. Thus it is impossible for SGM to correctly preserve this non-stationary steady state solution with a discontinuous bottom function. We also notice that even if the numerical fluxes at interfaces are correctly provided, with a cell average source term discretization, SGM still cannot correctly preserve such non-stationary steady state solution. This reveals the necessity of incorporating the interface type source term approximation [23] in our method.

Above discussed situation is illustrated in Fig. 1. In the figure the water surface level η^s is discontinuous at x_j as we discussed above. From the figure one can clearly see how SGM predicts wrong water surface level value

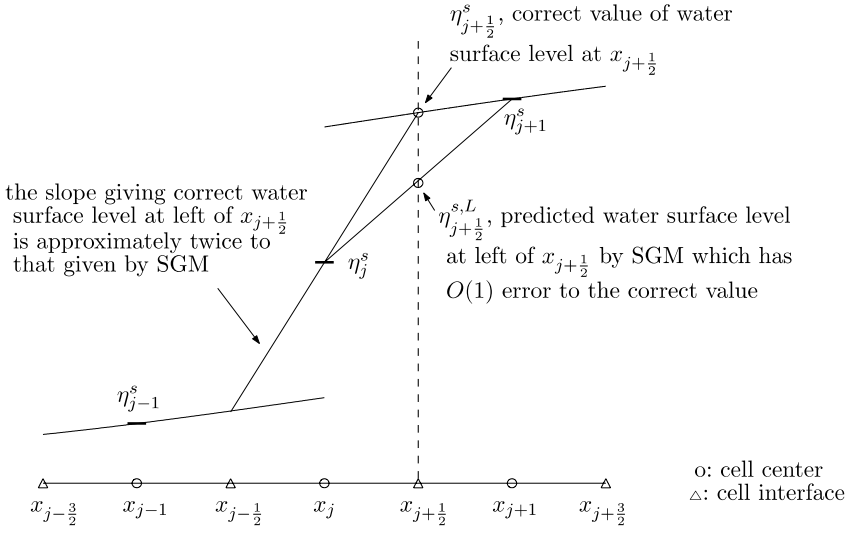

Fig. 1. Illustration of failure of SGM for predicting water surface level value at interface near bottom discontinuity.

on left side of interface $x_{j+\frac{1}{2}}$. The needed slope for water surface level in the cell $[x_{j-\frac{1}{2}}, x_{j+\frac{1}{2}}]$ should be sharper than that given by SGM in order to give correct water surface level value at the interface because this is the case water surface level has a standing discontinuity at x_j.

This gives light to our slope selecting strategy which aims at giving one side values of conserved variables on the interfaces near a bottom discontinuity from the cell average values with a o(1) error with regard to decreasing Δx. We achieve the aim by directly considering how to define the slope for water height in the cell $[x_{j-\frac{1}{2}}, x_{j+\frac{1}{2}}]$. We seek a slope formula $D(h_{j-1}, h_j, h_{j+1})$ in the cell, such that by defining

$$H^{\mathrm{L}}(h_{j-1}, h_j, h_{j+1}) = h_j - \frac{1}{2}\Delta x D(h_{j-1}, h_j, h_{j+1}), \tag{2.23}$$

$$H^{\mathrm{R}}(h_{j-1}, h_j, h_{j+1}) = h_j + \frac{1}{2}\Delta x D(h_{j-1}, h_j, h_{j+1}), \tag{2.24}$$

it holds that

$$H^{\mathrm{L}}(h^{\mathrm{s}}_{j-1}, h^{\mathrm{s}}_j, h^{\mathrm{s}}_{j+1}) = h^{\mathrm{s}}_{j-\frac{1}{2}} + \mathrm{o}(1), \quad H^{\mathrm{R}}(h^{\mathrm{s}}_{j-1}, h^{\mathrm{s}}_j, h^{\mathrm{s}}_{j+1}) = h^{\mathrm{s}}_{j+\frac{1}{2}} + \mathrm{o}(1), \tag{2.25}$$

where h^{s} is the steady state water height function in the above discussion for failure of SGM.

By substituting similar expression as (2.20) into above conditions (2.25) and assuming continuity of H^{L} and H^{R}, one gets

$$H^{\mathrm{L}}\left(h^{\mathrm{s}}_{j-\frac{1}{2}}, \frac{h^{\mathrm{s}}_{j-\frac{1}{2}} + h^{\mathrm{s}}_{j+\frac{1}{2}}}{2}, h^{\mathrm{s}}_{j+\frac{1}{2}}\right) = h^{\mathrm{s}}_{j-\frac{1}{2}} + \mathrm{o}(1), \tag{2.26}$$

$$H^{\mathrm{R}}\left(h^{\mathrm{s}}_{j-\frac{1}{2}}, \frac{h^{\mathrm{s}}_{j-\frac{1}{2}} + h^{\mathrm{s}}_{j+\frac{1}{2}}}{2}, h^{\mathrm{s}}_{j+\frac{1}{2}}\right) = h^{\mathrm{s}}_{j+\frac{1}{2}} + \mathrm{o}(1). \tag{2.27}$$

Since there are no constraints on $h^{\mathrm{s}}_{j-\frac{1}{2}}, h^{\mathrm{s}}_{j+\frac{1}{2}}$ except they are non-negative, conditions (2.27), (2.26) require

$$H^{\mathrm{L}}\left(a, \frac{a+b}{2}, b\right) = a, \quad H^{\mathrm{R}}\left(a, \frac{a+b}{2}, b\right) = b \quad \forall a, b > 0. \tag{2.28}$$

Since water height is a non-negative quantity, the obtained one side water height value on the interface should be ensured non-negative. So we impose the following conditions on H^{L} and H^{R}

$$H^{\mathrm{L}}(a, b, c) > 0, \quad H^{\mathrm{R}}(a, b, c) > 0 \quad \forall a, b, c > 0. \tag{2.29}$$

Thus we are seeking a slope expression $D(h_{j-1}, h_j, h_{j+1})$ such that the functions H^{L}, H^{R} defined by (2.23), (2.24) at least satisfy the conditions (2.28) and (2.29). There should be many available slope expressions which meet such requirement. For example, it is easily seen from the discussion of the failure of SGM that setting $D(h_{j-1}, h_j, h_{j+1}) = 2G(h_{j-1}, h_j, h_{j+1})$, where $G(h_{j-1}, h_j, h_{j+1})$ is a standard slope limiter, may serve the purpose. Here we propose a different formula. We assume the functions $H^{\mathrm{L}}, H^{\mathrm{R}}$ take the form

$$H^{\mathrm{L}}(a, b, c) = \alpha(a, c)b, \quad H^{\mathrm{R}}(a, b, c) = \beta(a, c)b.$$

Then conditions (2.28) require

$$\alpha(a, c) = \frac{2a}{a+c}, \quad \beta(a, c) = \frac{2c}{a+c}.$$

Thus the functions $H^{\mathrm{L}}, H^{\mathrm{R}}$ we have found by this way are

$$H^{\mathrm{L},*}(a, b, c) = \frac{2ab}{a+c}, \quad H^{\mathrm{R},*}(a, b, c) = \frac{2cb}{a+c}. \tag{2.30}$$

The corresponding slope expression is

$$D^*(h_{j-1}, h_j, h_{j+1}) = \frac{2h_j}{\Delta x}\frac{h_{j+1} - h_{j-1}}{h_{j+1} + h_{j-1}}. \tag{2.31}$$

This is the water height slope formula we propose in the cell $[x_{j-\frac{1}{2}}, x_{j+\frac{1}{2}}]$ from which the predicted one side water height values $H^{L,*}(h^s_{j-1}, h^s_j, h^s_{j+1})$ and $H^{R,*}(h^s_{j-1}, h^s_j, h^s_{j+1})$ on the interfaces $x_{j\pm\frac{1}{2}}$ satisfy the requirement (2.25) for a non-stationary steady state solution with a discontinuous bottom function. Moreover, it is easily seen that these predicted one side water height values are of $O(\Delta x)$ error when h^s is Lipschitz continuous at two sides of x_j, and are exact when h^s is a step function, which is the case when bottom B is a step function. Now that the water height slope has been determined by this formula, there is no need to give slope for water surface level in this cell since the purpose of defining surface gradient in SGM is to provide a reasonable way for giving water height slope.

Besides providing the water height slope in the cell $[x_{j-\frac{1}{2}}, x_{j+\frac{1}{2}}]$ containing a bottom discontinuity, our slope selecting strategy also involves modifying the slope for water surface level in the cells adjacent to this cell. Take the cell $[x_{j+\frac{1}{2}}, x_{j+\frac{3}{2}}]$ for example. Denote $\eta(x)$ to be the water surface level in a solution after initial time. The slope of water surface level provided by SGM in this cell is given by a standard slope limiter $G(\eta_j, \eta_{j+1}, \eta_{j+2})$ applying on the cell average values. However, since the bottom function has a discontinuity at x_j, it should be that $\eta(x)$ generally is discontinuous across x_j even when steady state is not reached in the solution. Denote $\eta^+_j = \eta(x^+_j)$. One can see a reasonable way to define the slope of water surface level in the cell $[x_{j+\frac{1}{2}}, x_{j+\frac{3}{2}}]$ is $G(\eta^+_j, \eta_{j+1}, \eta_{j+2})$. The slope specified by SGM turns to be replacing η^+_j in the expression by η_j. We assume it is more suitable in principle to define the slope of water surface level in this cell by replacing η^+_j more accurately in the expression $G(\eta^+_j, \eta_{j+1}, \eta_{j+2})$. By observing that η_j has a $O(1)$ error from η^+_j, we propose to replace η^+_j by a quantity more close to it. Define

$$\eta^*_{j+\frac{1}{2}} = H^{R,*}(h_{j-1}, h_j, h_{j+1}) + B_{j+\frac{1}{2}}, \tag{2.32}$$

where $H^{R,*}$ is given in (2.30).

Although the conditions (2.25) are obtained for discussing steady state solution, the solution is just assumed discontinuous across the bottom discontinuity and continuous on the two sides in the discussion. Thus the same conditions can be derived for general (unsteady state) solution with the same property. Therefore, one has

$$\eta^*_{j+\frac{1}{2}} = \eta_{j+\frac{1}{2}} + o(1) = \eta^+_j + o(1)$$

with regard to decreasing Δx.

Thus we propose to set water surface level slope in this cell $[x_{j+\frac{1}{2}}, x_{j+\frac{3}{2}}]$ to be $G(\eta^*_{j+\frac{1}{2}}, \eta_{j+1}, \eta_{j+2})$ with $\eta^*_{j+\frac{1}{2}}$ given by (2.32). We use the minmod slope limiter in this slope selecting strategy. Then the proposed slope for water surface level in this cell becomes

$$\frac{\operatorname{sign}\{\eta_{j+2} - \eta_{j+1}\} + \operatorname{sign}\{\eta_{j+1} - \eta^*_{j+\frac{1}{2}}\}}{2\Delta x} \min\{|\eta_{j+2} - \eta_{j+1}|, |\eta_{j+1} - \eta^*_{j+\frac{1}{2}}|\}.$$

The water surface level slope for the cell $[x_{j-\frac{3}{2}}, x_{j-\frac{1}{2}}]$ is similarly defined.

After above discussion, we now summarize our slope selecting strategy near the bottom discontinuity. For a cell $[x_{j-\frac{1}{2}}, x_{j+\frac{1}{2}}]$ containing a bottom discontinuity in the center, our slope selecting strategy involves setting slopes for this cell and its two adjacent cells. Define

$$h^*_{j-\frac{1}{2}} = \frac{2h_j h_{j-1}}{h_{j+1} + h_{j-1}}, \quad h^*_{j+\frac{1}{2}} = \frac{2h_j h_{j+1}}{h_{j+1} + h_{j-1}}, \tag{2.33}$$

$$\eta^*_{j\pm\frac{1}{2}} = h^*_{j\pm\frac{1}{2}} + B_{j\pm\frac{1}{2}}. \tag{2.34}$$

In the cell $[x_{j-\frac{1}{2}}, x_{j+\frac{1}{2}}]$ we directly define the water height slope to be

$$\frac{h^*_{j+\frac{1}{2}} - h^*_{j-\frac{1}{2}}}{\Delta x}.$$

In the two adjacent cells we set the water surface level slopes to be

$$S_{j-1} = \frac{\operatorname{sign}\{\eta_{j-1} - \eta_{j-2}\} + \operatorname{sign}\{\eta^*_{j-\frac{1}{2}} - \eta_{j-1}\}}{2\Delta x} \min\{|\eta_{j-1} - \eta_{j-2}|, |\eta^*_{j-\frac{1}{2}} - \eta_{j-1}|\}, \tag{2.35}$$

$$S_{j+1} = \frac{\operatorname{sign}\{\eta_{j+2} - \eta_{j+1}\} + \operatorname{sign}\{\eta_{j+1} - \eta^*_{j+\frac{1}{2}}\}}{2\Delta x} \min\{|\eta_{j+2} - \eta_{j+1}|, |\eta_{j+1} - \eta^*_{j+\frac{1}{2}}|\}. \tag{2.36}$$

The slopes for momentum in these cells are not changed. They are kept the same as in SGM as well as in solving homogeneous shallow water equations.

After implementation of the slope selecting strategy, another modification from SGM in our method is to incorporate the interface type source term approximation [23] in the cell $[x_{j-\frac{1}{2}}, x_{j+\frac{1}{2}}]$ containing a bottom discontinuity in the center. Consider the situation that our method uses a conservative scheme for the homogeneous shallow water equations with only numerical fluxes provided. We need to use the slope selecting strategy to provide the interface values of conserved variables required by the interface type source term approximation which the conservative scheme may not supply.

Before treating with source term approximation, we first calculate the numerical fluxes for this cell. The values of water height on the left and right of the cell interfaces $x_{j\pm\frac{1}{2}}$ are

$$h^{\mathrm{L}}_{j-\frac{1}{2}} = \left(\eta_{j-1} + \frac{1}{2}\Delta x S_{j-1}\right) - B_{j-\frac{1}{2}}, \quad h^{\mathrm{R}}_{j-\frac{1}{2}} = h^*_{j-\frac{1}{2}}, \tag{2.37}$$

$$h^{\mathrm{L}}_{j+\frac{1}{2}} = h^*_{j+\frac{1}{2}}, \quad h^{\mathrm{R}}_{j+\frac{1}{2}} = \left(\eta_{j+1} - \frac{1}{2}\Delta x S_{j+1}\right) - B_{j+\frac{1}{2}}, \tag{2.38}$$

with $h^*_{j\pm\frac{1}{2}}$ defined by (2.33) and $S_{j\pm1}$ set by (2.35), (2.36) in the slope selecting strategy. The left and right values of momentum are obtained standardly as in SGM. These left and right values of conserved variables at interfaces $x_{j\pm\frac{1}{2}}$ are used by the homogeneous equations conservative scheme to get the numerical fluxes for water height and momentum $m_{j\pm\frac{1}{2}}, e_{j\pm\frac{1}{2}}$.

Now we need to define the interface values of conserved variables in order to apply the interface type source term approximation. Instead of seeking the interface values of water height from the homogeneous equations scheme, we specify the quantities defined by (2.33) in the slope selecting strategy as the water height interface values at $x_{j\pm\frac{1}{2}}$. The interface values of velocity are then defined as

$$v^*_{j-\frac{1}{2}} = \frac{m_{j-\frac{1}{2}}}{h^*_{j-\frac{1}{2}}}, \quad v^*_{j+\frac{1}{2}} = \frac{m_{j+\frac{1}{2}}}{h^*_{j+\frac{1}{2}}}, \tag{2.39}$$

where $m_{j\pm\frac{1}{2}}$ are numerical fluxes for water height we already obtained above.

We notice that these defined interface values of conserved variables are just for the purpose of using in the source term approximation. While strictly obtain the numerical fluxes from the homogeneous equations conservative scheme, we use these defined interface values of conserved variables in the source term approximation instead of those interface values matching with the numerical fluxes, i.e. those interface values of conserved variables which give the numerical fluxes by substituting into the flux expression, which was used in the previous interface type methods [23,24]. Numerical experiments strongly support that this measure makes our slope selecting method keep similar steady state capturing efficiency as in our interface type methods [23,24] and in the same time get rid of the restriction on the homogeneous equations solver of providing interface values of conserved variables.

Once the interface values of conserved variables are defined at $j \pm \frac{1}{2}$, the following procedure is then similar to the interface type method described in Section 2.2. We define function $H(x)$ in the cell $[x_{j-\frac{1}{2}}, x_{j+\frac{1}{2}}]$ to be the *linear interpolant* through interpolating points $(x_i, h^*_i v^*_i),\ i = j-\frac{1}{2},\ j+\frac{1}{2}$, $G(x)$ in $[x_{j-\frac{1}{2}}, x_{j+\frac{1}{2}}]$ to be the linear interpolant through $(x_i, \frac{1}{2}(v^*_i)^2 + gh^*_i + gB_i),\ i = j-\frac{1}{2},\ j+\frac{1}{2}$, and $\widehat{B}(x)$ in $[x_{j-\frac{1}{2}}, x_{j+\frac{1}{2}}]$ to be the linear interpolant through $(x_i, B_i),\ i = j-\frac{1}{2},\ j+\frac{1}{2}$. Namely,

$$H(x_i) = h^*_i v^*_i, \quad G(x_i) = \frac{1}{2}(v^*_i)^2 + gh^*_i + gB_i, \quad \widehat{B}(x_i) = B_i, \quad i = j \pm \frac{1}{2}. \tag{2.40}$$

We then define smooth functions $\hat{h}, \hat{v}$ in cell $[x_{j-\frac{1}{2}}, x_{j+\frac{1}{2}}]$ satisfying

$$\hat{h}(x_i) = h_i^*, \quad \hat{v}(x_i) = v_i^*, \quad i = j - \frac{1}{2}, \quad j + \frac{1}{2} \tag{2.41}$$

and the identities

$$\hat{h}\hat{v} = H, \tag{2.42}$$

$$\frac{1}{2}\hat{v}^2 + g\hat{h} + g\widehat{B} = G, \tag{2.43}$$

or $\hat{h}$ can be determined by the relation

$$\frac{1}{2}\frac{H^2}{\hat{h}^2} + g\hat{h} + g\widehat{B} = G. \tag{2.44}$$

Then our slope selecting scheme in the cell $[x_{j-\frac{1}{2}}, x_{j+\frac{1}{2}}]$ takes the form

$$\partial_t h_j + \frac{m_{j+\frac{1}{2}} - m_{j-\frac{1}{2}}}{\Delta x} = 0, \tag{2.45}$$

$$\partial_t (hv)_j + \frac{e_{j+\frac{1}{2}} - e_{j-\frac{1}{2}}}{\Delta x} = -g\left(\frac{1}{\Delta x}\int_{x_{j-\frac{1}{2}}}^{x_{j+\frac{1}{2}}} \hat{h}\,\mathrm{d}x\right)\frac{B_{j+\frac{1}{2}} - B_{j-\frac{1}{2}}}{\Delta x}. \tag{2.46}$$

The numerical strategy for calculating the cell average of $\hat{h}$ in the source term approximation and the choice of $\hat{h}$ value from the algebraic equation (2.44), including the use of a transcritical fix to facilitate the choice of $\hat{h}$ in dealing with transcritical problems are the same to our method described in Section 2.2. One can refer the details in the paper [23].

We use the scheme of SGM in all the other cells do not containing a bottom discontinuity with the mention that the slope of water surface level in the cell adjacent to a bottom discontinuity is modified by our slope selecting strategy.

Because our method uses SGM in the cells where bottom is smooth, it can be similarly proved as in [40] that our slope selecting method satisfies the Z-property given in Definition 2.2. The Z-property is known to be an important property with which a scheme can efficiently preserve (stationary or non-stationary) steady state solution for shallow water equations with smooth bottom. But as have been shown, for shallow water equations with discontinuous bottom, a scheme with only Z-property, for example SGM, may be unreliable in (non-stationary) steady state preserving. Accordingly, we propose the following S-property which is useful for steady state preserving for shallow water equations with discontinuous bottom.

Definition 2.3. S-property: a numerical scheme exactly preserves the (stationary or non-stationary) steady state flow belonging to Definition 2.1 in which no stationary shock exists for the shallow water equations with a step function bottom.

We now prove that this S-property is *formally* satisfied by our slope selecting method.

Theorem 2.2. *When the bottom function is a step function, if the interface type source term approximation in the slope selecting method can be exactly computed, then the slope selecting scheme can preserve exactly any steady state solution belonging to Definition 2.1 in which the steady state conditions (2.3), (2.4) are hold anywhere including across the bottom discontinuity.*

Proof. Assume the bottom is a step function with left side value B_l and right side value B_r. We only need to prove our slope selecting scheme preserve the steady state solution exactly in the cell $[x_{j-\frac{1}{2}}, x_{j+\frac{1}{2}}]$ which contains the bottom discontinuity in the center. Consider a steady state solution in which the water height and velocity are step functions with left side values $h_\mathrm{l}, v_\mathrm{l}$ and right side values $h_\mathrm{r}, v_\mathrm{r}$, respectively, and it holds that

$$h_\mathrm{l} v_\mathrm{l} = h_\mathrm{r} v_\mathrm{r}, \tag{2.47}$$

$$\frac{1}{2}v_\mathrm{l}^2 + gh_\mathrm{l} + gB_\mathrm{l} = \frac{1}{2}v_\mathrm{r}^2 + gh_\mathrm{r} + gB_\mathrm{r}. \tag{2.48}$$

Denote $M = h_l v_l = h_r v_r$, then the cell average values of water height, water surface level and momentum in cells $j-1, j, j+1$ are respectively

$$\begin{aligned}
&h_{j-1} = h_l, \quad h_j = \frac{h_l + h_r}{2}, \quad h_{j+1} = h_r,\\
&\eta_{j-1} = h_l + B_l, \quad \eta_j = \frac{h_l + B_l + h_r + B_r}{2}, \quad \eta_{j+1} = h_r + B_r,\\
&m_i = M, \quad i = j-1, j, j+1.
\end{aligned}$$

Because $h_j = \frac{h_{j-1}+h_{j+1}}{2}$, the definition of values of water height at interfaces $j-\frac{1}{2}$, $j+\frac{1}{2}$ (2.33) gives

$$h^*_{j-\frac{1}{2}} = h_l, \quad h^*_{j+\frac{1}{2}} = h_r. \tag{2.49}$$

The definition of slopes for water surface level in cells $j-1, j+1$ (2.35), (2.36) gives

$$S_{j-1} = 0, \quad S_{j+1} = 0.$$

The values of water height on the left and right of the cell interfaces $x_{j\pm\frac{1}{2}}$ are given by (2.37), (2.38) as

$$\begin{aligned}
h^{\mathrm{L}}_{j-\frac{1}{2}} &= \left(\eta_{j-1} + \frac{1}{2}\Delta x S_{j-1}\right) - B_{j-\frac{1}{2}} = h_l,\\
h^{\mathrm{R}}_{j-\frac{1}{2}} &= h_l,\\
h^{\mathrm{L}}_{j+\frac{1}{2}} &= h_r,\\
h^{\mathrm{R}}_{j+\frac{1}{2}} &= \left(\eta_{j+1} - \frac{1}{2}\Delta x S_{j+1}\right) - B_{j+\frac{1}{2}} = h_r,
\end{aligned}$$

where $B_{j-\frac{1}{2}} = B_l$, $B_{j+\frac{1}{2}} = B_r$.

On the other hand, because the momentum are constant in all cells, the values of momentum on the left and right of any cell interface are given by M. So in solving the numerical fluxes by homogeneous equations conservative solver, the left and right side values at interface $j+\frac{1}{2}$ are the same which are (h_r, M). No matter what solver one uses, the numerical fluxes at interface $j+\frac{1}{2}$ are definitely given by $m_{j+\frac{1}{2}} = M$, $e_{j+\frac{1}{2}} = h_r v_r^2 + \frac{1}{2} g h_r^2$. In the same way, the numerical fluxes at interface $j-\frac{1}{2}$ are given by $m_{j-\frac{1}{2}} = M$, $e_{j-\frac{1}{2}} = h_l v_l^2 + \frac{1}{2} g h_l^2$.

Our slope selecting scheme in the cell $[x_{j-1/2}, x_{j+1/2}]$ (2.45), (2.46) thus can be rewritten as

$$\partial_t h_j + \frac{M - M}{\Delta x} = 0, \tag{2.50}$$

$$\partial_t (hv)_j + \frac{\left(h_r v_r^2 + \frac{1}{2} g h_r^2\right) - \left(h_l v_l^2 + \frac{1}{2} g h_l^2\right)}{\Delta x} = -\frac{g}{\Delta x} \int_{x_{j-\frac{1}{2}}}^{x_{j+\frac{1}{2}}} \hat{h} \widehat{B}_x \, \mathrm{d}x. \tag{2.51}$$

with the aid of $\widehat{B}(x)$ being linear function on $[x_{j-1/2}, x_{j+1/2}]$ with end point values $B_{j\pm\frac{1}{2}}$.

From (2.50) one knows the flux difference for water height is zero in the cell $[x_{j-1/2}, x_{j+1/2}]$. In the following we prove that the flux difference for momentum is also zero. Recall the fact (2.49) and from definition (2.39) one has

$$v^*_{j-\frac{1}{2}} = \frac{M}{h_l} = v_l, \quad v^*_{j+\frac{1}{2}} = \frac{M}{h_r} = v_r. \tag{2.52}$$

For steady state solutions satisfying one of conditions 2.7, 2.8 2.9 described in Definition 2.1, the transcritical fix in our source term approximation does not apply. So the endpoint values for functions $\hat{h}, \hat{v}$ are given by (2.41), which are given by (2.49) and (2.52). Recalling the identities (2.42), (2.43), the flux difference for momentum in scheme (2.51) can be calculated as

$$\frac{\left(h_r v_r^2+\frac{1}{2}gh_r^2\right)-\left(h_l v_l^2+\frac{1}{2}gh_l^2\right)}{\Delta x}+\frac{g}{\Delta x}\int_{x_{j-\frac{1}{2}}}^{x_{j+\frac{1}{2}}}\hat{h}\widehat{B}_x\,\mathrm{d}x=\frac{1}{\Delta x}\int_{x_{j-\frac{1}{2}}}^{x_{j+\frac{1}{2}}}\left[(\hat{h}\hat{v}^2)_x+\left(\frac{1}{2}g\hat{h}^2\right)_x+g\hat{h}\widehat{B}_x\right]\mathrm{d}x$$
$$=\frac{1}{\Delta x}\int_{x_{j-\frac{1}{2}}}^{x_{j+\frac{1}{2}}}[(\hat{h}\hat{v})_x\hat{v}+(\hat{h}\hat{v})\hat{v}_x+g\hat{h}\hat{h}_x+g\hat{h}\widehat{B}_x]\,\mathrm{d}x$$
$$=\frac{1}{\Delta x}\int_{x_{j-\frac{1}{2}}}^{x_{j+\frac{1}{2}}}[H_x\hat{v}+\hat{h}(\hat{v}\hat{v}_x+g\hat{h}_x+g\widehat{B}_x)]\,\mathrm{d}x$$
$$=\frac{1}{\Delta x}\int_{x_{j-\frac{1}{2}}}^{x_{j+\frac{1}{2}}}[H_x\hat{v}+\hat{h}G_x]\,\mathrm{d}x. \tag{2.53}$$

Finally, recall the definitions of H, G (2.40) and the facts (2.47), (2.48), one knows H, G indeed are constants in the cell $[x_{j-1/2}, x_{j+1/2}]$. So the function in the integration (2.53) is identically zero and the flux difference for momentum in scheme (2.51) is zero. Thus this steady state solution is exactly preserved by our slope selecting scheme. □

Remark 2.1. In practical computation, the integral $\int_{x_{j-\frac{1}{2}}}^{x_{j+\frac{1}{2}}}\hat{h}\,\mathrm{d}x$ in the interface type source term approximation (2.46) cannot be exactly computed. This is because the values of $\hat{h}$ is solved by Newton iteration from the algebraic equation (2.44), and the integral is approximated by composite quadrature rules. Therefore in practical use the slope selecting method generally cannot exactly preserve a non-stationary steady state solution across the bottom step. However, the integral $\int_{x_{j-\frac{1}{2}}}^{x_{j+\frac{1}{2}}}\hat{h}\,\mathrm{d}x$ in the source term approximation can be computed *with any desired accuracy* by specifying the accuracy of the Newton iteration for computing values of $\hat{h}$ and using enough nodal number in the integral quadrature. Thus in practical computation the slope selecting method can be designed to preserve the steady state solution described in Theorem 2.2 *with any desired accuracy* at one time step.

Satisfying Z-property exactly and S-property *with any desired accuracy* enables our slope selecting method to be efficient in steady state preserving for shallow water equation with general discontinuous and variable bottom topography. The steady state capturing property of our method *cannot* be similarly proved as for the method in [23] due to the complication of defining interface values of conserved variables by the slope selecting strategy used for the source term approximation. We leave the efficiency of our method in steady state capturing demonstrated by numerical experiments. For example, our method gives satisfactory convergent solutions for the shallow water Riemann problems with a bottom step, as shown in Examples 2.1 and 2.2.

2.4. Extension of the slope selecting method to 2D shallow water equations

In two space dimensions the shallow water equations are given by

$$h_t+(hu)_x+(hv)_y=0, \tag{2.54}$$
$$(hu)_t+\left(hu^2+\frac{1}{2}gh^2\right)_x+(huv)_y=-ghB_x, \tag{2.55}$$
$$(hv)_t+(huv)_x+\left(hv^2+\frac{1}{2}gh^2\right)_y=-ghB_y, \tag{2.56}$$

where h is the water height, u, v are the velocity in x, y direction, respectively, and B is the bottom topography. g is the gravitational constant.

In two space dimension one cannot derive an algebraic relation like (2.3) and (2.4) for the steady state solution. Therefore, we will just extend our 1D slope selecting method to 2D dimension-by-dimension.

For a general quantity q, its two dimensional cell average value q_{ij} is given by

$$q_{ij}=\frac{1}{\Delta x\Delta y}\int_{x_{i-\frac{1}{2}}}^{x_{i+\frac{1}{2}}}\int_{y_{j-\frac{1}{2}}}^{y_{j+\frac{1}{2}}}q(x,y)\,\mathrm{d}x\,\mathrm{d}y,$$

while the one-dimensional average is defined, for example, by

$$q_{i+\frac{1}{2},\mathrm{j}} = \frac{1}{\Delta y}\int_{y_{j-\frac{1}{2}}}^{y_{j+\frac{1}{2}}} q(x_{i+\frac{1}{2}}, y)\,\mathrm{d}y.$$

The cell average method for (2.54)–(2.56) takes the form

$$\partial_t h_{ij} + \frac{m1_{i+\frac{1}{2},\mathrm{j}} - m1_{i-\frac{1}{2},\mathrm{j}}}{\Delta x} + \frac{m2_{i,\mathrm{j}+\frac{1}{2}} - m2_{i,\mathrm{j}-\frac{1}{2}}}{\Delta y} = 0, \tag{2.57}$$

$$\partial_t (hu)_{ij} + \frac{e1_{i+\frac{1}{2},\mathrm{j}} - e1_{i-\frac{1}{2},\mathrm{j}}}{\Delta x} + \frac{e2_{i,\mathrm{j}+\frac{1}{2}} - e2_{i,\mathrm{j}-\frac{1}{2}}}{\Delta y} = -gh_{ij}\frac{B_{i+\frac{1}{2},\mathrm{j}} - B_{i-\frac{1}{2},\mathrm{j}}}{\Delta x}, \tag{2.58}$$

$$\partial_t (hv)_{ij} + \frac{f1_{i+\frac{1}{2},\mathrm{j}} - f1_{i-\frac{1}{2},\mathrm{j}}}{\Delta x} + \frac{f2_{i,\mathrm{j}+\frac{1}{2}} - f2_{i,\mathrm{j}-\frac{1}{2}}}{\Delta y} = -gh_{ij}\frac{B_{i,\mathrm{j}+\frac{1}{2}} - B_{i,\mathrm{j}-\frac{1}{2}}}{\Delta y}, \tag{2.59}$$

where $m1_{i\pm\frac{1}{2},\mathrm{j}}$, $m2_{i,\mathrm{j}\pm\frac{1}{2}}$, $e1_{i\pm\frac{1}{2},\mathrm{j}}$, $e2_{i,\mathrm{j}\pm\frac{1}{2}}$, $f1_{i\pm\frac{1}{2},\mathrm{j}}$, $f2_{i,\mathrm{j}\pm\frac{1}{2}}$ are the corresponding numerical fluxes at interfaces given by a conservative solver for the 1D homogeneous shallow water equations in x and y direction, respectively. Similar to 1D case, in 2D SGM [40] is also based on the same numerical scheme as the cell average method with the two sides values of water height used for solving the numerical fluxes at a mesh interface obtained through gradient of water surface level.

In this paper, we only consider the simple situation that the bottom discontinuous line locates on the center line of a cell. That is, for a cell centered at (x_k, y_l), the bottom discontinuous line occupies either the line segment $(x_{k-\frac{1}{2}}, y_l) - (x_{k+\frac{1}{2}}, y_l)$, or the line segment $(x_k, y_{l-\frac{1}{2}}) - (x_k, y_{l+\frac{1}{2}})$. It is not clear yet whether the present scheme can be *directly* applied to the more general case of the bottom discontinuous line slantwise crossing a cell, e.g. cutting a corner of a cell. Investigating for such general case will be of help for designing efficient numerical method for 2D shallow water equations with curved bottom discontinuous line using a uniform mesh, and is of interest in the future study.

When a cell centered at (x_k, y_l) contains discontinuous line of bottom, we add in our slope selecting strategy in the cell and its adjacent cells on the basis of SGM. In the following we discuss the case that the discontinuous line of B occupies the line segment $(x_k, y_{l-\frac{1}{2}}) - (x_k, y_{l+\frac{1}{2}})$. We define the quantities at $(k-\frac{1}{2}, l), (k+\frac{1}{2}, l)$

$$h^*_{k-\frac{1}{2},\mathrm{l}} = \frac{2h_{kl}h_{k-1,\mathrm{l}}}{h_{k+1,\mathrm{l}} + h_{k-1,\mathrm{l}}}, \quad h^*_{k+\frac{1}{2},\mathrm{l}} = \frac{2h_{kl}h_{k+1,\mathrm{l}}}{h_{k+1,\mathrm{l}} + h_{k-1,\mathrm{l}}}, \tag{2.60}$$

$$\eta^*_{k\pm\frac{1}{2},\mathrm{l}} = h^*_{k\pm\frac{1}{2},\mathrm{l}} + B_{k\pm\frac{1}{2},\mathrm{l}}. \tag{2.61}$$

We set the x-directional water height slope in the cell (k, l) to be

$$\frac{h^*_{k+\frac{1}{2},\mathrm{l}} - h^*_{k-\frac{1}{2},\mathrm{l}}}{\Delta x}$$

and modify the slopes for water surface level in x-direction in cells $(k-1, l), (k+1, l)$ to be

$$S_{k-1,\mathrm{l}} = \frac{\mathrm{sign}\{\eta_{k-1,\mathrm{l}} - \eta_{k-2,\mathrm{l}}\} + \mathrm{sign}\{\eta^*_{k-\frac{1}{2},\mathrm{l}} - \eta_{k-1,\mathrm{l}}\}}{2\Delta x}\min\{|\eta_{k-1,\mathrm{l}} - \eta_{k-2,\mathrm{l}}|, |\eta^*_{k-\frac{1}{2},\mathrm{l}} - \eta_{k-1,\mathrm{l}}|\}, \tag{2.62}$$

$$S_{k+1,\mathrm{l}} = \frac{\mathrm{sign}\{\eta_{k+2,\mathrm{l}} - \eta_{k+1,\mathrm{l}}\} + \mathrm{sign}\{\eta_{k+1,\mathrm{l}} - \eta^*_{k+\frac{1}{2},\mathrm{l}}\}}{2\Delta x}\min\{|\eta_{k+2,\mathrm{l}} - \eta_{k+1,\mathrm{l}}|, |\eta_{k+1,\mathrm{l}} - \eta^*_{k+\frac{1}{2},\mathrm{l}}|\}. \tag{2.63}$$

Since the bottom discontinuous line is vertical in the cell (k, l), we do not modify the y-directional slopes in this cell and its adjacent cells.

Above are the description of our slope selecting strategy near this cell (k, l). We then present our slope selecting scheme in this cell. First we calculate the numerical fluxes for this cell from solving homogeneous equations.

With the application of our slope selecting strategy, the values of water height on the two sides of the cell interfaces $(x_{k\pm\frac{1}{2}}, y_l)$ are

$$h^{\mathrm{L}}_{k-\frac{1}{2},\mathrm{l}} = \left(\eta_{k-1,\mathrm{l}} + \frac{1}{2}\Delta x S_{k-1,\mathrm{l}}\right) - B_{k-\frac{1}{2},\mathrm{l}}, \quad h^{\mathrm{R}}_{k-\frac{1}{2},\mathrm{l}} = h^{*}_{k-\frac{1}{2},\mathrm{l}},$$
$$h^{\mathrm{L}}_{k+\frac{1}{2},\mathrm{l}} = h^{*}_{k+\frac{1}{2},\mathrm{l}}, \quad h^{\mathrm{R}}_{k+\frac{1}{2},\mathrm{l}} = \left(\eta_{k+1,\mathrm{l}} - \frac{1}{2}\Delta x S_{k+1,\mathrm{l}}\right) - B_{k+\frac{1}{2},\mathrm{l}}$$

with $h^{*}_{k\pm\frac{1}{2},\mathrm{l}}$ defined in (2.60) and $S_{k\pm1,l}$ defined in (2.62), (2.63).

The left and right values of momentum are obtained in the same way as SGM. These two sides values of conserved variables at interfaces $(x_{k\pm\frac{1}{2}}, y_1)$ are used in solving the x-directional 1D homogeneous shallow water equations to get the x-directional numerical fluxes $m1_{k\pm\frac{1}{2},\mathrm{l}} e1_{k\pm\frac{1}{2},\mathrm{l}}$, $f1_{k\pm\frac{1}{2},\mathrm{l}}$.

We define the quantities at $(k-\frac{1}{2}, l)$, $(k+\frac{1}{2}, l)$

$$u^{*}_{k-\frac{1}{2},\mathrm{l}} = \frac{m1_{k-\frac{1}{2},\mathrm{l}}}{h^{*}_{k-\frac{1}{2},\mathrm{l}}}, \quad u^{*}_{k+\frac{1}{2},\mathrm{l}} = \frac{m1_{k+\frac{1}{2},\mathrm{l}}}{h^{*}_{k+\frac{1}{2},\mathrm{l}}}. \tag{2.64}$$

The y-directional numerical fluxes $m2_{k,\mathrm{l}\pm\frac{1}{2}}$, $e2_{k,\mathrm{l}\pm\frac{1}{2}}$, $f2_{k,\mathrm{l}\pm\frac{1}{2}}$ in this cell are obtained without modification to SGM since the y-directional slopes near this cell are not modified.

We then use the one dimensional interface type source term approximation with needed interface values of water height and x-directional velocity chosen to be (2.60) and (2.64) to replace the cell average source term discretization in formula (2.58) which SGM uses. Namely, we replace the formula (2.58) in the cell average scheme in this cell by

$$\partial_t (hu)_{kl} + \frac{e1_{k+\frac{1}{2},\mathrm{l}} - e1_{k-\frac{1}{2},\mathrm{l}}}{\Delta x} + \frac{e2_{k,\mathrm{l}+\frac{1}{2}} - e2_{k,\mathrm{l}-\frac{1}{2}}}{\Delta y} = -g\left(\frac{1}{\Delta x}\int_{x_{k-\frac{1}{2}}}^{x_{k+\frac{1}{2}}} \hat{h}\,\mathrm{d}x\right)\frac{B_{k+\frac{1}{2},\mathrm{l}} - B_{k-\frac{1}{2},\mathrm{l}}}{\Delta x}, \tag{2.65}$$

where as in one dimension, the function $\hat{h}$ is defined together with function $\hat{u}$ in the interval $[x_{k-\frac{1}{2}}, x_{k+\frac{1}{2}}]$ by

$$\hat{h}\hat{u} = H, \tag{2.66}$$
$$\frac{1}{2}\hat{u}^2 + g\hat{h} + g\widehat{B} = G, \tag{2.67}$$

or $\hat{h}$ can be determined by

$$\frac{1}{2}\frac{H^2}{\hat{h}^2} + g\hat{h} + g\widehat{B} = G \tag{2.68}$$

with functions H, G, $\widehat{B}$ in the interval $[x_{k-\frac{1}{2}}, x_{k+\frac{1}{2}}]$ set to be linear satisfying the endpoint values

$$H(x_i) = h^{*}_{il}u^{*}_{il}, \quad G(x_i) = \frac{1}{2}\left(u^{*}_{il}\right)^2 + gh^{*}_{il} + gB_{il}, \quad \widehat{B}(x_i) = B_{il}, \quad i = k \pm \frac{1}{2}. \tag{2.69}$$

As the same to our 1D method, we use the Newton iteration to solve values of $\hat{h}$ from (2.68) and use the numerical integration to evaluate the integral of function $\hat{h}$ to deal with the source term approximation in the scheme (2.65).

If the discontinuous line of B occupies the line segment $(x_{k-\frac{1}{2}}, y_1) - (x_{k+\frac{1}{2}}, y_1)$, the application of our slope selecting strategy in y-direction on the basis of SGM, and the replacement of the cell average formula (2.59) by our interface-type scheme is similar.

We use the scheme of SGM in all the other cells do not containing a bottom discontinuous line with the mention that the slope of water surface level in the cell adjacent to a bottom discontinuous line is modified by our slope selecting strategy.

2.5. Numerical examples

In this section, we give five 1D numerical examples and one 2D example. We use the second order TVD Runge–Kutta time discretization [35] for all the examples. Examples 2.1 and 2.2 are Riemann problems from

[1] and have been tested by our methods in [23,24]. These two examples are used to show that our method works well for calculating unsteady state solutions for shallow water equations with discontinuous bottom. The gravitational constant is set to be 9.8. These two Riemann problems are defined on the domain $[-10, 10]$. The zeroth order extrapolation is used as numerical boundary condition. The exact solutions are available for these problems [1], and we can perform the convergence rates tests for our numerical solutions in these examples.

Example 2.3 is a steady state capturing problem tested in [24] and shows that our method is efficient in steady state capturing calculation.

Examples 2.4 and 2.5 are used to test the steady state preserving property of our method. Example 2.4 is a problem of tidal wave propagating over a discontinuous bottom and Example 2.5 is a quasi-steady state computing problem. These two examples show that our method has strong ability to preserve steady state solutions when bottom contains both discontinuities and variable continuous part.

Example 2.6 is a 2D Riemann problem tested in [24] and is used to test the effectiveness of the extension of our slope selecting method to 2D problem.

Example 2.1. A Riemann problem with solution in supercritical state.

The initial data are given by $(h, v, B) = (4, -10, 0)$ when $x < 0$ and $(h, v, B) = (1, -6, 1)$ when $x > 0$. This is a supercritical case. We take $\frac{\Delta t}{\Delta x} = 1/20$, and compute the solution using HLLE solver and relaxation scheme. See Appendix A for the description of the numerical fluxes provided by these solvers for shallow water equations. The constant $\widehat{C}$ (defined in Appendix A) in subcharacteristic condition in relaxation scheme is chosen as 50. The results by using 100 cells are plotted in Figs. 2–4 versus the exact solution. One can see our solutions correctly predict that the energy is constant across the bottom step. The exact solution for this example is given in Appendix B.

Table 1 lists the relative l^1-errors of the computed conserved variables on the whole computational domain with different meshes by our method using both solvers. The results present to be approximately first order convergent, showing the effectiveness of our method for computing unsteady state solution for discontinuous bottom problem.

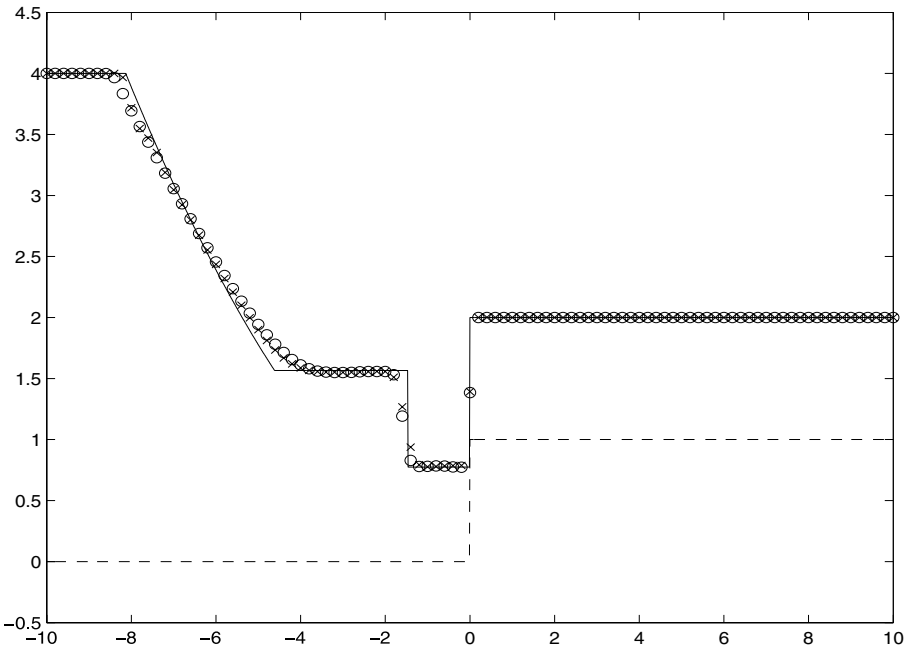

Fig. 2. Example 2.1, the supercritical case. Water level at $t = 0.5$ along with the bottom topography. Solid line: the exact solution; "○": the solution of HLLE solver using 100 cells; "×": the solution of relaxation scheme using 100 cells; dashed line: bottom topography.

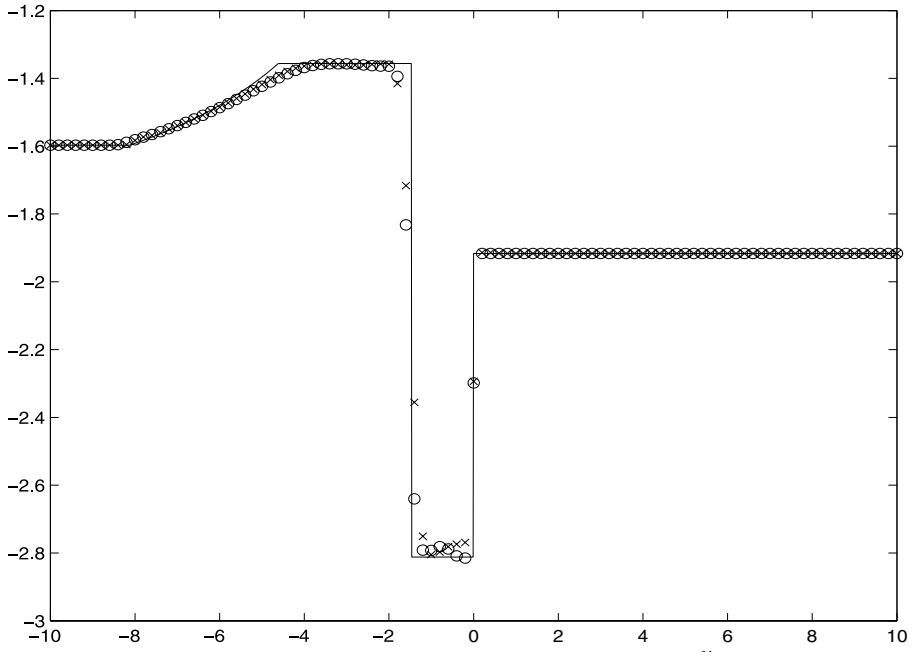

Fig. 3. Example 2.1, supercritical case. Froude number $\frac{v}{\sqrt{gh}}$ at $t = 0.5$. Solid line: the exact solution; "○": the solution of HLLE solver using 100 cells; "×": the solution of relaxation scheme using 100 cells.

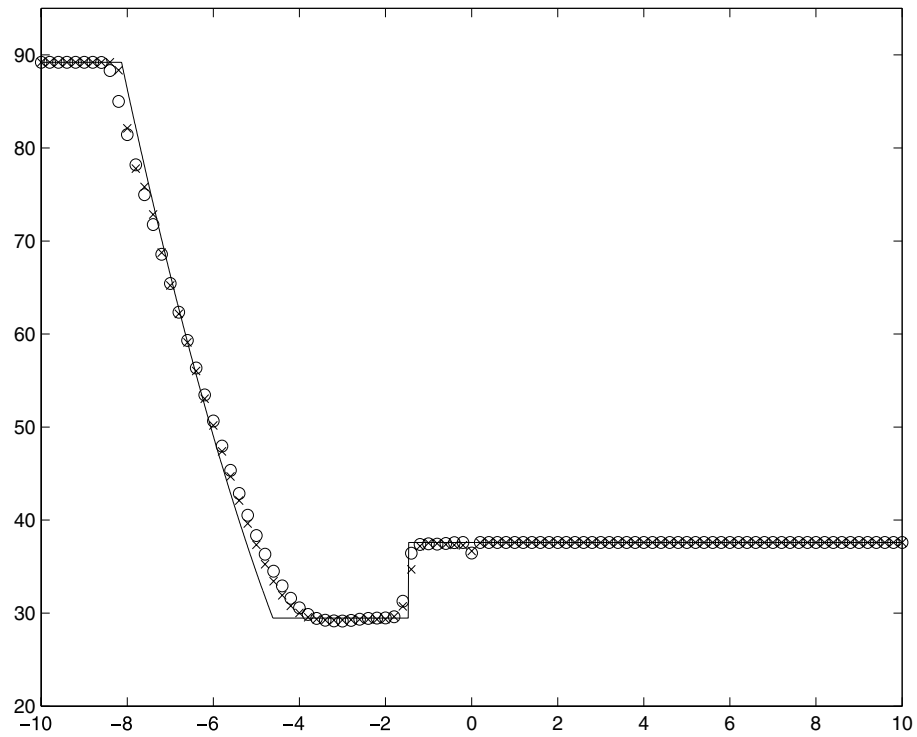

Fig. 4. Example 2.1, supercritical case. Energy $\frac{1}{2}v^2 + g(h + B)$ at $t = 0.5$. Solid line: the exact solution; "○": the solution of HLLE solver using 100 cells; "×": the solution of relaxation scheme using 100 cells.

We can show the effectiveness of our method by another numerical test. Consider the homogeneous shallow water Riemann problem with the same gravitational constant with initial data

$$(h, v) = \begin{cases} (4, -10), & x < 0, \\ (h_R, v_R), & x > 0, \end{cases} \tag{2.70}$$

where h_R, v_R are the solution values in the exact solution of this example to the left of the bottom jump and to the right of the left going shock. According to Appendix B, $v_R = \frac{-6}{h_R}$, and the six effective number truncation for h_R is 0.774464. In our computation these values are chosen such that the truncation errors have insignificant influence on the results of the following numerical test.

The solution of the homogeneous Riemann problem with initial data (2.70) on $x > 0$ is its initial right state, and on $x < 0$ is the same as the exact solution on $x < 0$ for this example. Thus we can use the homogeneous shallow water equations solver used in the slope selecting method to solve this homogeneous Riemann problem and compare the solution errors on $x < 0$ with those by the slope selecting method for this example.

We choose the HLLE scheme to perform the test. In Table 2 we list, respectively, the relative l^1-errors on $[-10, -0.5]$ of the computed conserved variables by the slope selecting method using HLLE scheme for this example and by HLLE scheme for the homogeneous Riemann problem.

These errors are comparable and those by the slope selecting method are slightly larger. In fact, one cannot expect the solution errors by the slope selecting method are even smaller since the solved problem contains a bottom step across which the solution errors are produced. The similarity of the solution errors shows that the solution errors across the bottom step in this example are much small compared with those away from bottom step produced by the shock capturing scheme, and exhibits the effectiveness of our slope selecting method to control the energy conservation across the bottom step in this unsteady state example.

Example 2.2. A Riemann problem with solution in the transcritical state.

The initial data are $(h, v, B) = (4, -10, 0)$ when $x < 0$ and $(h,\ v, B) = (2, 0, 1)$ when $x > 0$. This is a transcritical case. The solution reaches the critical state at the right side of the bottom jump. We take $\frac{\Delta t}{\Delta x} = 1/20$. We choose the constant $\widehat{C}$ in subcharacteristic condition in relaxation scheme as 50. The solutions obtained by HLLE solver and relaxation scheme using 200 cells, along with the exact solution, are plotted in Figs. 5–7. The results can correctly predict that the Froude number $\frac{v}{\sqrt{gh}}$ reaches -1 at the right side of the bottom jump. This is due to the fix used in our source term approximation for the transcritical case. The exact solution for this example is given in Appendix B.

Table 1
Relative l^1-errors of computed conserved variables for Example 2.1 in the computational domain $[-10, 10]$

Errors	100 Cells	200 Cells	400 Cells	800 Cells	1600 Cells
HLLE scheme					
h	1.8283E − 2	9.7519E − 3	4.6468E − 3	2.4952E − 3	1.1722E − 3
m	2.4744E − 2	1.2808E − 2	6.4067E − 3	3.2823E − 3	1.6203E − 3
Relaxation scheme					
h	1.4742E − 2	7.7922E − 3	3.7653E − 3	2.4373E − 3	1.1651E − 3
m	1.8481E − 2	9.4937E − 3	4.8174E − 3	3.4457E − 3	1.7094E − 3

Table 2
Relative l^1-errors of computed conserved variables in the domain $[-10, -0.5]$ using HLLE scheme

Errors	100 Cells	200 Cells	400 Cells	800 Cells
Riemann problem with bottom step				
h	2.5618E − 2	1.3745E − 2	6.5361E − 3	3.5176E − 3
m	3.3155E − 2	1.7229E − 2	8.6187E − 3	4.4153E − 3
Homogeneous Riemann problem				
h	2.3660E − 2	1.3103E − 2	6.2982E − 3	3.4202E − 3
m	3.1075E − 2	1.6420E − 2	8.2996E − 3	4.2824E − 3

There is a visible spike in the numerical solutions of energy at bottom discontinuity. As mentioned in [24], this spike is a numerical artifact, due to the use of numerical viscosity. This phenomenon was analyzed in [22]. Even with mesh refinement, this spike does not disappear. This phenomenon is reasonable since one does not necessarily expect the numerical solutions to be convergent in l^∞-norm in the cell containing a bottom discontinuity since the solutions are discontinuous in that cell. This numerical spike does not effect the other part of the numerical solution, i.e. does not effect the l^1-convergence of the numerical solutions, as seen from the l^1-errors of our numerical solutions presented in the following.

In Table 3 we present the relative l^1-errors of the computed conserved variables on the whole computational domain with different meshes by our slope selecting method using both solvers. Again it is shown that the numerical solutions for this example are convergent with approximate first order rate. This whole computational domain l^1-convergence rate is the same as that by using second order shock capturing scheme to solve homogeneous shallow water Riemann problem.

Example 2.3. A steady state capturing calculation.

This is a problem tested in [24]. The computational domain is $[-10, 10]$. We choose the bottom function to be

$$B(x) = \begin{cases} 0, & x < -4, \\ 1 + \cos\left(\frac{\pi x}{8}\right), & -4 < x < 4, \\ 1, & x > 4, \end{cases}$$

as shown by the dashed line in Fig. 8. The initial conditions are given by

$$h(x,0) = 3 - B(x),$$
$$v(x,0) = \frac{2}{h(x,0)},$$

the boundary conditions are given as $hv|_{x=-10} = 2, h|_{x=10} = 2$. The gravitational constant is set to be 9.8. We take $\frac{\Delta t}{\Delta x} = 1/10$ and use HLLE solver to solve the homogeneous shallow water equations. Figs. 9–11 show,

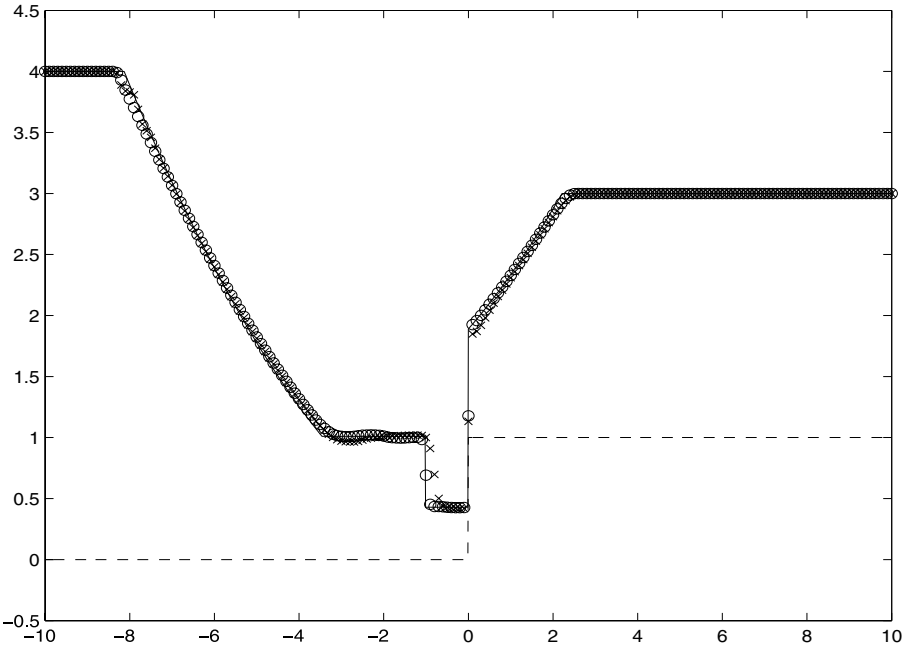

Fig. 5. Example 2.2, transcritical case. Water level at $t = 0.5$ along with bottom topography; solid line: the exact solution; "○": the solution of HLLE solver using 200 cells; "×": the solution of relaxation scheme using 200 cells; dashed line: bottom topography.

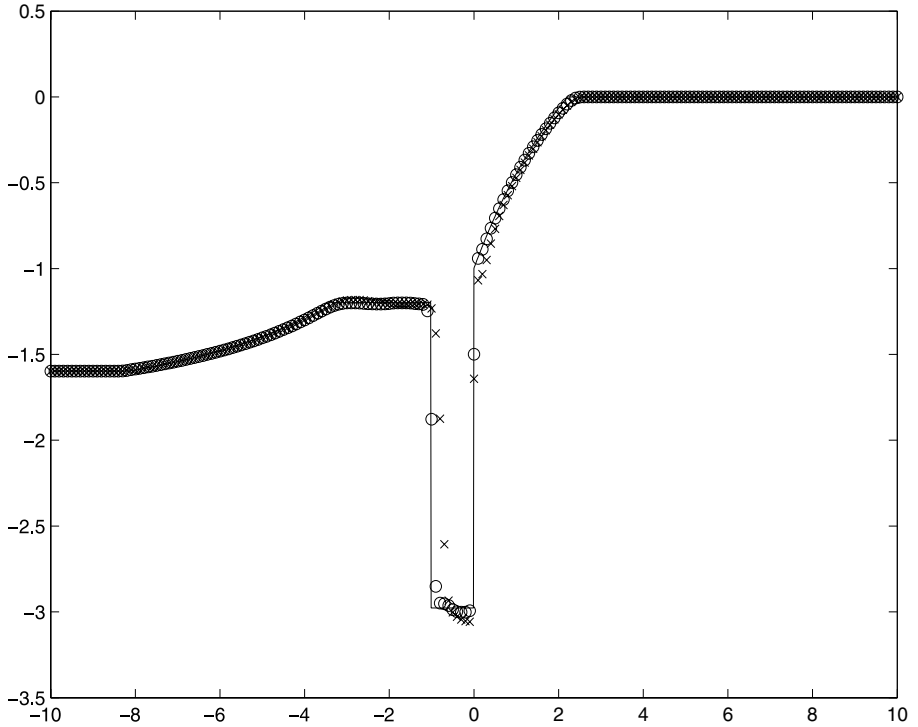

Fig. 6. Example 2.2, transcritical case. Froude number $\frac{v}{\sqrt{gh}}$ at $t = 0.5$; solid line: the exact solution; "○": the solution of HLLE solver using 200 cells; "×": the solution of relaxation scheme using 200 cells.

respectively, the water surface, Froude number $\frac{v}{\sqrt{gh}}$ and energy $\frac{1}{2}v^2 + g(h + B)$ in the obtained steady state solutions by our slope selecting method. These results match with those given in [24]. The results of our method using 100 cells agrees well with that using 400 cells and show accurately the energy are equal at two sides of bottom discontinuity at $x = -4$. The steady state solution belongs to Definition 2.1 with states at two sides of bottom discontinuity being both subcritical. The steady state solution is subcritical at left of the domain and transfers into supercritical at $x = 0$ which is the maximum bottom point, and again transfers back to subcritical through a standing transcritical shock.

Example 2.4. A tidal wave flow over discontinuous bottom.

This is a problem modified from [39]. The domain for this problem is $[0, 1500]$. In this example we choose the bottom function to be a variable discontinuous one

$$B(x) = \begin{cases} 8 + \sin\left(\frac{x}{50}\right), & \frac{3}{8} \times 1500 \leqslant x \leqslant \frac{5}{8} \times 1500, \\ 0, & \text{else.} \end{cases}$$

The initial and boundary conditions are

$$h(x, 0) = H(x),$$
$$v(x, 0) = 0$$

and

$$h(0, t) = H(0) + 4 - 4 \sin\left[\pi\left(\frac{4t}{86400} + \frac{1}{2}\right)\right],$$
$$v(L, t) = 0,$$

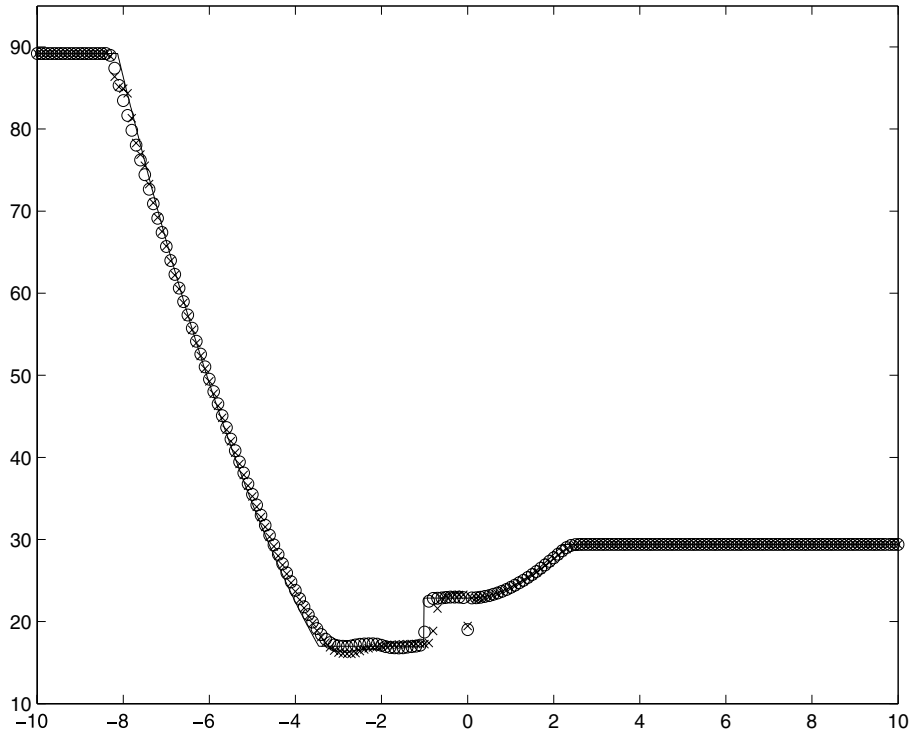

Fig. 7. Example 2.2, transcritical case. Energy $\frac{1}{2}v^2 + g(h+B)$ at $t = 0.5$; solid line: the exact solution; "○": the solution of HLLE solver using 200 cells; "×": the solution of relaxation scheme using 200 cells.

Table 3
Relative l^1-errors of computed conserved variables for Example 2.2 in the computational domain $[-10, 10]$

Errors	100 Cells	200 Cells	400 Cells	800 Cells	1600 Cells
HLLE scheme					
h	1.7959E − 2	9.0223E − 3	4.4579E − 3	2.6792E − 3	1.3661E − 3
m	3.5572E − 2	1.8205E − 2	9.1940E − 3	6.0454E − 3	3.0565E − 3
Relaxation scheme					
h	2.5314E − 2	1.2827E − 2	6.1377E − 3	2.8983E − 3	1.5084E − 3
m	3.3850E − 2	1.7393E − 2	8.8757E − 3	4.4184E − 3	2.3131E − 3

where $H(x) = H(0) - B(x)$, $H(0) = 16$ and $L = 1500$.

An asymptotic analytical solution is given by [3,39]

$$h(x,t) = H(x) + 4 - 4\sin\left[\pi\left(\frac{4t}{86400} + \frac{1}{2}\right)\right], \tag{2.71}$$

$$u(x,t) = \frac{(x-L)\pi}{5400h(x,t)}\cos\left[\pi\left(\frac{4t}{86400} + \frac{1}{2}\right)\right]. \tag{2.72}$$

This asymptotic solution does not depend on gravitational constant g since this solution is obtained by asymptotic expansion with respect to small Froude number [3]. In this example, we choose the gravitational constant $g = 9.81 \times 16$ so that the corresponding Froude number is small enough. We use the relaxation scheme with the constant $\widehat{C}$ in subcharacteristic condition set from the initial data. We use 96 cells to let the discontinuity of bottom located in the cell center and take $\frac{\Delta t}{\Delta x} = 1/60$. We plot the water height and velocity of our method at

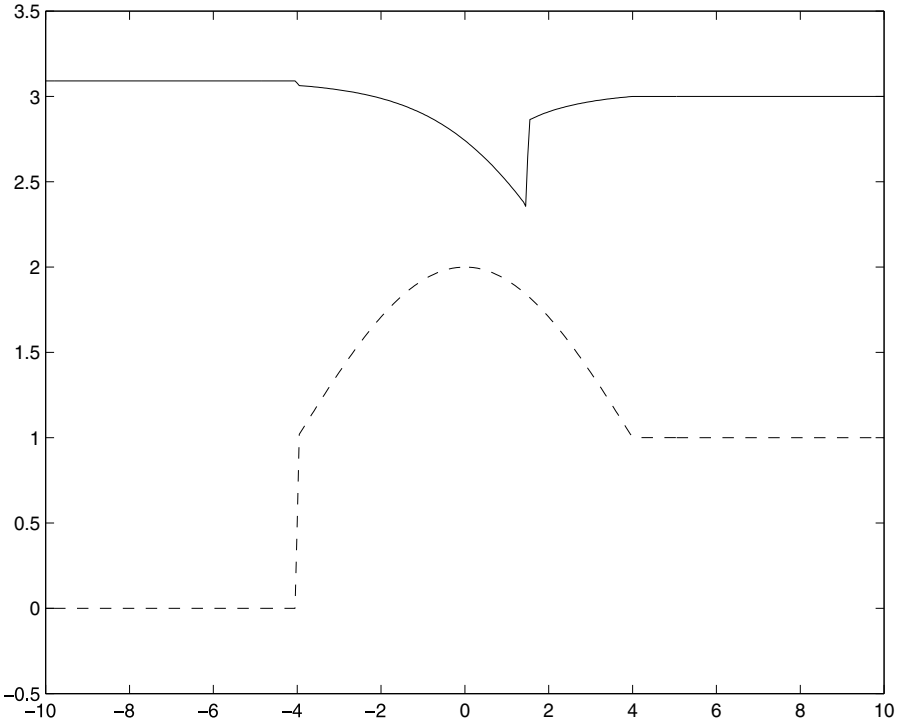

Fig. 8. Example 2.3, steady state capturing. Water surface at steady state along with bottom topography; solid line: water surface; dashed line: bottom topography.

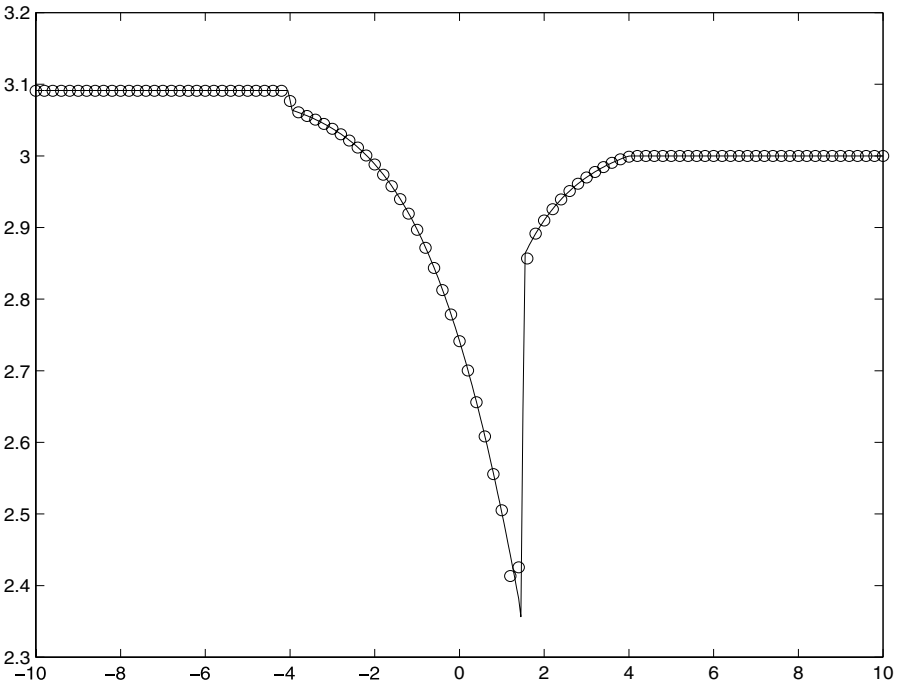

Fig. 9. Example 2.3, steady state capturing. Water surface at steady state by the slope selecting method; solid line: solution using 400 cells; "○": solution using 100 cells.

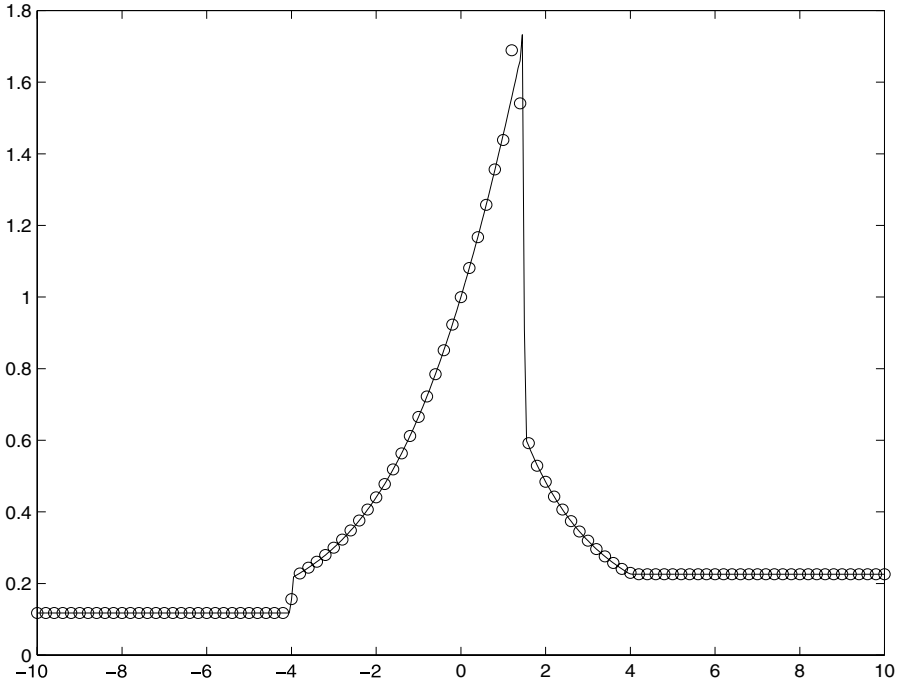

Fig. 10. Example 2.3, steady state capturing. Froude number $\frac{v}{\sqrt{gh}}$ at steady state by the slope selecting method; solid line: solution using 400 cells; "○": solution using 100 cells.

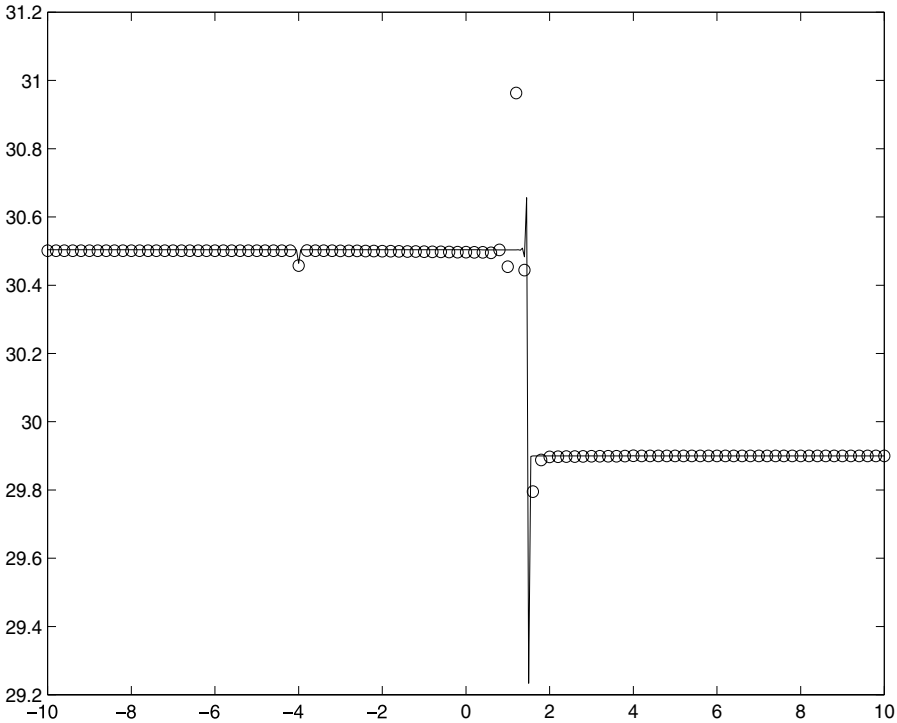

Fig. 11. Example 2.3, steady state capturing. Energy $\frac{1}{2}v^2 + g(h + B)$ at steady state by the slope selecting method; solid line: solution using 400 cells; "○": solution using 100 cells.

$t = 10{,}800$, which is one quarter of the tidal period in Figs. 12 and 13 and the velocity at $t = 32{,}400$, which is three quarter of the tidal period in Fig. 14 along with the asymptotic solutions. Our solutions match with the asymptotic solutions well in these results.

Example 2.5. A quasi-steady propagation.

In this example we test a quasi-steady problem using our slope selecting scheme. This quasi-steady problem is similar to the example tested by LeVeque in [30] but we now choose a discontinuous bottom and non-stationary steady state. We choose bottom function as

$$B(x) = \begin{cases} \cos\left(\frac{\pi x}{8}\right), & 0 \leqslant x \leqslant 4, \\ 0, & \text{else} \end{cases}$$

on $-10 < x < 10$, as shown by the dashed line in Fig. 15. The gravitational constant is set to be 9.8. We choose a subcritical steady state solution h_0, v_0 on $[-10, 10]$ belonging to Definition 2.1 satisfying

$$h_0 v_0 = 1,$$
$$\frac{1}{2} v_0^2 + g(h_0 + B) = 19.6.$$

We choose initial water height value and velocity value as

$$h(x,0) = \begin{cases} h_0 + \frac{1}{98}, & -8 \leqslant x \leqslant -5, \\ h_0, & \text{else} \end{cases}$$

and $v(x,0) = \frac{1}{h(x,0)}$. The initial water surface and Froude number are plotted in Figs. 16 and 17, respectively. In our scheme the zeroth order extrapolation is used as numerical boundary condition. We use HLLE scheme as the homogeneous shallow water equations solver and obtain the reference solution using our slope selecting method with 2000 grid points. We use 100 cells and take $\frac{\Delta t}{\Delta x} = 1/10$. The initial disturbance splits into two

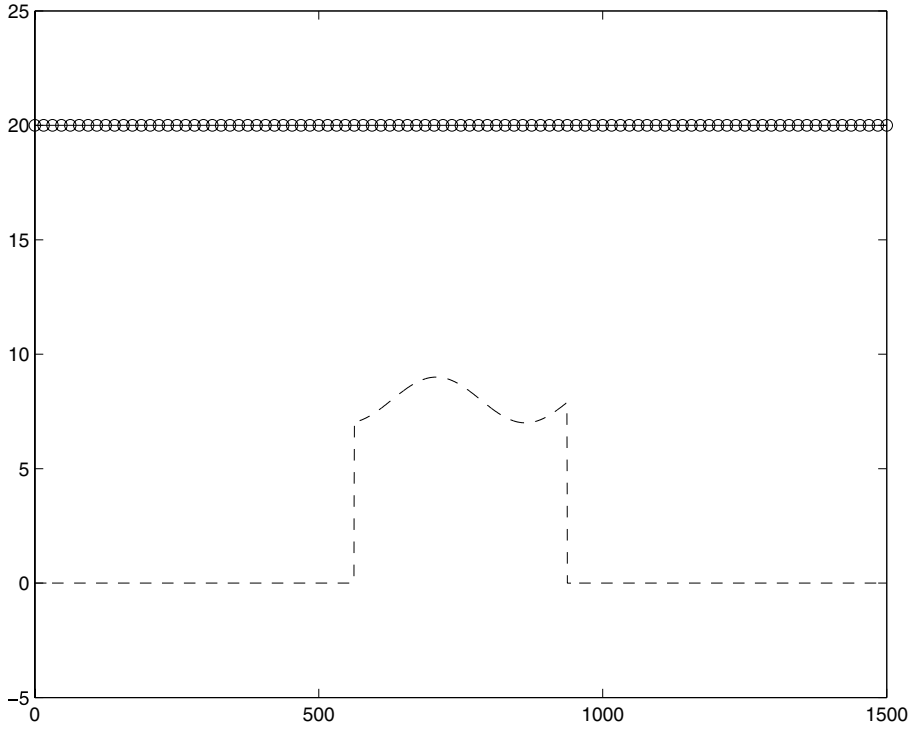

Fig. 12. Example 2.4, tidal flow. Water height at $t = 10{,}800$; solid line: the asymptotic solution; "○": the solution of the slope selecting method using 96 cells; dashed line: bottom topography.

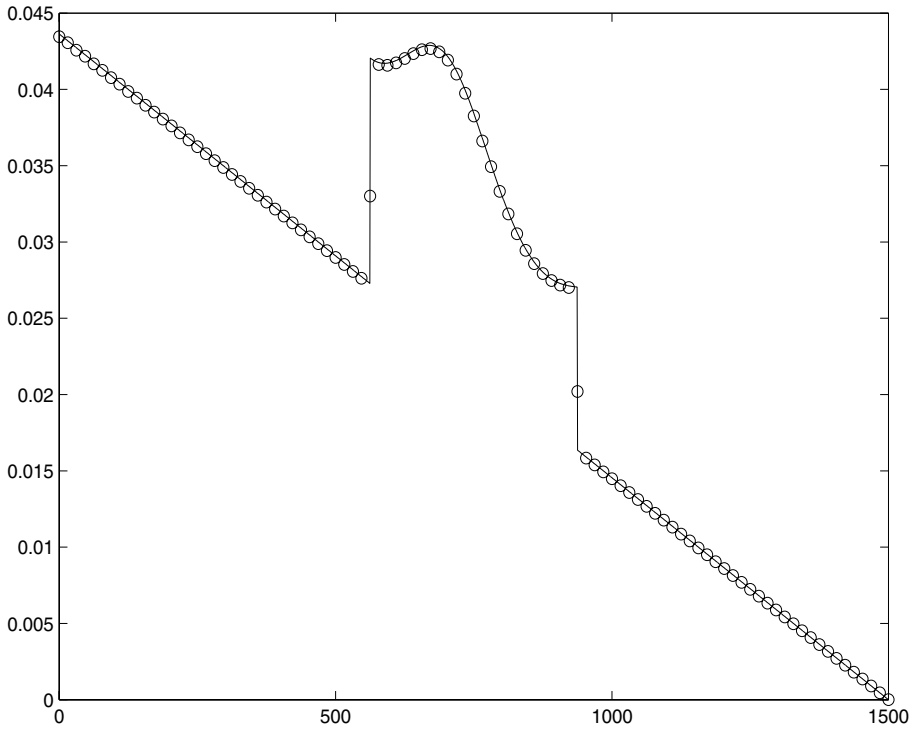

Fig. 13. Example 2.4, tidal flow. Velocity at $t = 10{,}800$; solid line: the asymptotic solution; "○": the solution of the slope selecting method using 96 cells.

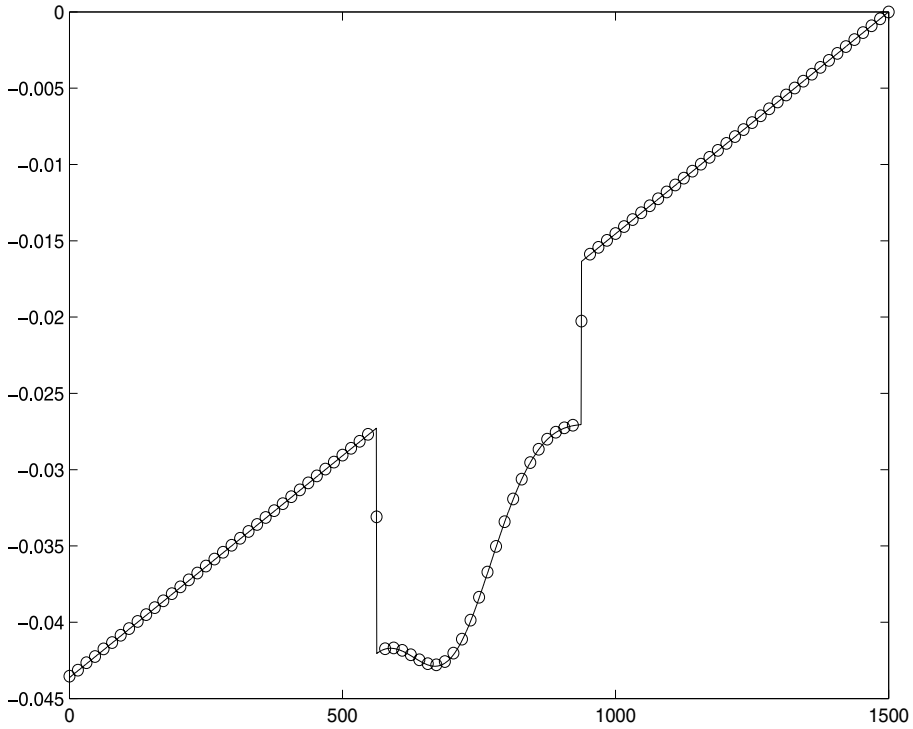

Fig. 14. Example 2.4, tidal flow. Velocity at $t = 32{,}400$; solid line: the asymptotic solution; "○": the solution of the slope selecting method using 96 cells.

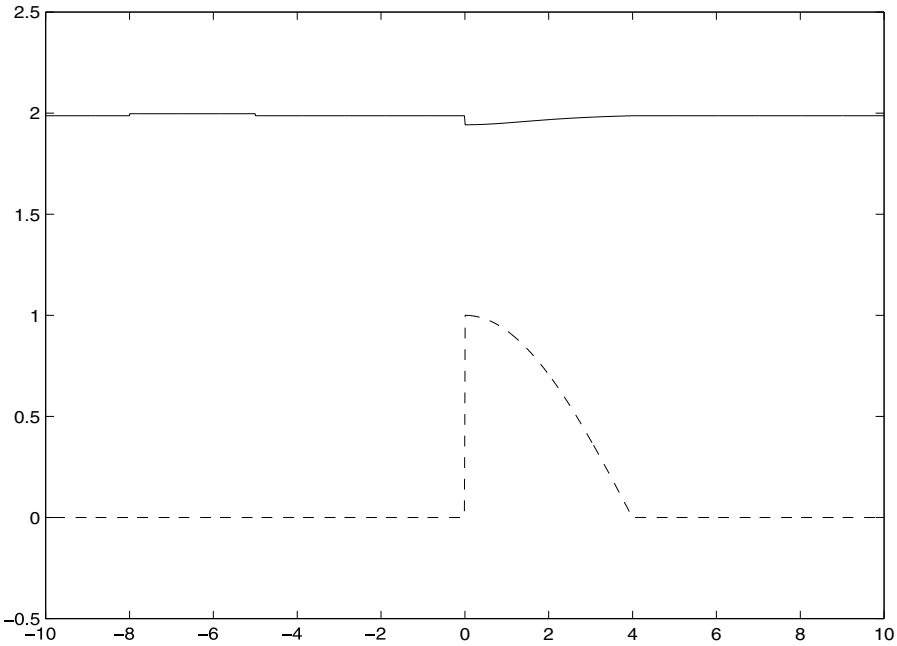

Fig. 15. Example 2.5, quasi-steady problem. Initial water surface along with bottom topography; solid line: water surface; dashed line: bottom topography.

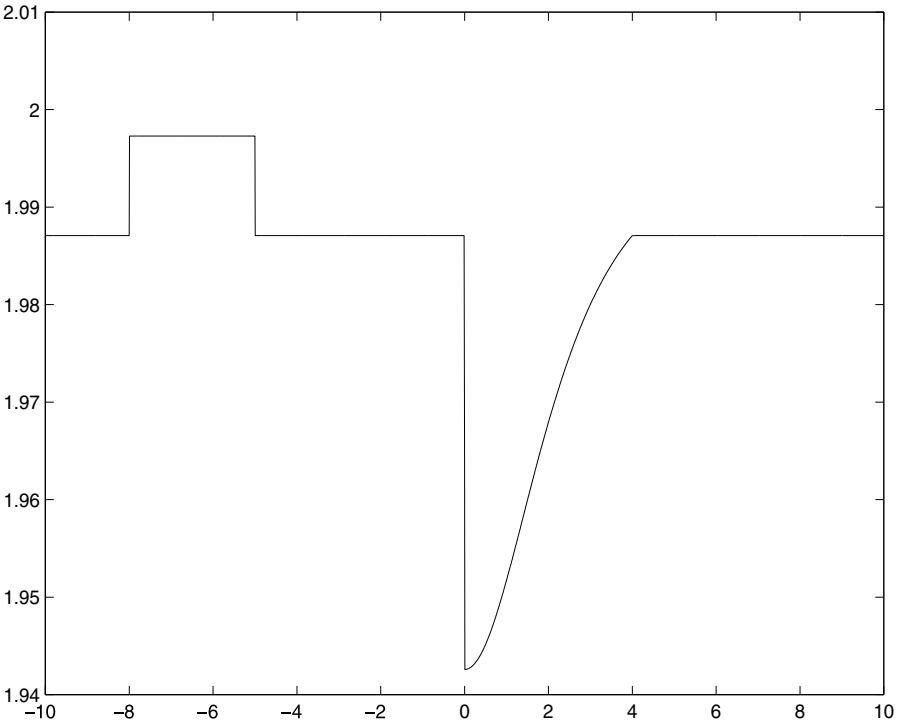

Fig. 16. Example 2.5, quasi-steady problem. Initial water surface.

waves propagating in different directions, as shown in Fig. 18, which shows the numerical solutions of water surface at $t = 0.5$. As the right going disturbance reaches the position of bottom discontinuity, it again splits into two disturbances – one goes back to the left and one continue going to the right. Fig. 19 show the

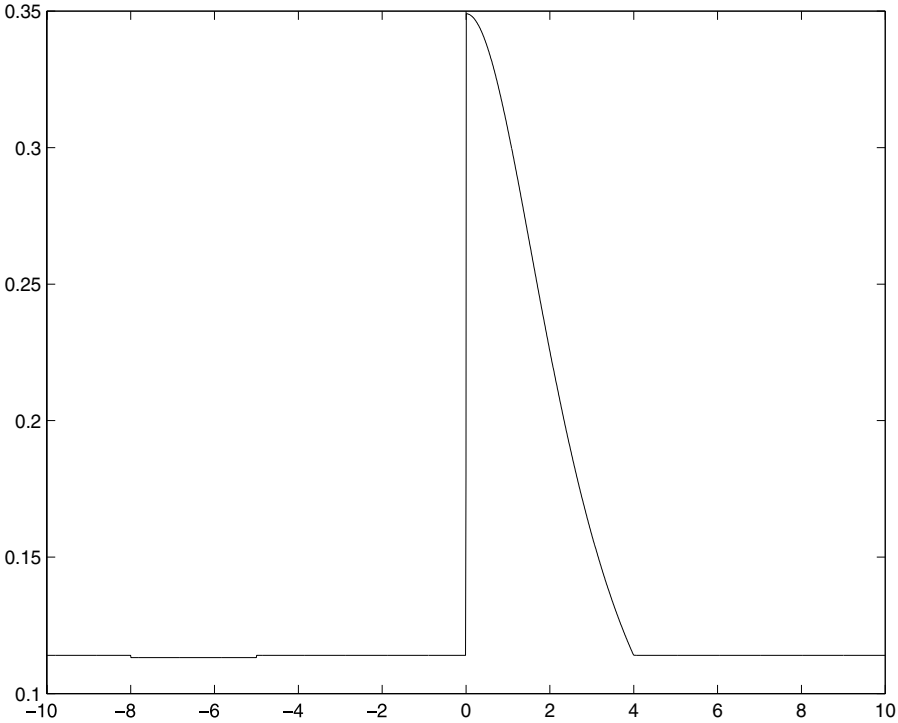

Fig. 17. Example 2.5, quasi-steady problem. Initial Froude number.

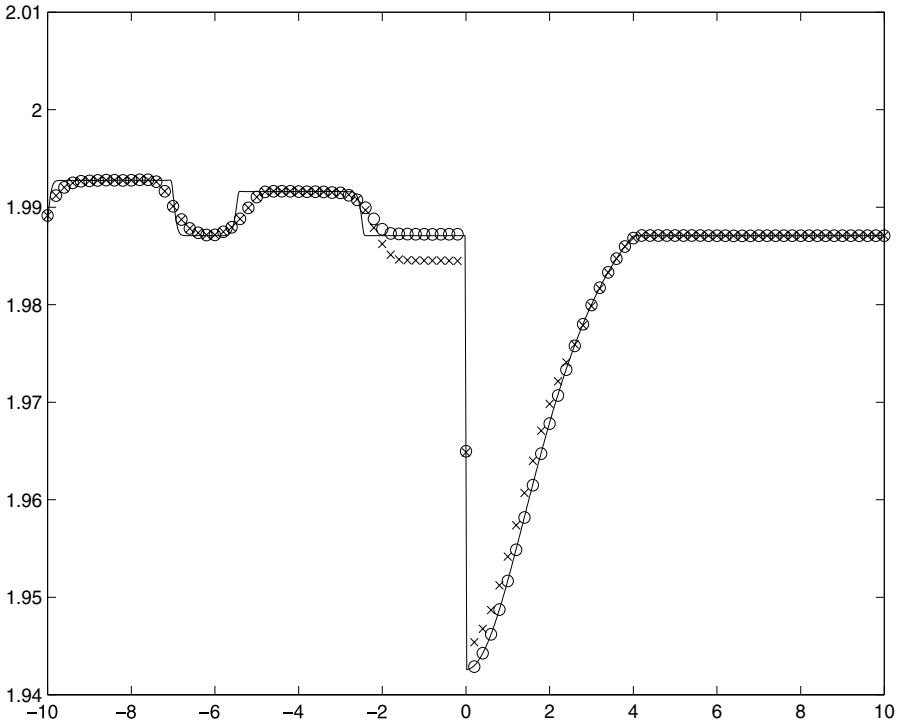

Fig. 18. Example 2.5, quasi-steady problem. Water surface at $t = 0.5$; solid line: the reference solution; "○": the solution of the slope selecting method using 100 cells; "×": the solution of SGM using 100 cells.

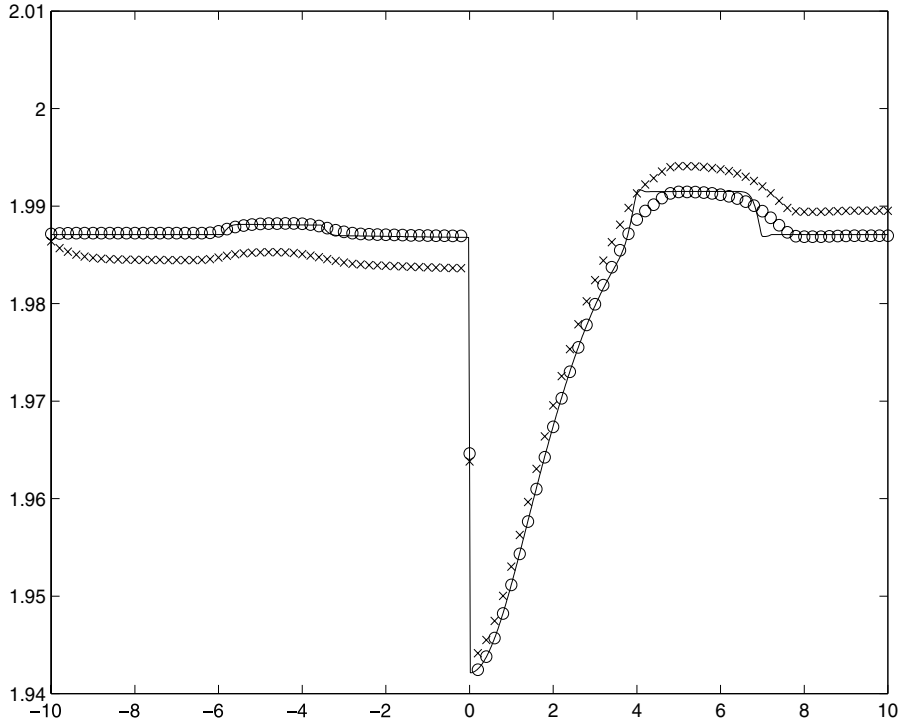

Fig. 19. Example 2.5, quasi-steady problem. Water surface at $t = 2.5$; solid line: the reference solution; "○": the solution of the slope selecting method using 100 cells; "×": the solution of SGM using 100 cells.

solutions of water surface at $t = 2.5$. At this time, the initially left going disturbance already leaves the domain and the two visible disturbances are split from the initially right going disturbance. Compared with the reference solutions, the solutions by our slope selecting scheme using 100 cells can efficiently preserve the steady state solution and correctly predict the positions of propagating disturbances. In comparison, Figs. 18 and 19 also depict the solution given by SGM. SGM fails to preserve the subcritical equal energy solution across the bottom discontinuity. In Fig. 18 the solution near bottom discontinuity should remain unchanged as predicted by the slope selecting method since the disturbance does not reach there yet, but the solution by SGM shows a substantial change near the bottom discontinuity. As mentioned formerly, SGM does not hold the *S*-property, and is improper in preserving (non-stationary) steady state solution when bottom is discontinuous.

Example 2.6. A 2D Riemann problem.

In this example we consider the calculation of unsteady state solution of a 2D Riemann problem with discontinuous bottom. The problem is defined in the square $(x, y) \in [0, 200] \times [0, 200]$. The initial data are $(h, u, v, B) = (15, -0.1, 0.1, 0)$ when $(x, y) \in [0, 100] \times [100, 200]$ and $(h, u, v, B) = (10, -0.1, 0.1, 10)$ elsewhere. The solution of this problem describe the motion of water outside the square $[0, 100] \times [100, 200]$ into this region across the bottom discontinuous line. The gravitational constant is chosen to be 9.8. We use the zeroth order extrapolation boundary condition. We use the uniform space mesh and take $\frac{\Delta t}{\Delta x} = \frac{\Delta t}{\Delta y} = 1/20$.

In the space discretization we use the Roe solver for 1D homogeneous shallow water equations in x or y direction [37] to obtain the numerical fluxes. Figs. 20 and 21 draw, respectively, the water surface and the quantity $\frac{1}{2}u^2 + g(h + B)$ at $t = 4$ by our 2D slope selecting method using 100×100 cells. In the quantity $\frac{1}{2}u^2 + g(h + B)$, u is the x-directional velocity. This quantity represents the sum of potential energy and x-directional kinetic energy.

In Figs. 22–25, we plot, respectively, water surface and the quantity $\frac{1}{2}u^2 + g(h + B)$ at $y = 180, 120$ at $t = 4$ by our 2D slope selecting method using 100×100, 400×400 and 800×800 cells. The comparison between numerical solutions by different meshes show the convergence of the numerical solutions. In particular, our results using 100×100 cells already have high resolution near bottom discontinuous line.

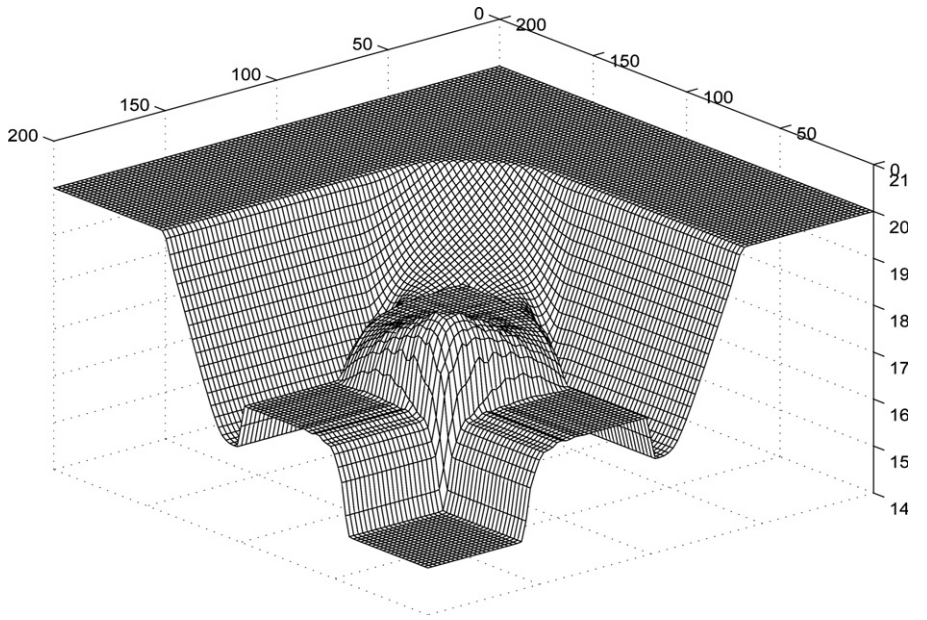

Fig. 20. Example 2.6, a 2D Riemann problem. Water surface at $t = 4$ by the 2D slope selecting method using 100×100 cells.

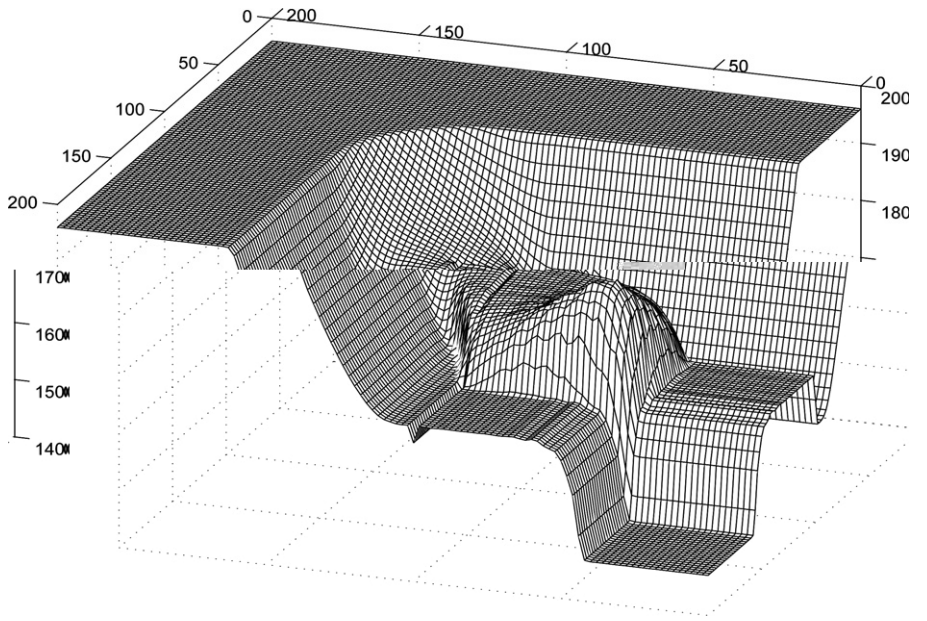

Fig. 21. Example 2.6, a 2D Riemann problem. $\frac{1}{2}u^2 + g(h + B)$ at $t = 4$ by the 2D slope selecting method using 100×100 cells.

Since this example has no exact solution available, a feasible way to check the validity of our numerical results is to compare the results with those computed by another method with different mechanism. The match of the results by two methods designed by different principle will make it sound that both methods are valid. In [24], the *continuous bottom cell average method* (CBCAM) has been used to compare with the interface type methods designed there. The CBCAM is a reasonable approach for discontinuous bottom problem by replacing the bottom discontinuity (line) with a continuous bottom transition zone. The conventional cell average method is applied to the regularized continuous bottom problem with enough cell numbers putting in the

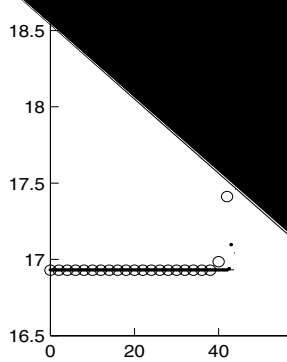

Fig. 23. Example 2.6, a 2D Riemann problem. Water surface at $t = 4$, $\ldots$ 800×800 cells; "·": solution using 400×400 cells; "○": solution using $1\ldots$

transition zone. The transition zone width tends to zero with regard $\ldots$ in [24]. This CBCAM has been tested to work for 1D discontinuous botto$\ldots$ nter-face type methods in [24] have been checked to match well with those by C$\ldots$ n using

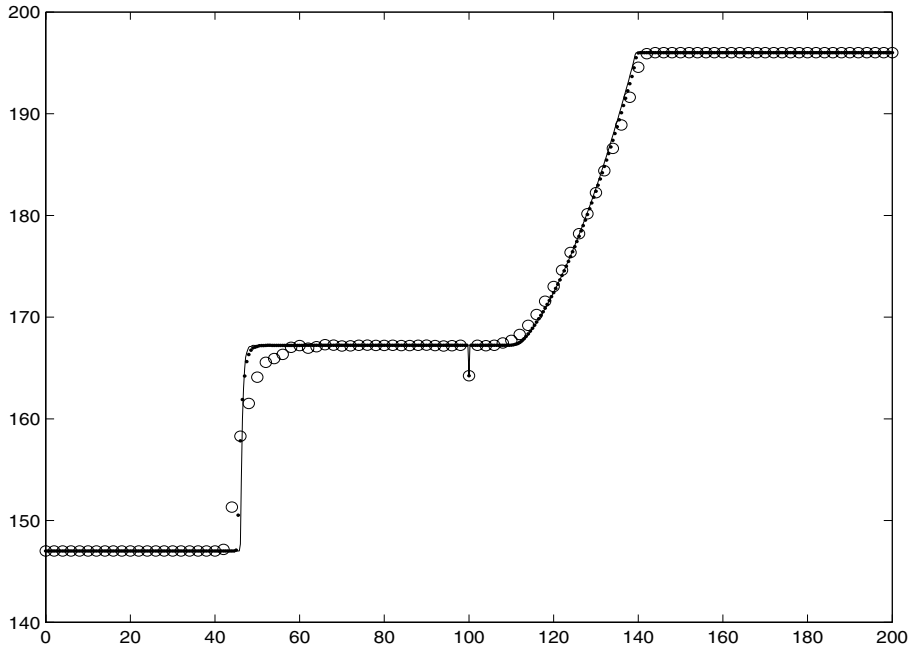

Fig. 24. Example 2.6, a 2D Riemann problem. $\frac{1}{2}u^2 + g(h+B)$ at $t = 4$, $y = 180$ by the 2D slope selecting method; solid line: solution using 800×800 cells; "·": solution using 400×400 cells; "○": solution using 100×100 cells.

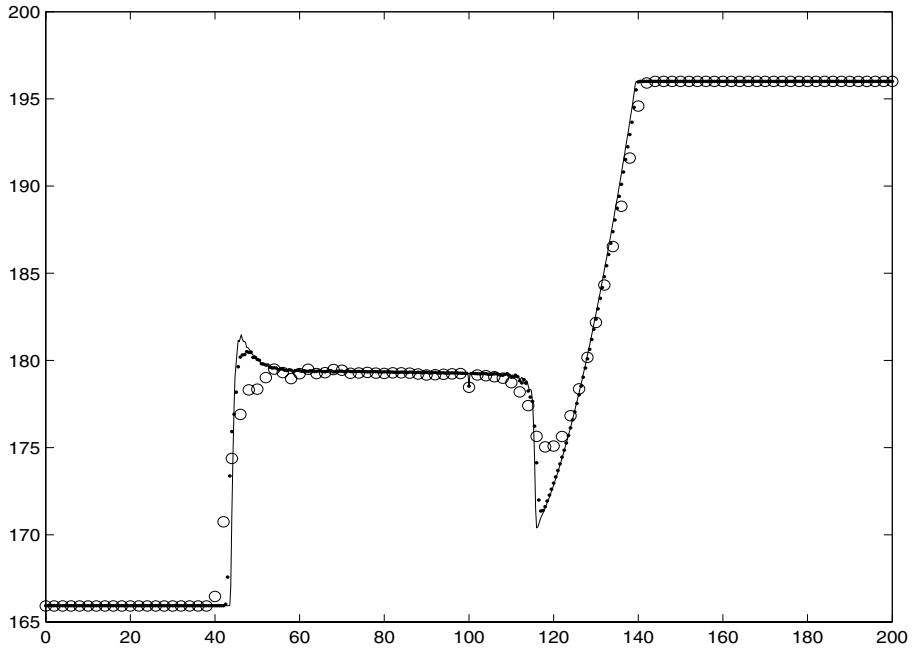

Fig. 25. Example 2.6, a 2D Riemann problem. $\frac{1}{2}u^2 + g(h+B)$ at $t = 4$, $y = 120$ by the 2D slope selecting method; solid line: solution using 800×800 cells; "·": solution using 400×400 cells; "○": solution using 100×100 cells.

course mesh, the interface type methods in [24] are shown to be more effective than CBCAM since the regularization of the source term in CBCAM makes the solution lose resolution near bottom discontinuous line. The results by our slope selecting method are similar to those given by the interface type methods in [24]. They match with those given by CBCAM using fine mesh, and have much higher resolution near bottom discontinuous line than those by CBCAM when using coarse mesh.

From the results by our slope selecting method as well as comparable results by other methods, one observes the phenomenon that across the bottom discontinuous line the potential energy plus normal directional kinetic energy is equal. For example, the quantity $\frac{1}{2}u^2 + g(h+B)$ is equal across a bottom discontinuous line which is parallel to y axis, as shown in Figs. 24 and 25.

3. The isothermal nozzle flow equations

Consider the system describing the evolution of an isothermal fluid in a nozzle

$$\partial_t(a\rho) + \partial_x(a\rho v) = 0, \tag{3.1}$$

$$\partial_t(a\rho v) + \partial_x(a\rho v^2 + ka\rho^\gamma) = p(\rho)\partial_x a, \tag{3.2}$$

where ρ, v represent density and velocity of the fluid, $a(x) > 0$ is the cross-sectional area, $p(\rho)$ is the pressure given by the relation

$$p(\rho) = k\rho^\gamma.$$

Equations (3.1), (3.2) reduce to the standard isentropic equations when $a(x)$ is constant.

The cell average method for above isothermal nozzle flow equations takes the form

$$\partial_t(a\rho)_j + \frac{m_{j+\frac{1}{2}} - m_{j-\frac{1}{2}}}{\Delta x} = 0, \tag{3.3}$$

$$\partial_t(a\rho v)_j + \frac{e_{j+\frac{1}{2}} - e_{j-\frac{1}{2}}}{\Delta x} = k\rho_j^\gamma \frac{a_{j+\frac{1}{2}} - a_{j-\frac{1}{2}}}{\Delta x}, \tag{3.4}$$

where $m_{j-\frac{1}{2}}$, $m_{j+\frac{1}{2}}$, $e_{j-\frac{1}{2}}$, $e_{j+\frac{1}{2}}$ denote, respectively, numerical fluxes for conserved variables $a\rho$ and $a\rho v$ at interfaces $j-\frac{1}{2}$, $j+\frac{1}{2}$ obtained by solving the homogeneous part of equations (3.1), (3.2).

When the steady state solution is smooth, the steady state solutions satisfy

$$a\rho v = C_1, \tag{3.5}$$

$$\frac{1}{2}v^2 + k\frac{\gamma}{\gamma-1}\rho^{\gamma-1} = C_2. \tag{3.6}$$

In the study [28] for isothermal nozzle flow Riemann problem with a cross-sectional step, the authors construct a wide class of solutions under the smooth steady state conditions across the cross-sectional step. Similar for the shallow water equations, in the smooth steady state conditions across the cross-sectional step, the momentum and energy conservation (3.5), (3.6) hold. The two sides states can be both subsonic $\frac{|v|}{\sqrt{k\gamma\rho^{\gamma-1}}} < 1$ or be both supersonic $\frac{|v|}{\sqrt{k\gamma\rho^{\gamma-1}}} > 1$, but a direct transition between subsonic and supersonic states across the cross-sectional step is not allowed. The subsonic or supersonic state can be connected with a transonic state $\frac{|v|}{\sqrt{k\gamma\rho^{\gamma-1}}} = 1$ to compose the smooth steady state flow across the cross-sectional step with the condition that the transonic state is reached at the lower cross-sectional area step side.

With the above steady state conditions across the cross-sectional discontinuity, we define the corresponding steady state solutions for the isothermal nozzle flow equations (3.1), (3.2) with discontinuous cross-sectional area as follows.

Definition 3.1. Steady state solutions to isothermal nozzle flow equations with discontinuous cross-sectional area: for a given initial condition to isothermal nozzle flow equations (3.1), (3.2) with discontinuous cross-sectional area, the solution will remain unchanged, i.e. the initial condition is the steady state solution for isothermal nozzle flow equations with discontinuous cross-sectional area, if the initial condition is steady state solution on continuous cross-sectional part, and across the cross-sectional discontinuity the conditions (3.5), (3.6) hold, namely

$$a_l\rho_l v_l = a_r\rho_r v_r, \tag{3.7}$$

$$\frac{1}{2}v_l^2 + k\frac{\gamma}{\gamma-1}(\rho_l)^{\gamma-1} = \frac{1}{2}v_r^2 + k\frac{\gamma}{\gamma-1}(\rho_r)^{\gamma-1}, \tag{3.8}$$

where ρ_l, v_l, a_l and ρ_r, v_r, a_r are the density, velocity in the initial condition and the cross-sectional area at two sides of the cross-sectional discontinuity, and one of the following situations occurs

$$\text{(i)} \quad \frac{|v_l|}{\sqrt{k\gamma\rho_l^{\gamma-1}}} < 1, \quad \frac{|v_r|}{\sqrt{k\gamma\rho_r^{\gamma-1}}} < 1, \tag{3.9}$$

$$\text{(ii)} \quad \frac{|v_l|}{\sqrt{k\gamma\rho_l^{\gamma-1}}} > 1, \quad \frac{|v_r|}{\sqrt{k\gamma\rho_r^{\gamma-1}}} > 1, \tag{3.10}$$

$$\text{(iii)} \quad \begin{cases} \frac{|v_l|}{\sqrt{k\gamma\rho_l^{\gamma-1}}} = 1 & \text{if } a_l < a_r, \\ \frac{|v_r|}{\sqrt{k\gamma\rho_r^{\gamma-1}}} = 1 & \text{if } a_l > a_r. \end{cases} \tag{3.11}$$

It is shown in [28] that the solutions constructed under such smooth steady state conditions described in Definition 3.1 across the cross-sectional step form rich solution patterns. Therefore, such problems are commonly encountered in which the solutions evolve to the steady state solutions belonging to Definition 3.1. In this section, we are concerned with the steady state capturing and preserving for such steady state solutions belonging to Definition 3.1.

3.1. Density gradient method (DGM)

We first study the steady state preserving method for isothermal nozzle flow Eq. (3.1), (3.2) when the cross-sectional area is continuous. When the cross-sectional area is continuously variable, the cell average method does not effectively preserve steady state solutions. In this case, similar to dealing with shallow water equations, one can use a special data reconstruction procedure to combine with the cell average method to achieve the steady state preserving role. Observe in the stationary steady state, (3.6) gives that the density is a constant. In the same principle as SGM, one can take the following data reconstruction procedure based on the gradient of density.

(1) In the step of defining the slopes of conserved variables $a\rho, a\rho v$ in each cell. Instead of defining the slope of $a\rho$, define the slope(denoted by $\widehat{S}_k$) for density

$$\widehat{S}_k = G(\rho_{k-1}, \rho_k, \rho_{k+1}),$$

where G is a standard slope limiter [29]. The slope of the conserved variable $a\rho v$ is still defined since $a\rho v$ is a constant in the steady state.

(2) The values of $a\rho$ on the left and right of the cell interface $x_{k+\frac{1}{2}}$ are

$$(a\rho)^{\mathrm{L}}_{k+\frac{1}{2}} = a_{k+\frac{1}{2}}\left(\rho_k + \frac{1}{2}\Delta x\widehat{S}_k\right), \quad (a\rho)^{\mathrm{R}}_{k+\frac{1}{2}} = a_{k+\frac{1}{2}}\left(\rho_{k+1} - \frac{1}{2}\Delta x\widehat{S}_{k+1}\right).$$

The left and right values of $a\rho v$ are still obtained by its cell average values and slopes. These left and right values of conserved variables at interface $x_{k+\frac{1}{2}}$ are used by a homogeneous isothermal nozzle flow equations solver to get the numerical fluxes $m_{k+\frac{1}{2}}$, $e_{k+\frac{1}{2}}$.

(3) Once the numerical fluxes for conserved variables are obtained, one can use the cell average formula (3.3), (3.4) as the numerical scheme.

Since this method uses the gradient of density instead of that of the conserved variable $a\rho$ in constructing the two sides values at the interface, we name this method as the *density gradient method* (DGM). Similar to proving Z-property of SGM, one can prove that DGM can exactly preserve the *stationary* flow for isothermal nozzle flow equations with a continuously variable cross-sectional area (Z-property).

3.2. The slope selecting method

In the same principle as the shallow water equations, our slope selecting method for isothermal nozzle flow equations can be described as follows. Our method is based on DGM, incorporating the slope selecting

strategy and interface type source term approximation near or in the cell containing the cross-sectional area discontinuity. Assume a discontinuity of cross-section is contained in the center of the cell $[x_{j-\frac{1}{2}}, x_{j+\frac{1}{2}}]$. Let a_i be the interface values of a at $x_i (i = j-\frac{1}{2}, j+\frac{1}{2})$. Now define the quantities at interfaces $j-\frac{1}{2},\ j+\frac{1}{2}$

$$(a\rho)^*_{j-\frac{1}{2}} = \frac{2(a\rho)_j (a\rho)_{j-1}}{(a\rho)_{j+1} + (a\rho)_{j-1}}, \quad (a\rho)^*_{j+\frac{1}{2}} = \frac{2(a\rho)_j (a\rho)_{j+1}}{(a\rho)_{j+1} + (a\rho)_{j-1}}, \tag{3.12}$$

$$\rho^*_{j\pm\frac{1}{2}} = \frac{(a\rho)^*_{j\pm\frac{1}{2}}}{a_{j\pm\frac{1}{2}}}. \tag{3.13}$$

In the cell centered at x_j we directly define the slope for the conserved variable $a\rho$ to be

$$\frac{(a\rho)^*_{j+\frac{1}{2}} - (a\rho)^*_{j-\frac{1}{2}}}{\Delta x}. \tag{3.14}$$

In cells $j-1, j+1$ we set slopes for density ρ to be

$$\widehat{S}_{j-1} = \frac{\operatorname{sign}\{\rho_{j-1} - \rho_{j-2}\} + \operatorname{sign}\{\rho^*_{j-\frac{1}{2}} - \rho_{j-1}\}}{2\Delta x} \min\{|\rho_{j-1} - \rho_{j-2}|, |\rho^*_{j-\frac{1}{2}} - \rho_{j-1}|\}, \tag{3.15}$$

$$\widehat{S}_{j+1} = \frac{\operatorname{sign}\{\rho_{j+2} - \rho_{j+1}\} + \operatorname{sign}\{\rho_{j+1} - \rho^*_{j+\frac{1}{2}}\}}{2\Delta x} \min\{|\rho_{j+2} - \rho_{j+1}|, |\rho_{j+1} - \rho^*_{j+\frac{1}{2}}|\}. \tag{3.16}$$

The values of $a\rho$ on the left and right of the cell interfaces $x_{j\pm\frac{1}{2}}$ are

$$(a\rho)^{\mathrm{L}}_{j-\frac{1}{2}} = a_{j-\frac{1}{2}}\left(\rho_{j-1} + \frac{1}{2}\Delta x \widehat{S}_{j-1}\right), \quad (a\rho)^{\mathrm{R}}_{j-\frac{1}{2}} = (a\rho)^*_{j-\frac{1}{2}},$$

$$(a\rho)^{\mathrm{L}}_{j+\frac{1}{2}} = (a\rho)^*_{j+\frac{1}{2}}, \quad (a\rho)^{\mathrm{R}}_{j+\frac{1}{2}} = a_{j+\frac{1}{2}}\left(\rho_{j+1} - \frac{1}{2}\Delta x \widehat{S}_{j+1}\right)$$

with $(a\rho)^*_{j\pm\frac{1}{2}},\ \widehat{S}_{j\pm1}$ defined in (3.12), (3.15) and (3.16).

The left and right values of $a\rho v$ are obtained as in DGM. These left and right values of conserved variables at interfaces $x_{j\pm\frac{1}{2}}$ are used by a homogeneous isothermal nozzle flow equations conservative scheme to get the numerical fluxes $m_{j\pm\frac{1}{2}},\ e_{j\pm\frac{1}{2}}$.

Define quantities at $j \pm \frac{1}{2}$

$$v^*_{j-\frac{1}{2}} = \frac{m_{j-\frac{1}{2}}}{(a\rho)^*_{j-\frac{1}{2}}}, \quad v^*_{j+\frac{1}{2}} = \frac{m_{j+\frac{1}{2}}}{(a\rho)^*_{j+\frac{1}{2}}}. \tag{3.17}$$

We then apply the interface type source term approximation described in [23] with the needed interface values of ρ, v defined by (3.13), (3.17). Denote $H_i = a_i \rho^*_i v^*_i,\ G_i = \frac{1}{2}(v^*_i)^2 + k\frac{\gamma}{\gamma-1}(\rho^*_i)^{\gamma-1},\ i = j-\frac{1}{2},\ j+\frac{1}{2}$. We choose $\hat{a}, H, G$ to be linear functions on $[x_{j-\frac{1}{2}}, x_{j+\frac{1}{2}}]$ so that

$$\hat{a}(x_i) = a_i, \quad H(x_i) = H_i, \quad G(x_i) = G_i, \quad i = j-\frac{1}{2}, j+\frac{1}{2}. \tag{3.18}$$

We choose smooth $\hat{\rho},\ \hat{v}$ on $[x_{j-\frac{1}{2}}, x_{j+\frac{1}{2}}]$ from

$$\hat{a}\hat{\rho}\hat{v} = H, \tag{3.19}$$

$$\frac{1}{2}\hat{v}^2 + k\frac{\gamma}{\gamma-1}\hat{\rho}^{\gamma-1} = G, \tag{3.20}$$

or $\hat{\rho}$ from

$$\frac{1}{2}\frac{H^2}{\hat{a}^2\hat{\rho}^2} + k\frac{\gamma}{\gamma-1}\hat{\rho}^{\gamma-1} = G, \tag{3.21}$$

with endpoint values

$$\hat{\rho}(x_i) = \rho^*_i, \quad \hat{v}(x_i) = v^*_i, \quad i = j-\frac{1}{2}, j+\frac{1}{2}. \tag{3.22}$$

We then can use the following expression

$$k\left(\frac{1}{\Delta x}\int_{x_{j-\frac{1}{2}}}^{x_{j+\frac{1}{2}}}\hat{\rho}^{\gamma}\,\mathrm{d}x\right)\frac{a_{j+\frac{1}{2}}-a_{j-\frac{1}{2}}}{\Delta x}$$

to replace the source term approximation in cell average method (3.4). To obtain the integration value in the above expression, we use the same numerical strategy as for shallow water equations. The values of $\hat{\rho}$ are solved from (3.21) according to the subsonic or supersonic state of the computed solution. When dealing with the transonic problems, one also needs to add a transonic fix in the source term approximation. These are in the same principle as the method in [23] and the details are presented there.

We use the scheme of DGM in all the other cells do not containing a cross-sectional discontinuity with the mention that the slope of density in the cell adjacent to a cross-sectional discontinuity is modified by our slope selecting strategy.

Similar to the conclusions for the shallow water equations, one can prove that our slope selecting method for isothermal nozzle flow equations *formally* exactly preserves the (stationary or non-stationary) steady state solutions belonging to Definition 3.1 in which no stationary shock exists when cross-sectional area is a step function (S-property). The proof is given in Appendix C.

3.3. Numerical examples

We use numerical examples to demonstrate that our slope selecting method works well for unsteady calculation, steady state capturing and preserving for the isothermal nozzle flow equations with discontinuous cross-sectional area. The second order TVD Runge–Kutta method [35] is used for time discretization in all the examples. We choose $k = 1,\ \gamma = 4/3$ in the computation.

Examples 3.1 and 3.2 are Riemann problems studied in [28] and have been tested by our methods in [23,24]. These two Riemann problems are solved numerically on the domain $[-6, 6]$. For spatial discretization, we use the HLLE solver or relaxation scheme for the homogeneous part of equations (3.1), (3.2). See Appendix A for the description of the numerical fluxes provided by these solvers for isothermal nozzle flow equations. We take $\frac{\Delta t}{\Delta x} = 1/5$ for both problems. The zeroth extrapolation is used for numerical boundary conditions. The exact solutions are available for these problems [28], and we show the slope selecting method gives convergent solutions for these examples.

Example 3.3 is a steady state capturing problem tested in [24] and is used to show our method is efficient in calculating steady state solution for isothermal nozzle flow equations with discontinuous cross-sectional area with an improvement from our method in [24] in overcoming "slow convergence" phenomenon by using shock capturing scheme with larger numerical viscosity.

Example 3.4 is quasi-steady computation problems and is used to test the steady state preserving property of our method. This example shows that our slope selecting method has strong ability to preserve steady state solutions when cross-section contains both discontinuities and continuous variable part.

Example 3.1. A Riemann problem with solution in the transonic state.

The initial data are $(\rho, v, a) = (4, -1.8, 1.5)$ when $x < 0$ and $(\rho, v, a) = (1, 2, 2.5)$ when $x > 0$. This is a transonic case. The solution reaches critical state at the left side of the cross-sectional jump. The constant $\widehat{C}$ in subcharacteristic condition in relaxation scheme is chosen to be 8. The solutions of the slope selecting method based on HLLE solver and relaxation scheme using 100 cells along with the exact solution are plotted in Figs. 26–28. The transonic fix used in the source term approximation ensures our method correctly capture the transonic flow across the cross-sectional jump. The exact solution for this example is given in Appendix B. Table 4 lists the relative l^1-errors of the computed conserved variables on the whole computational domain with different meshes by our method using both solvers. The first order convergence rate of our numerical solutions can be observed in this table.

Example 3.2. A Riemann problem with solution in both super- and sub-sonic state.

The initial data are $(\rho, v, a) = (4, -1.6, 1.5)$ when $x < 0$ and $(\rho, v, a) = (6, 1, 2.5)$ when $x > 0$. This is a mixed sub- and super-sonic case. The constant $\widehat{C}$ in subcharacteristic condition in relaxation scheme is chosen to be 8. The solutions from the slope selecting method based on HLLE solver and relaxation scheme by using 100 cells along with the exact solution are shown in Fig. 29–31. The exact solution for this example is given in Appendix B. Table 5 lists the relative l^1-errors of the computed conserved variables on the whole computational domain with different meshes by our method using both solvers. One can observe our method gives first order convergent numerical solutions for this example.

Example 3.3. A steady state capturing calculation.

The problem is defined in $[-6, 6]$. We choose the cross-sectional area to be

$$a(x) = \begin{cases} 2, & x < -2, \\ 2 + \frac{1}{2}\cos\left(\frac{\pi x}{4}\right), & -2 < x < 0, \\ 2.5 - \frac{1}{2}\cos\left(\frac{\pi x}{6}\right), & 0 < x < 3, \\ 2.5, & x > 3. \end{cases}$$

as shown in Fig. 32. The initial conditions are given by

$$\rho(x, 0) = 4,$$
$$v(x, 0) = \frac{3}{a(x)\rho(x, 0)},$$

the boundary conditions are given by $\rho v|_{x=-6} = 1.2, \rho|_{x=6} = 4$. The exact steady state solutions $\rho_e(x), v_e(x)$ are the subsonic solutions belonging to Definition 3.1 determined by the steady state equations

$$a(x)\rho_e(x)v_e(x) = 2.4,$$
$$\frac{1}{2}(v_e(x))^2 + k\frac{\gamma}{\gamma - 1}(\rho_e(x))^{\gamma - 1} = 0.0288 + 4^{4/3}.$$

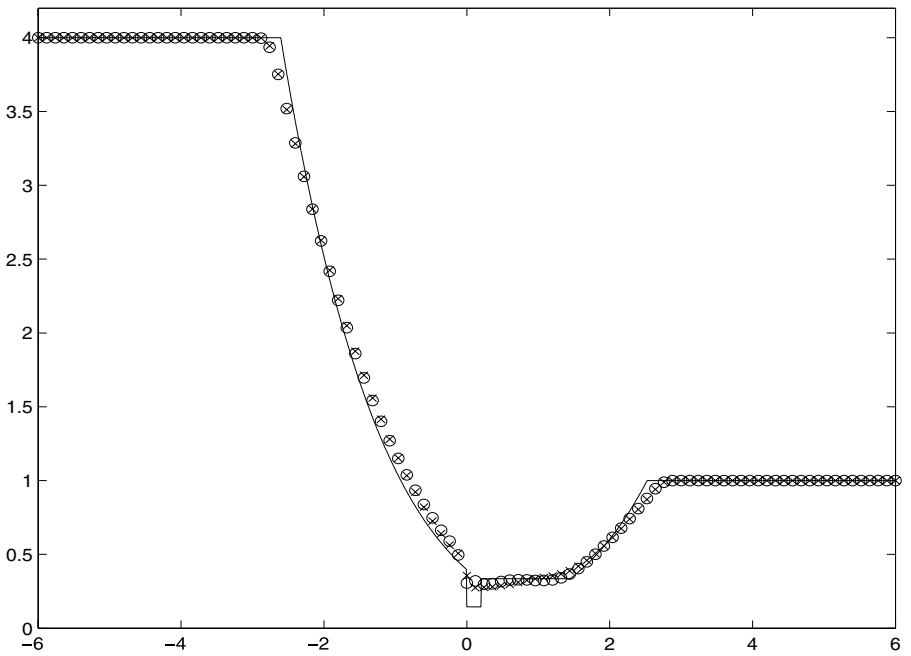

Fig. 26. Example 3.1, transonic case. Density at $t = 0.8$; solid line: the exact solution; "○": the solution of HLLE solver using 100 cells; "×": the solution of relaxation scheme using 100 cells.

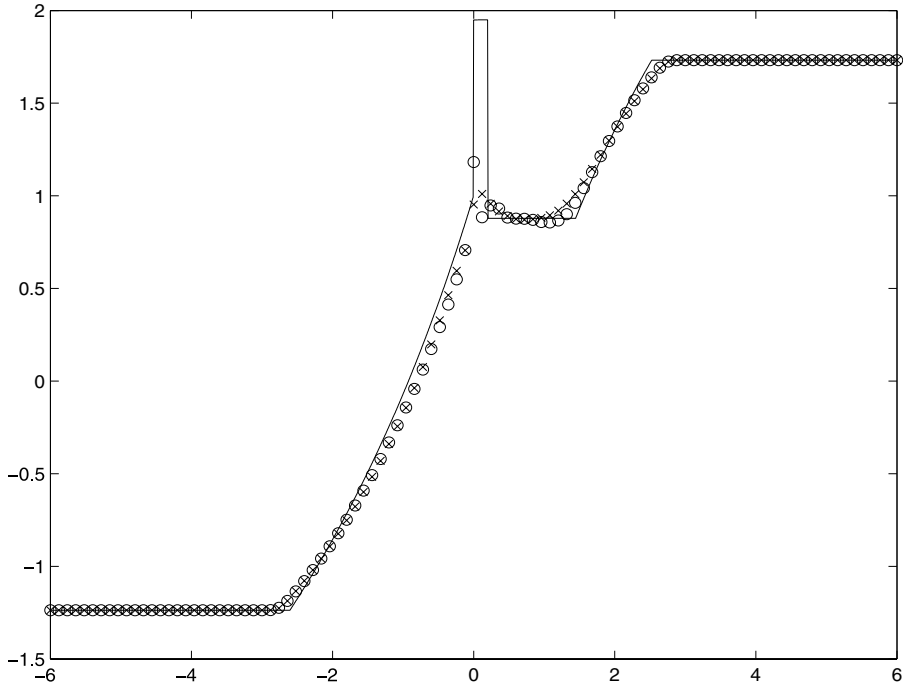

Fig. 27. Example 3.1, transonic case. Mach number $\frac{v}{\sqrt{k\gamma\rho^{\gamma-1}}}$ at $t = 0.8$; solid line: the exact solution; "○": the solution of HLLE solver using 100 cells; "×": the solution of relaxation scheme using 100 cells.

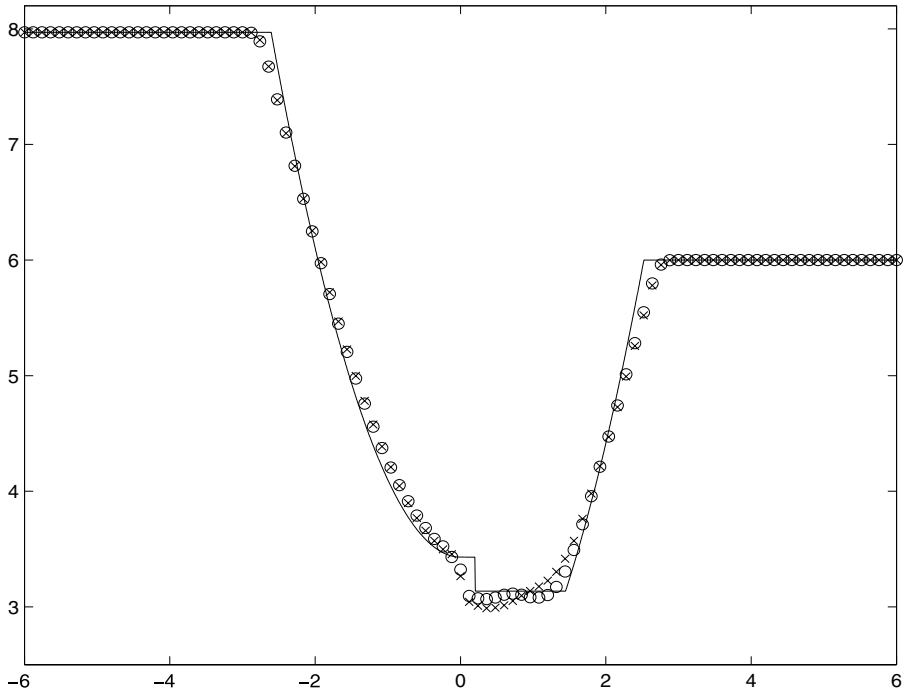

Fig. 28. Example 3.1, transonic case. Energy $\frac{1}{2}v^2 + k\frac{\gamma}{\gamma-1}\rho^{\gamma-1}$ at $t = 0.8$; solid line: the exact solution; "○": the solution of HLLE solver using 100 cells; "×": the solution of relaxation scheme using 100 cells.

Table 4
Relative l^1-errors of computed conserved variables for Example 3.1 in the computational domain $[-6,6]$

Errors	100 Cells	200 Cells	400 Cells	800 Cells
HLLE scheme				
ρ	1.7226E − 2	8.7752E − 3	4.3618E − 3	2.2309E − 3
m	1.9711E − 2	1.0194E − 2	5.1879E − 3	2.6164E − 3
Relaxation scheme				
ρ	1.8507E − 2	1.0311E − 2	5.5495E − 3	2.6851E − 3
m	2.1113E − 2	1.1272E − 2	5.8273E − 3	2.9305E − 3

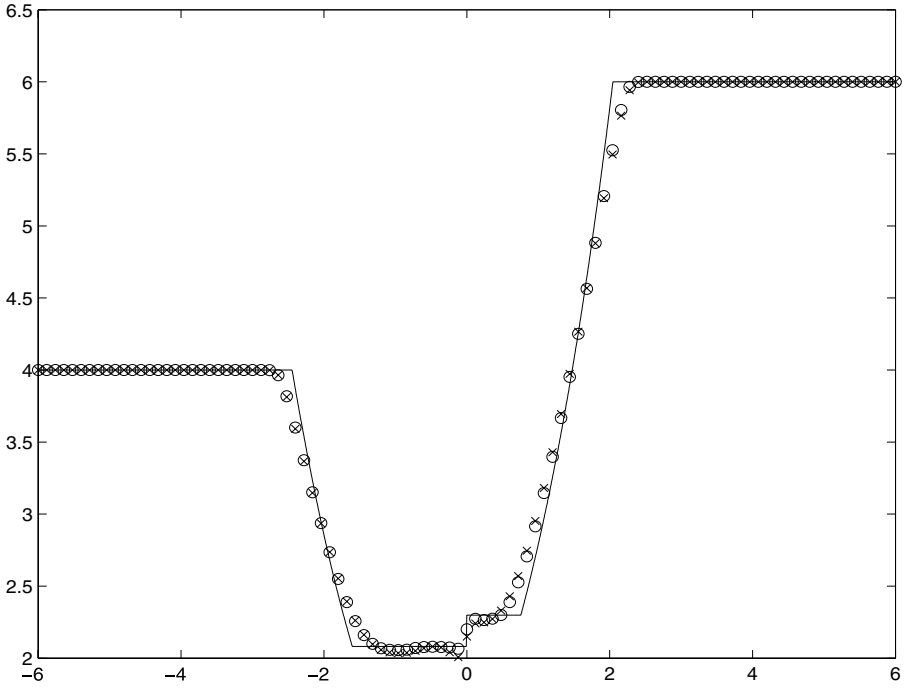

Fig. 29. Example 3.2, mixed sub- and super-sonic case. Density at $t = 0.8$; solid line: the exact solution; "○": the solution of HLLE solver using 100 cells; "×": the solution of relaxation scheme using 100 cells.

We take $\frac{\Delta t}{\Delta x} = 1/2$ and use HLLE solver to solve the homogeneous part of isothermal nozzle flow equations. Figs. 33–35 show, respectively, the numerical steady state density, Mach number $\frac{v}{\sqrt{k\gamma\rho^{\gamma-1}}}$ and energy $\frac{1}{2}v^2 + k\frac{\gamma}{\gamma-1}\rho^{\gamma-1}$ by our slope selecting method. The numerical results show the energy are equal at two sides of cross-sectional discontinuity with high accuracy. Table 6 lists the l^1-norm of the errors between exact and numerical steady state densities on different meshes. In this table, one can observe that the l^1-convergence rate of numerical steady state solutions are second order in both $[-6,-0.2]$ and $[0.2,6]$, but is first order in the entire domain $[-6,6]$ which includes the cross-sectional area discontinuity. These results show that our method is able to capture the steady state solution with second order accuracy in the domain where the cross-sectional area and solution are smooth due to the effectiveness of our method in controlling energy conservation across the cross-sectional discontinuity.

For this problem our methods in [24] using Roe solver encounter "slow convergence" phenomenon when l^∞-error between numerical solutions at two adjacent time step reaches about 1E − 3. The slope selecting method in this paper using HLLE solver does not encounter this phenomenon at least when the above mentioned l^∞-error decreases to less than 1E − 6. According to the analysis in [22], the "slow convergence" phenomenon is related to the stability of the discrete viscous profile of the used scheme and can be alleviated by using scheme having larger viscosity. The HLLE solver, which has larger numerical viscosity than the Roe solver, performs better in reducing the "slow convergence" phenomenon in this problem.

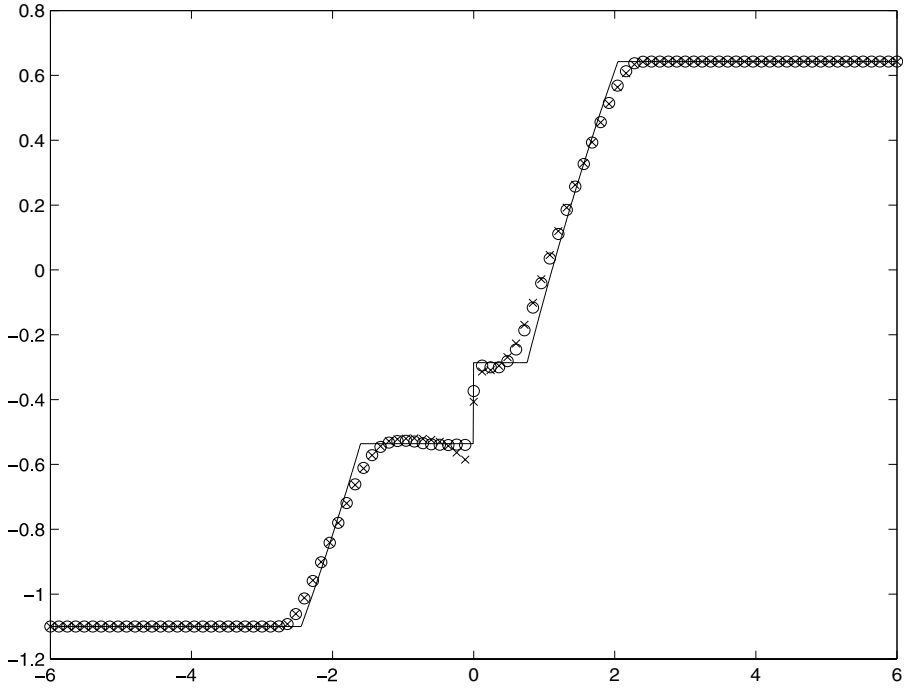

Fig. 30. Example 3.2, mixed sub- and super-sonic case. Mach number $\frac{v}{\sqrt{k\gamma\rho^{\gamma-1}}}$ at $t = 0.8$; solid line: the exact solution; "○": the solution of HLLE solver using 100 cells; "×": the solution of relaxation scheme using 100 cells.

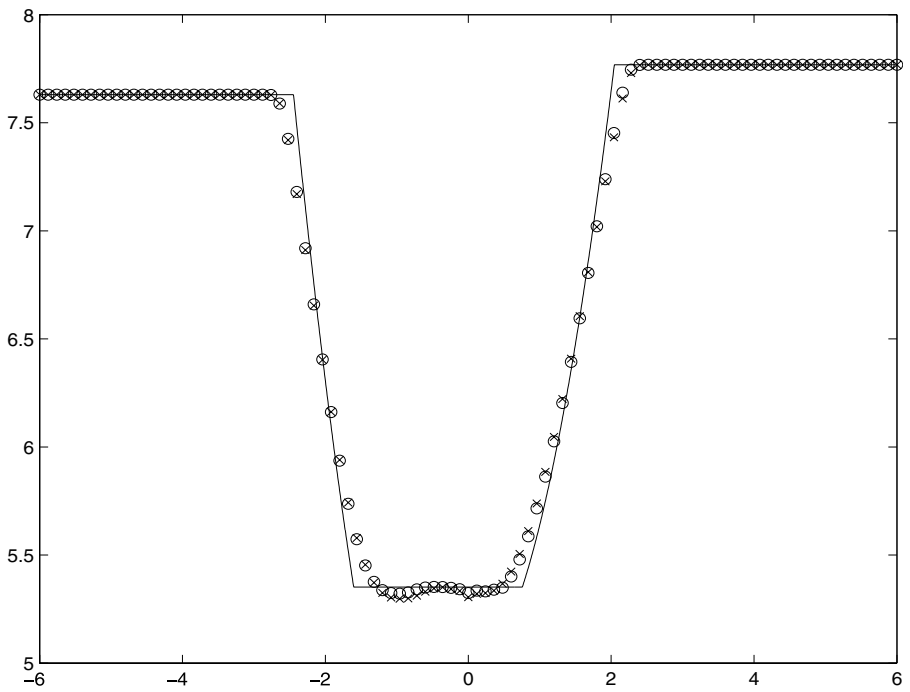

Fig. 31. Example 3.2, mixed sub- and super-sonic case. Energy $\frac{1}{2}v^2 + k\frac{\gamma}{\gamma-1}\rho^{\gamma-1}$ at $t = 0.8$; solid line: the exact solution; "○": the solution of HLLE solver using 100 cells; "×": the solution of relaxation scheme using 100 cells.

Table 5
Relative l^1-errors of computed conserved variables for Example 3.2 in the computational domain $[-6,6]$

Errors	100 Cells	200 Cells	400 Cells	800 Cells
HLLE scheme				
ρ	9.7698E − 3	4.9695E − 3	2.4871E − 3	1.2436E − 3
m	1.8490E − 2	9.4172E − 3	4.7348E − 3	2.3807E − 3
relaxation scheme				
ρ	1.1542E − 2	5.8071E − 3	2.8531E − 3	1.4003E − 3
m	2.1156E − 2	1.0709E − 2	5.2692E − 3	2.6037E − 3

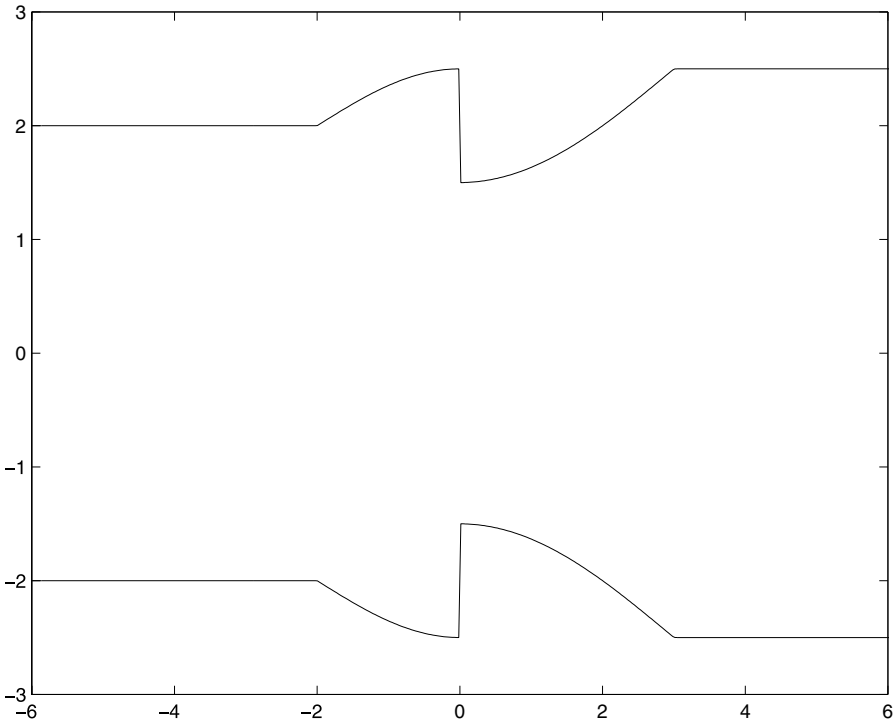

Fig. 32. Example 3.3, steady state capturing. The nozzle cross-sectional area.

This example reveals that it is frequently encountered that one may need to use different schemes to efficiently deal with different problems. Thus the ability of our slope selecting method to be applicable to more general shock capturing scheme for the homogeneous hyperbolic system makes our method more flexible in dealing with various problems.

Example 3.4. Quasi-steady problems.

In this example we test quasi-steady problems using our slope selecting scheme. We use the zeroth order extrapolation as numerical boundary condition in this example. We use HLLE scheme as the homogeneous equations solver and obtain the reference solution using our method with 2000 grid points. The cross-sectional area is chosen to be

$$a(x) = \begin{cases} 2.5 - \cos\left(\frac{\pi x}{6}\right), & 0 \leqslant x \leqslant 3, \\ 2.5, & \text{else} \end{cases}$$

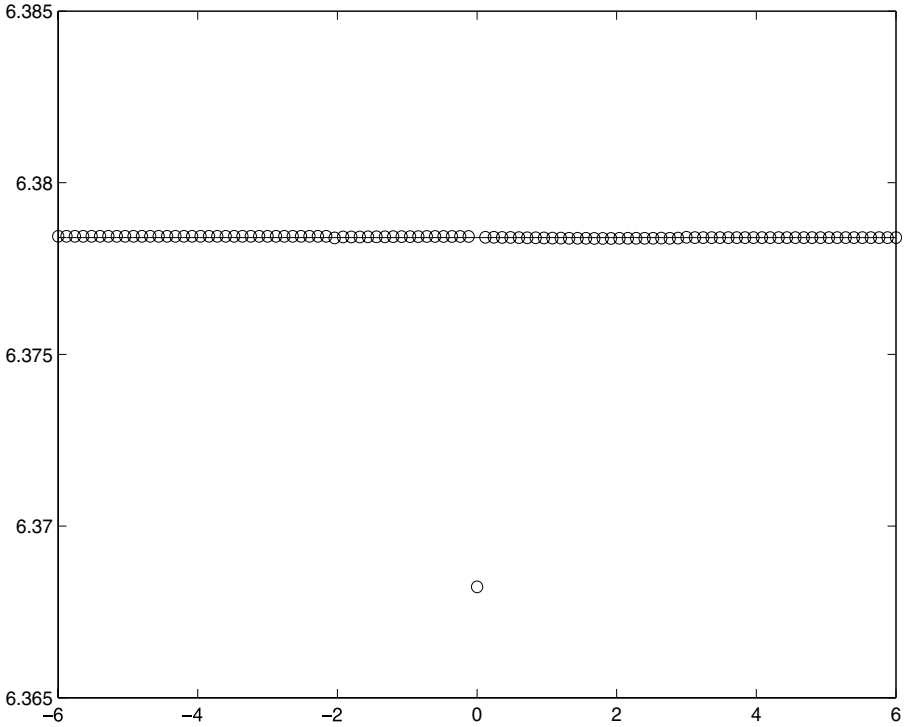

Fig. 35. Example 3.3, steady state capturing. Energy $\frac{1}{2}v^2 + k\frac{\gamma}{\gamma-1}\rho^{\gamma-1}$ at steady state; solid line: exact solution; "○" solution of the slope selecting method using 100 cells.

Table 6
l^1-Norm of errors of steady state density in different domains

Errors	$[-6,-0.2]$	$[0.2,6]$	$[-6,6]$
50 Cells	2.807471E − 4	8.256022E − 5	5.725880E − 4
100 Cells	6.246616E − 5	1.642795E − 5	2.410718E − 4
200 Cells	1.208474E − 5	4.294303E − 6	1.090404E − 4

on $-6 < x < 6$, as shown in Fig. 36.

First we test a case of the disturbance propagating in a stationary steady state. We choose the steady state solution ρ_0, v_0 on $[-6,6]$ to be $\rho_0 = 3.375, v_0 = 0$. We choose initial density value and velocity value as

$$\rho(x,0) = \begin{cases} \rho_0 + 10^{-2}, & -4 \leqslant x \leqslant -2, \\ \rho_0, & \text{else} \end{cases}$$

and $v(x,0) = v_0$. The initial density is plotted in Fig. 37. We use 100 cells and take $\frac{\Delta t}{\Delta x} = 1/2$. The propagation phenomenon of the initial disturbance is similar to that of shallow water flow. We plot our solutions of density at $t = 2.5, 4$ in Figs. 38 and 39, respectively. At $t = 2.5$, the right going disturbance begin to encounter the cross-sectional discontinuity and at $t = 4$, the initially left going disturbance leaves the domain and the two remaining visible disturbance are split from the initially right going disturbance.

We then test our scheme in predicting the propagation of disturbance in non-stationary steady state solution. The cross-sectional area is the same. We choose a subcritical steady state solution ρ_0, v_0 on $[-6,6]$ belonging to Definition 3.1 satisfying

$$a\rho_0 v_0 = -3,$$
$$\frac{1}{2}v_0^2 + k\frac{\gamma}{\gamma-1}\rho_0^{\gamma-1} = 6.$$

We choose initial density value and velocity value as

$$\rho(x,0) = \begin{cases} \rho_0 + 0.05, & -4 \leqslant x \leqslant -2, \\ \rho_0, & \text{else} \end{cases}$$

and $v(x,0) = \frac{-3}{a\rho(x,0)}$. The initial density and Mach number $\frac{v}{\sqrt{k\gamma\rho^{\gamma-1}}}$ are plotted in Figs. 40 and 41, respectively. We use 100 cells and take $\frac{\Delta t}{\Delta x} = 1/2$. We plot in Fig. 42 the solutions of density at $t = 1.5$, when the two disturbance visible is split from the initial disturbance, and plot in Fig. 43 the solutions of density at $t = 4.5$, when the two disturbance visible is split from the initially right going disturbance.

For both cases, compared with reference solutions, the solutions by our slope selecting scheme using 100 cells can efficiently preserve the steady state solution and correctly predict the positions of propagating disturbances.

4. The non-isothermal nozzle flow equations

The one-dimensional non-isothermal nozzle flow equations can be described by the following Euler equations with a geometric source term

$$\partial_t(a\rho) + \partial_x(a\rho v) = 0, \tag{4.1}$$

$$\partial_t(a\rho v) + \partial_x(a\rho v^2 + Pa) = P\partial_x a, \tag{4.2}$$

$$\partial_t(aE) + \partial_x(v(E+P)a) = 0, \tag{4.3}$$

where ρ, v, P, E are, respectively, density, velocity, pressure, and total energy, $a(x) > 0$ is area of the nozzle. For a polytropic gas, the equation of state is given by

$$P = (\gamma - 1)\left(E - \frac{1}{2}\rho v^2\right). \tag{4.4}$$

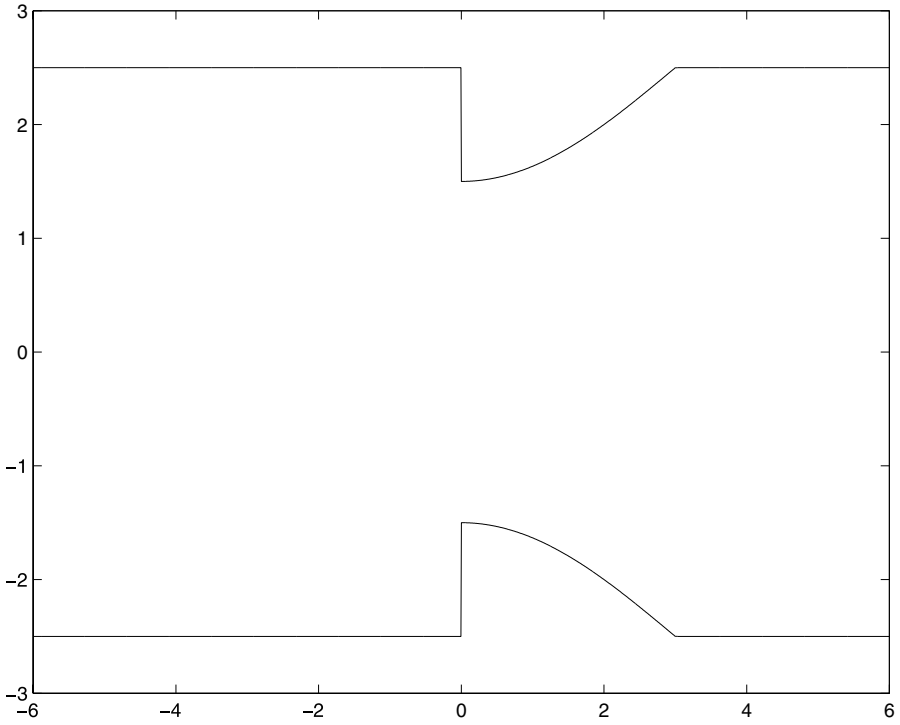

Fig. 36. Example 3.4, quasi-steady problem. The nozzle cross-sectional area.

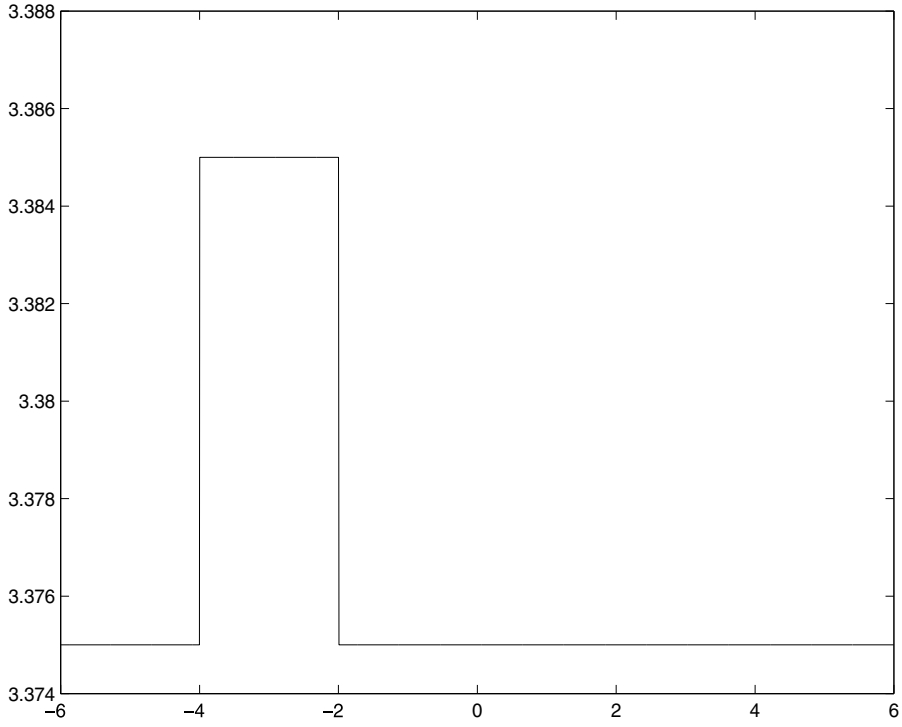

Fig. 37. Example 3.4, stationary quasi-steady problem. Density at initial time.

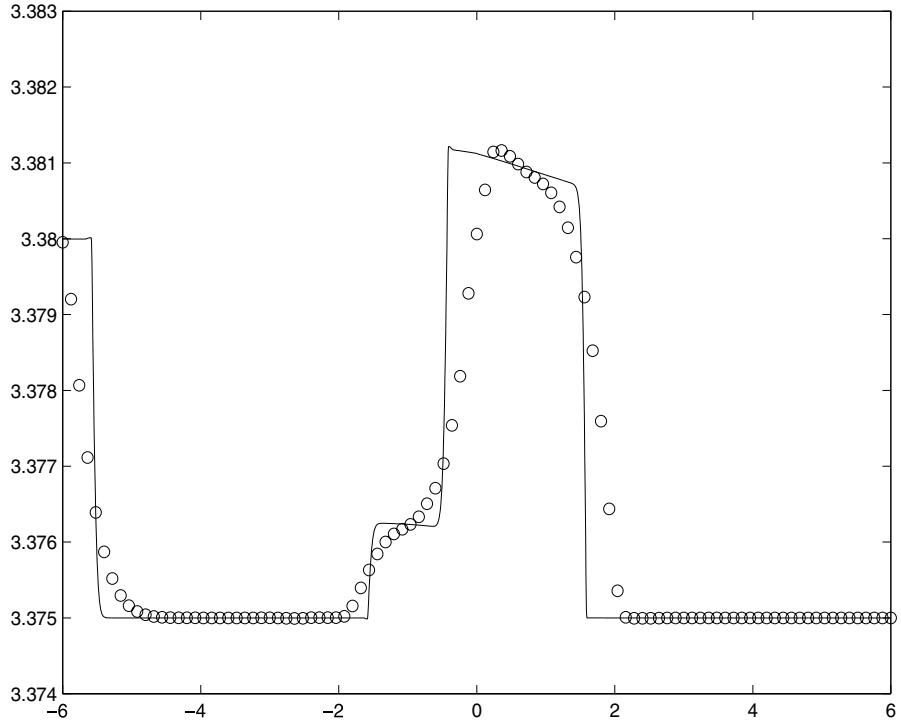

Fig. 38. Example 3.4, stationary quasi-steady problem. Density at $t = 2.5$; solid line: the reference solution; "○": the solution of the slope selecting method using 100 cells.

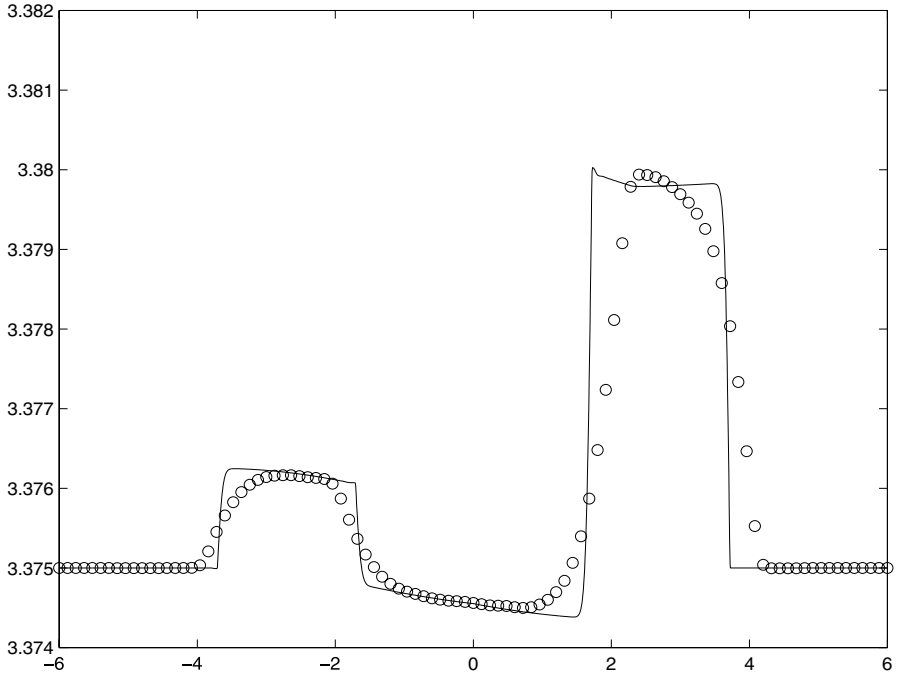

Fig. 39. Example 3.4, stationary quasi-steady problem. Density at $t = 4$; solid line: the reference solution; "○": the solution of the slope selecting method using 100 cells.

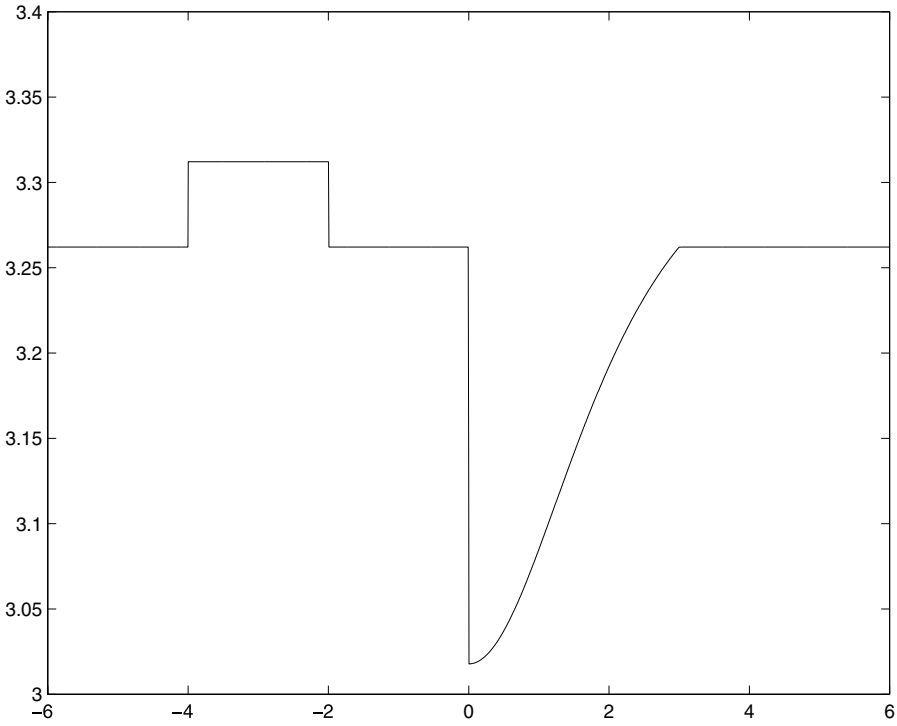

Fig. 40. Example 3.4, non-stationary quasi-steady problem. Density at initial time.

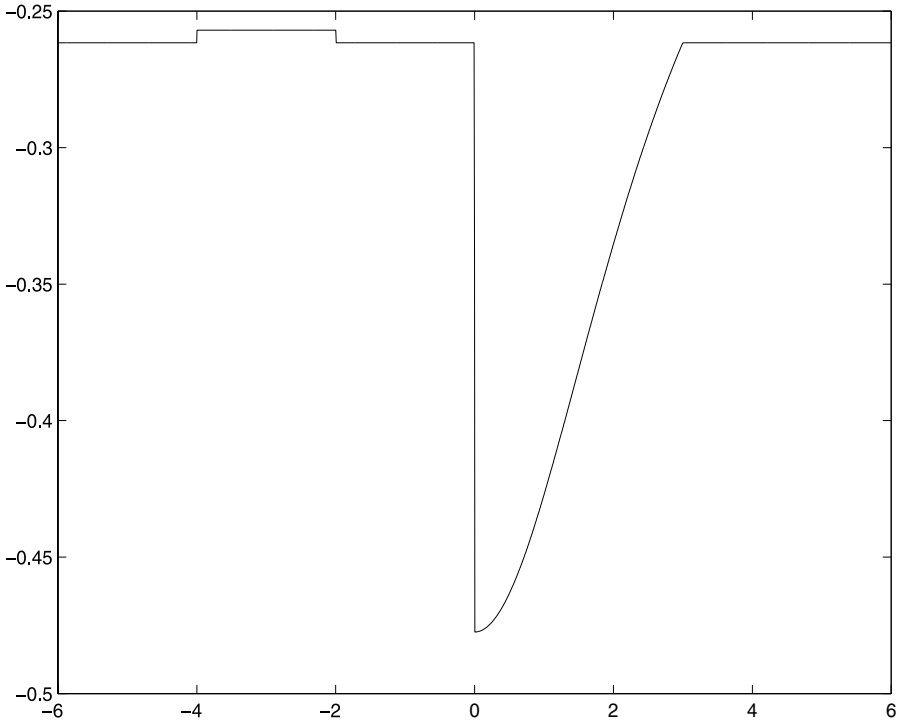

Fig. 41. Example 3.4, non-stationary quasi-steady problem. Mach number $\frac{v}{\sqrt{k_7\rho^{\gamma-1}}}$ at initial time.

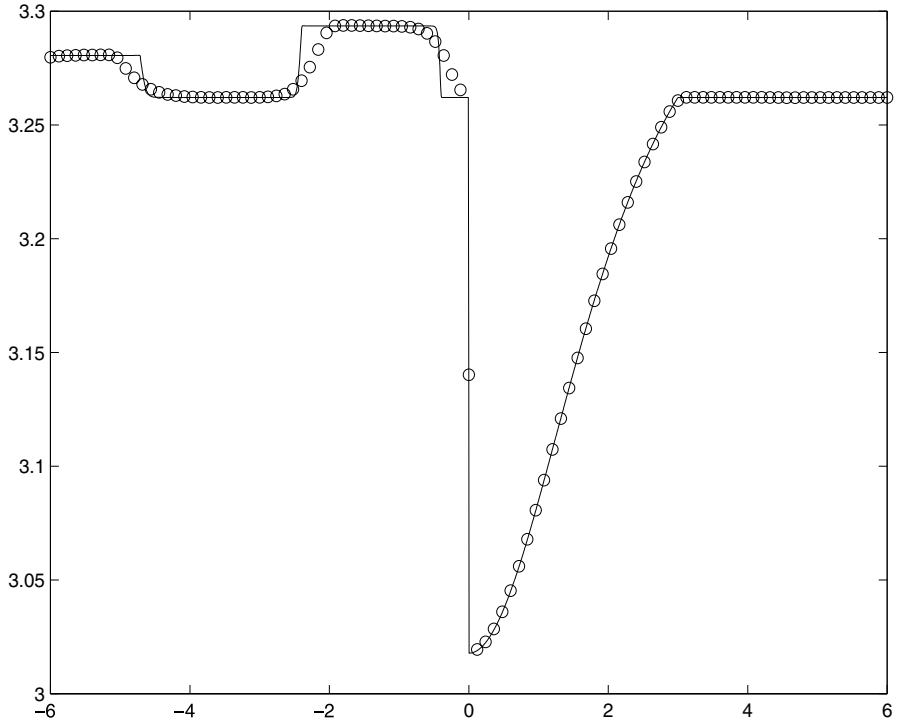

Fig. 42. Example 3.4, non-stationary quasi-steady problem. Density at $t = 1.5$; solid line: the reference solution; "○": the solution of the slope selecting method using 100 cells.

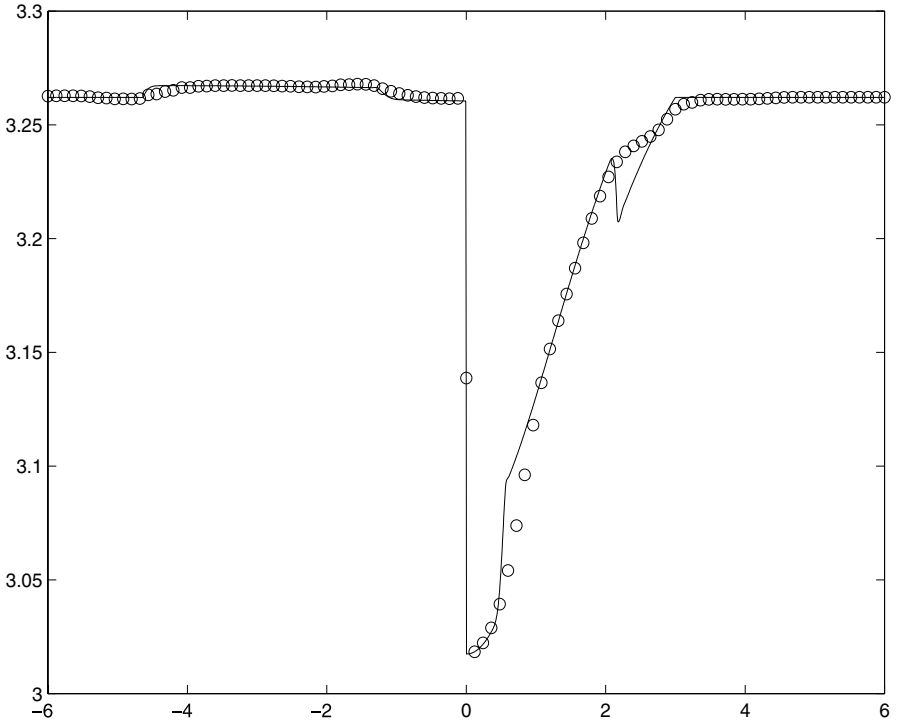

Fig. 43. Example 3.4, non-stationary quasi-steady problem. Density at $t = 4.5$; solid line: the reference solution; "○": the solution of the slope selecting method using 100 cells.

The cell average method for above non-isothermal nozzle flow equations takes the form

$$\partial_t(a\rho)_j + \frac{m_{j+\frac{1}{2}} - m_{j-\frac{1}{2}}}{\Delta x} = 0, \tag{4.5}$$

$$\partial_t(a\rho v)_j + \frac{e_{j+\frac{1}{2}} - e_{j-\frac{1}{2}}}{\Delta x} = P_j \frac{a_{j+\frac{1}{2}} - a_{j-\frac{1}{2}}}{\Delta x}, \tag{4.6}$$

$$\partial_t(aE)_j + \frac{f_{j+\frac{1}{2}} - f_{j-\frac{1}{2}}}{\Delta x} = 0, \tag{4.7}$$

where $a_{j+\frac{1}{2}} = a(x_{j+\frac{1}{2}})$ and $m_{j-\frac{1}{2}},\ m_{j+\frac{1}{2}},\ e_{j-\frac{1}{2}},\ e_{j+\frac{1}{2}},\ f_{j-\frac{1}{2}},\ f_{j+\frac{1}{2}}$ denote, respectively, numerical fluxes for conserved variables $a\rho, a\rho v$ and aE at interfaces $j-\frac{1}{2},\ j+\frac{1}{2}$ obtained by solving the homogeneous part of the non-isothermal nozzle flow equations (4.1)–(4.3), namely the Euler equations.

The stationary steady state equations are given by

$$v = 0, \tag{4.8}$$

$$P = (\gamma - 1)E = C. \tag{4.9}$$

The non-stationary steady state equations are given by

$$a\rho v = C_1, \tag{4.10}$$

$$av\left(\gamma E - \frac{\gamma - 1}{2}\rho v^2\right) = C_2, \tag{4.11}$$

$$\frac{\rho^\gamma}{E - \frac{1}{2}\rho v^2} = C_3. \tag{4.12}$$

Similar to shallow water equations and isothermal nozzle flow equations, we can define the steady state solutions for non-isothermal nozzle flow equations with discontinuous cross-sectional area associated with smooth

steady state conditions across the cross-sectional discontinuity. The definitions are given, respectively, for stationary and non-stationary case since the steady state conditions are different.

Definition 4.1. Stationary steady state solutions to non-isothermal nozzle flow equations with discontinuous cross-sectional area: for a given initial condition to non-isothermal nozzle flow equations (4.1)–(4.3) with discontinuous cross-sectional area, the solution will remain unchanged, i.e. the initial condition is the steady state solution for non-isothermal nozzle flow equations with discontinuous cross-sectional area, if the initial condition satisfies (4.8) and (4.9) anywhere including across the cross-sectional discontinuity.

Definition 4.2. Non-stationary steady state solutions to non-isothermal nozzle flow equations with discontinuous cross-sectional area: for a given initial condition to non-isothermal nozzle flow equations (4.1)–(4.3) with discontinuous cross-sectional area, the solution will remain unchanged, i.e. the initial condition is the steady state solution for non-isothermal nozzle flow equations with discontinuous cross-sectional area, if the initial condition is non-stationary steady state solution i.e. velocity and density are non-zero in the solution on continuous cross-sectional part, and across the cross-sectional discontinuity the conditions (4.10)–(4.12) hold, namely

$$a_l\rho_l v_l = a_r\rho_r v_r, \tag{4.13}$$

$$a_l v_l\left(\gamma E_l - \frac{\gamma-1}{2}\rho_l (v_l)^2\right) = a_r v_r\left(\gamma E_r - \frac{\gamma-1}{2}\rho_r (v_r)^2\right), \tag{4.14}$$

$$\frac{\rho_l^\gamma}{E_l - \frac{1}{2}\rho_l (v_l)^2} = \frac{\rho_r^\gamma}{E_r - \frac{1}{2}\rho_r (v_r)^2}, \tag{4.15}$$

where ρ_l, v_l, E_l, a_l and ρ_r, v_r, E_r, a_r are the density, velocity, total energy in the initial condition and the cross-sectional area at two sides of the cross-sectional discontinuity, and one of the following situations occurs

$$\text{(i)} \quad \frac{|v_l|}{\sqrt{\gamma P_l/\rho_l}} < 1, \quad \frac{|v_r|}{\sqrt{\gamma P_r/\rho_r}} < 1, \tag{4.16}$$

$$\text{(ii)} \quad \frac{|v_l|}{\sqrt{\gamma P_l/\rho_l}} > 1, \quad \frac{|v_r|}{\sqrt{\gamma P_r/\rho_r}} > 1, \tag{4.17}$$

$$\text{(iii)} \quad \begin{cases} \frac{|v_l|}{\sqrt{\gamma P_l/\rho_l}} = 1 & \text{if } a_l < a_r, \\ \frac{|v_r|}{\sqrt{\gamma P_r/\rho_r}} = 1 & \text{if } a_l > a_r, \end{cases} \tag{4.18}$$

where P_l, P_r are pressure in the initial condition at two sides of the cross-sectional discontinuity which are $P_l = (\gamma-1)(E_l - \frac{1}{2}\rho_l v_l^2)$, $P_r = (\gamma-1)(E_r - \frac{1}{2}\rho_r v_r^2)$.

4.1. Energy gradient method (EGM)

When the cross-sectional area is continuously variable, similar to dealing with isothermal nozzle flow equations or shallow water equations, one can obtain a steady state preserving method by adding a data reconstruction procedure into the cell average method. Since in stationary steady state, the pressure as well as the total energy are constant, so we can use a data reconstruction procedure based on total energy as follows.

(1) In the step of defining the slopes of conserved variables $a\rho, a\rho v, aE$ in each cell. Instead of defining the slope of aE, define the slope (denoted by S_k^2) for the total energy E

$$S_k^2 = G(E_{k-1}, E_k, E_{k+1}),$$

where G is a standard slope limiter [29]. The slopes of $a\rho$, $a\rho v$ are still defined.

(2) The values of aE on the left and right of the cell interface $x_{k+\frac{1}{2}}$ are

$$(aE)^L_{k+\frac{1}{2}} = a_{k+\frac{1}{2}}\left(E_k + \frac{1}{2}\Delta x S_k^2\right), \quad (aE)^R_{k+\frac{1}{2}} = a_{k+\frac{1}{2}}\left(E_{k+1} - \frac{1}{2}\Delta x S_{k+1}^2\right).$$

The left and right values of $a\rho, a\rho v$ are obtained by their cell average values and slopes. These left and right values of conserved variables at interface $x_{k+\frac{1}{2}}$ are used by a homogeneous non-isothermal nozzle flow equations solver to get the numerical fluxes $m_{k+\frac{1}{2}}$, $e_{k+\frac{1}{2}}$, $f_{k+\frac{1}{2}}$.

(3) Once the numerical fluxes for conserved variables are obtained, one can use the cell average formula (4.5)–(4.7) as the numerical scheme.

Since this method uses the gradient of total energy instead of that of the conserved variable aE in constructing the two sides values at the interface, we name this method as the *energy gradient method* (EGM). Similar to proving Z-property of SGM, one can prove that EGM can exactly preserve the *stationary* flow for non-isothermal nozzle flow equations with a continuously variable cross-sectional area (Z-property) provided the homogeneous system (Euler equations) solver used by the EGM holds the following property.

Definition 4.3. Property: a Euler equations conservative scheme exactly preserves the stationary steady state flow. Namely, when the conserved variables values at two sides of an interface for the Euler equations are given by

$$\rho^{\mathrm{L}}_{j+\frac{1}{2}} = \rho_{\mathrm{L}}, \quad (\rho v)^{\mathrm{L}}_{j+\frac{1}{2}} = 0, \quad E^{\mathrm{L}}_{j+\frac{1}{2}} = \widetilde{E},$$
$$\rho^{\mathrm{R}}_{j+\frac{1}{2}} = \rho_{\mathrm{R}}, \quad (\rho v)^{\mathrm{R}}_{j+\frac{1}{2}} = 0, \quad E^{\mathrm{R}}_{j+\frac{1}{2}} = \widetilde{E},$$

where $\rho_{\mathrm{L}}, \rho_{\mathrm{R}}$ may not be equal, the scheme can give the exact numerical flux at the interface $(0, (\gamma-1)\widetilde{E}, 0)$.

This is a reasonable requirement since Euler equations is got from the non-isothermal nozzle flow equations with the cross-sectional area being a constant. So property in Definition 4.3 is the simplest case of Z-property for non-isothermal nozzle flow equations when the cross-sectional area is a constant.

4.2. The slope selecting method

In the slope selecting method, we start from EGM and add in slope selecting strategy and interface type source term approximation near or in the cell containing the cross-sectional discontinuity. Assume a discontinuity of cross-sectional area is contained in the center of a cell $[x_{j-\frac{1}{2}}, x_{j+\frac{1}{2}}]$. Let a_i be the interface values of a at x_i, $i = j-\frac{1}{2}$, $j+\frac{1}{2}$. We define the quantities at interfaces $j-\frac{1}{2}$, $j+\frac{1}{2}$

$$(a\rho)^*_{j-\frac{1}{2}} = \frac{2(a\rho)_j(a\rho)_{j-1}}{(a\rho)_{j+1}+(a\rho)_{j-1}}, \quad (a\rho)^*_{j+\frac{1}{2}} = \frac{2(a\rho)_j(a\rho)_{j+1}}{(a\rho)_{j+1}+(a\rho)_{j-1}}, \tag{4.19}$$

$$(aE)^*_{j-\frac{1}{2}} = \frac{2(aE)_j(aE)_{j-1}}{(aE)_{j+1}+(aE)_{j-1}}, \quad (aE)^*_{j+\frac{1}{2}} = \frac{2(aE)_j(aE)_{j+1}}{(aE)_{j+1}+(aE)_{j-1}}, \tag{4.20}$$

$$\rho^*_{j\pm\frac{1}{2}} = (a\rho)^*_{j\pm\frac{1}{2}}/a_{j\pm\frac{1}{2}}, \quad E^*_{j\pm\frac{1}{2}} = (aE)^*_{j\pm\frac{1}{2}}/a_{j\pm\frac{1}{2}}. \tag{4.21}$$

We set the slopes for $a\rho$ in cells $j-1, j, j+1$ as

$$S^1_j = \frac{(a\rho)^*_{j+\frac{1}{2}} - (a\rho)^*_{j-\frac{1}{2}}}{\Delta x}, \tag{4.22}$$

$$S^1_{j-1} = \frac{\mathrm{sign}\{(a\rho)_{j-1}-(a\rho)_{j-2}\} + \mathrm{sign}\{(a\rho)^*_{j-\frac{1}{2}} - (a\rho)_{j-1}\}}{2\Delta x} \min\{|(a\rho)_{j-1}-(a\rho)_{j-2}|, |(a\rho)^*_{j-\frac{1}{2}} - (a\rho)_{j-1}|\}, \tag{4.23}$$

$$S^1_{j+1} = \frac{\mathrm{sign}\{(a\rho)_{j+2}-(a\rho)_{j+1}\} + \mathrm{sign}\{(a\rho)_{j+1} - (a\rho)^*_{j+\frac{1}{2}}\}}{2\Delta x} \min\{|(a\rho)_{j+2}-(a\rho)_{j+1}|, |(a\rho)_{j+1} - (a\rho)^*_{j+\frac{1}{2}}|\}. \tag{4.24}$$

We set the slope for aE in cell j as

$$\frac{(aE)^*_{j+\frac{1}{2}} - (aE)^*_{j-\frac{1}{2}}}{\Delta x}. \tag{4.25}$$

We set the slopes for E in cells $j-1, j+1$ as

$$S^2_{j-1} = \frac{\operatorname{sign}\{E_{j-1}-E_{j-2}\}+\operatorname{sign}\{E^*_{j-\frac{1}{2}}-E_{j-1}\}}{2\Delta x}\min\{|E_{j-1}-E_{j-2}|,|E^*_{j-\frac{1}{2}}-E_{j-1}|\}, \tag{4.26}$$

$$S^2_{j+1} = \frac{\operatorname{sign}\{E_{j+2}-E_{j+1}\}+\operatorname{sign}\{E_{j+1}-E^*_{j+\frac{1}{2}}\}}{2\Delta x}\min\left\{|E_{j+2}-E_{j+1}|,|E_{j+1}-E^*_{j+\frac{1}{2}}|\right\}. \tag{4.27}$$

The values of aE on the left and right of the cell interfaces $x_{j\pm\frac{1}{2}}$ are

$$(aE)^{\mathrm{L}}_{j-\frac{1}{2}} = a_{j-\frac{1}{2}}\left(E_{j-1}+\frac{1}{2}\Delta x S^2_{j-1}\right),\quad (aE)^{\mathrm{R}}_{j-\frac{1}{2}} = (aE)^*_{j-\frac{1}{2}},$$

$$(aE)^{\mathrm{L}}_{j+\frac{1}{2}} = (aE)^*_{j+\frac{1}{2}},\quad (aE)^{\mathrm{R}}_{j+\frac{1}{2}} = a_{j+\frac{1}{2}}\left(E_{j+1}-\frac{1}{2}\Delta x S^2_{j+1}\right)$$

with $(aE)^*_{j\pm\frac{1}{2}}$, $S^2_{j\pm1}$ defined in (4.20), (4.26) and (4.27).

The left and right values of $a\rho, a\rho v$ are still obtained by their cell average values and slopes. These left and right values of conserved variables at interfaces $x_{j\pm\frac{1}{2}}$ are used by a homogeneous non-isothermal nozzle flow equations conservative scheme to get the numerical fluxes $m_{j\pm\frac{1}{2}}$, $e_{j\pm\frac{1}{2}}$, $f_{j\pm\frac{1}{2}}$.

From the above obtained quantities, define

$$v^*_{j\pm\frac{1}{2}} = \frac{m_{j\pm\frac{1}{2}}}{(a\rho)^*_{j\pm\frac{1}{2}}},\quad P^*_{j\pm\frac{1}{2}} = (\gamma-1)\left(E^*_{j\pm\frac{1}{2}}-\frac{1}{2}\rho^*_{j\pm\frac{1}{2}}(v^*_{j\pm\frac{1}{2}})^2\right). \tag{4.28}$$

If $v^*_{j-\frac{1}{2}} = v^*_{j+\frac{1}{2}} = 0$, this is the stationary case. We use the following expression

$$\frac{P^*_{j-\frac{1}{2}}+P^*_{j+\frac{1}{2}}}{2}\frac{a_{j+\frac{1}{2}}-a_{j-\frac{1}{2}}}{\Delta x} \tag{4.29}$$

to replace the source term approximation in cell average method (4.6). This is the interface scheme introduced in [21].

In other non-stationary cases, as in [23], denote $H_i = a_i\rho^*_i v^*_i$, $G_i = a_i v^*_i(\gamma E^*_i - \frac{\gamma-1}{2}\rho^*_i(v^*_i)^2)$, $F_i = \frac{(\rho^*_i)^\gamma}{E^*_i-\frac{1}{2}\rho^*_i(v^*_i)^2}$, $i = j\pm\frac{1}{2}$. We choose $\hat{a}, H, G, F$ to be linear functions on $[x_{j-\frac{1}{2}}, x_{j+\frac{1}{2}}]$ with

$$\hat{a}(x_i) = a_i,\quad H(x_i) = H_i,\quad G(x_i) = G_i,\quad F(x_i) = F_i,\quad i = j\pm\frac{1}{2}. \tag{4.30}$$

We choose smooth $\hat{\rho}$, $\hat{v}$, $\widehat{E}$ on $[x_{j-\frac{1}{2}}, x_{j+\frac{1}{2}}]$ satisfying

$$\hat{a}\hat{\rho}\hat{v} = H, \tag{4.31}$$

$$\hat{a}\hat{v}\left(\gamma\widehat{E}-\frac{\gamma-1}{2}\hat{\rho}\hat{v}^2\right) = G, \tag{4.32}$$

$$\frac{\hat{\rho}^\gamma}{\widehat{E}-\frac{1}{2}\hat{\rho}\hat{v}^2} = F \tag{4.33}$$

with endpoint values

$$\hat{\rho}(x_i) = \rho^*_i,\quad \hat{v}(x_i) = v^*_i,\quad \widehat{E}(x_i) = E^*_i,\quad i = j\pm\frac{1}{2}. \tag{4.34}$$

Define $\widehat{P}$ by

$$\widehat{P} = (\gamma-1)\left(\widehat{E}-\frac{1}{2}\hat{\rho}\hat{v}^2\right). \tag{4.35}$$

We then use the following expression

$$\left(\frac{1}{\Delta x}\int_{x_{j-\frac{1}{2}}}^{x_{j+\frac{1}{2}}}\widehat{P}\,\mathrm{d}x\right)\frac{a_{j+\frac{1}{2}}-a_{j-\frac{1}{2}}}{\Delta x} \tag{4.36}$$

to replace the source term approximation in cell average method (4.6) to define our scheme. The numerical integration strategy is similar as mentioned for shallow water equations and isothermal nozzle flow equations.

The values of $\hat{\rho}$, $\hat{v}$, $\widehat{E}$ are chosen from (4.31)–(4.33) according to the sub- or super-sonic states of the solution. When the flow is transonic over the cross-sectional discontinuity, we should do the fix operation to help choosing these values from (4.31)–(4.33). This is essentially the same as the isothermal nozzle flow equations.

We use the scheme of EGM in all the other cells do not containing a cross-sectional discontinuity with the mention that the slopes of energy and $a\rho$ in the cell adjacent to a cross-sectional discontinuity is modified by our slope selecting strategy.

Similar to the conclusions for the shallow water equations and isothermal nozzle flow equations, one can prove that our slope selecting method for non-isothermal nozzle flow equations preserves exactly the stationary steady state solutions belonging to Definition 4.1 provided the homogeneous system solver satisfies Definition 4.3, and *formally* exactly preserves the non-stationary steady state solutions belonging to Definition 4.2 in which no stationary shock exists when cross-sectional area is a step function (*S*-property). The proof is given in Appendix D.

4.3. Numerical examples

We now give two numerical examples. The first example illustrates that our method works well for calculating both unsteady and steady state solution for the non-isothermal nozzle flow equations. The second example is a quasi-steady problem.

Example 4.1. Steady and unsteady state calculation.

This is a problem modified from [11] and has been tested by our method in [23]. The steady state solution for this problem contains a transonic shock. Consider a discontinuous nozzle

$$a(x) = \begin{cases} 1.05, & 0 \leqslant x \leqslant 2, \\ 1.4452 + 0.3\tanh(0.8x - 4), & 2 < x \leqslant 10 \end{cases}$$

shown in Fig. 44. The computational domain is $0 \leqslant x \leqslant 10$. The left boundary conditions are $(\rho_l, v_l, E_l) = (0.502, 1.299, 1.378)$, the right boundary conditions are $\rho_r = 0.776$. We choose the initial values

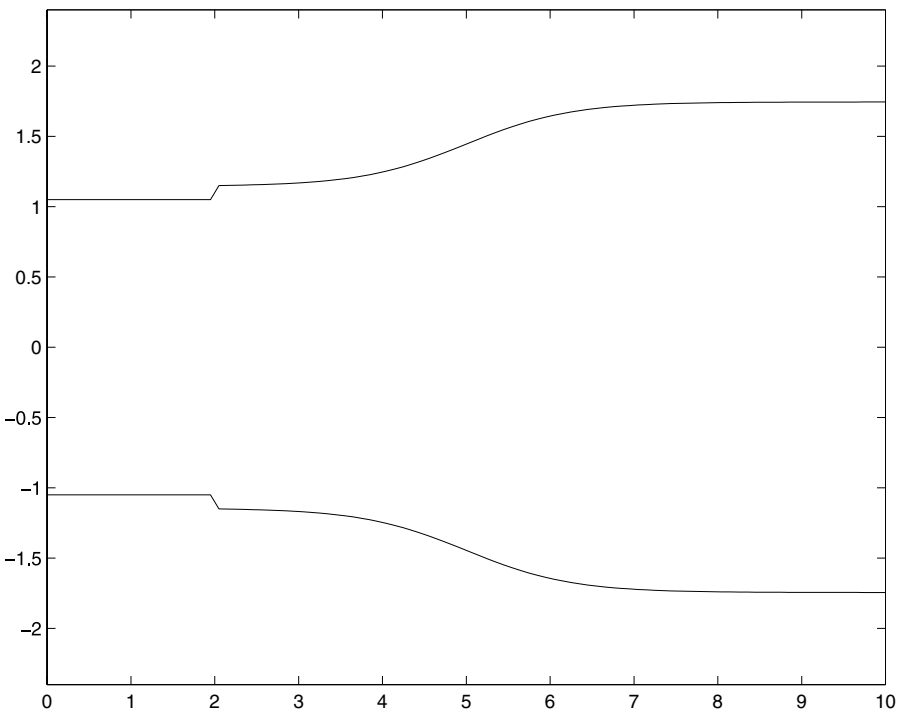

Fig. 44. Example 4.1, steady and unsteady calculation. A nozzle with discontinuous cross-sectional area.

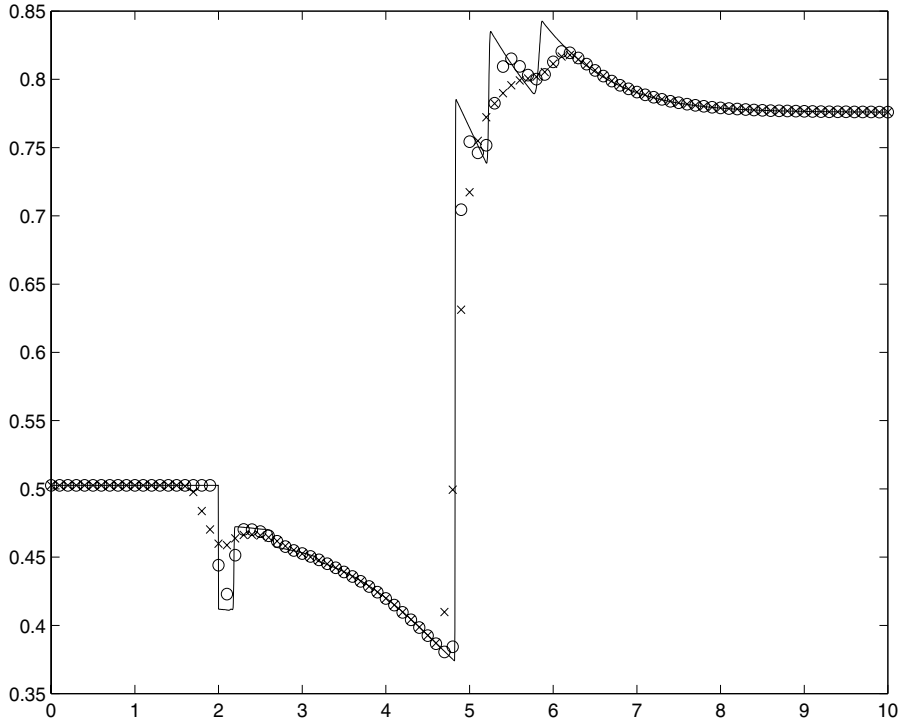

Fig. 45. Example 4.1, steady and unsteady calculation. Density at $t = 0.5$; solid line: the reference solution; "○": the solution of Roe solver using 100 cells; "×": the solution of relaxation scheme using 100 cells.

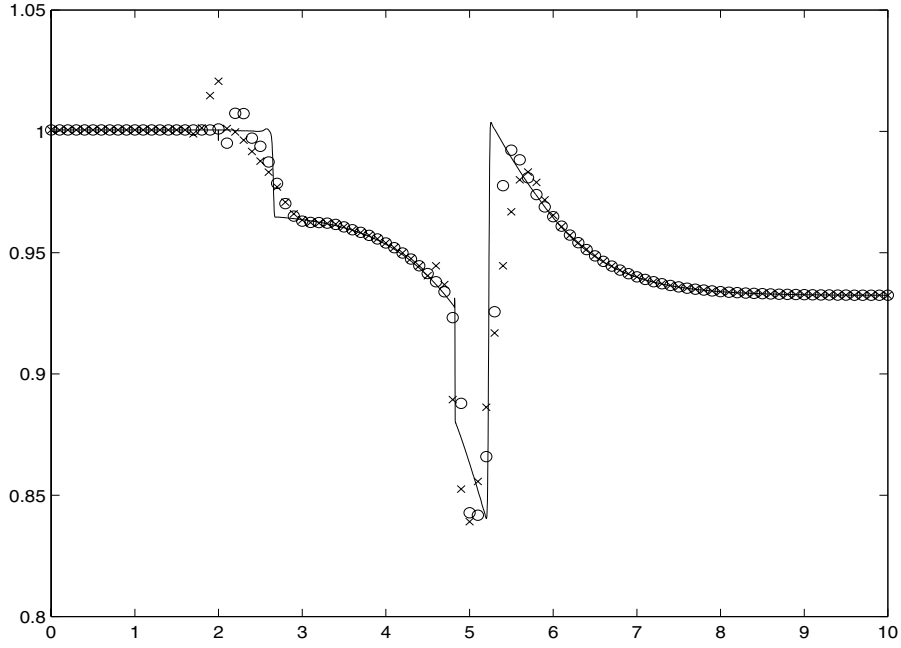

Fig. 46. Example 4.1, steady and unsteady calculation. Solutions of $\frac{\rho^\gamma}{P}$ at $t = 0.5$; solid line: the reference solution; "○": the solution of Roe solver using 100 cells; "×": the solution of relaxation scheme using 100 cells.

as $a(\rho, \rho v, E) = (0.528, 0.686, 1.447)$ when $x < 5$ and $a(\rho, \rho v, E) = (1.354, 0.686, 3.454)$ when $x > 5$. We take $\frac{\Delta t}{\Delta x} = 1/4$, use the Roe solver and relaxation scheme for the convection and the second order TVD Runge–Kutta time discretization [35]. The constant $\widehat{C}$ in subcharacteristic condition in relaxation scheme is chosen to be 10.

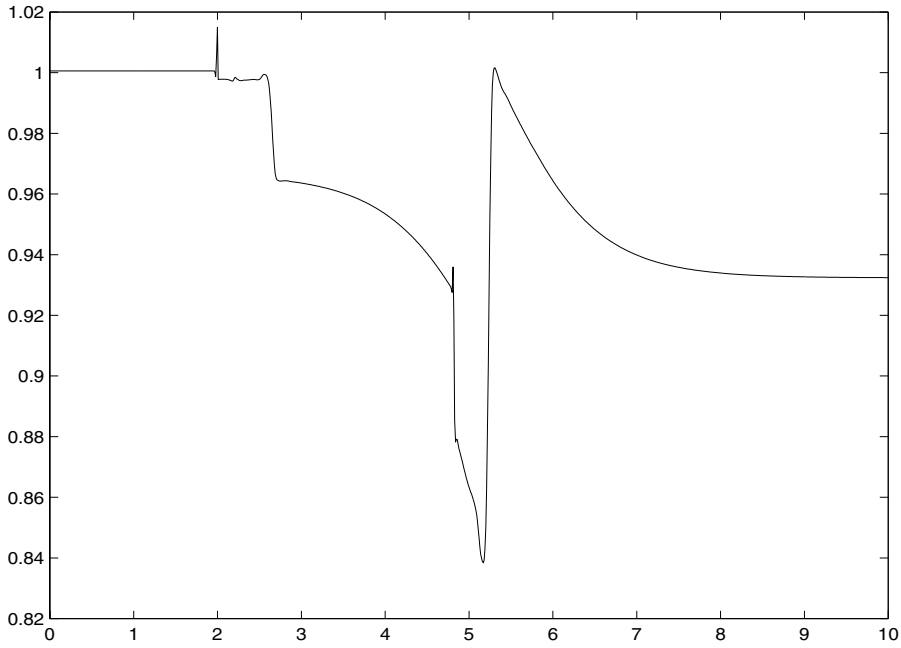

Fig. 47. Example 4.1, steady and unsteady calculation. Solutions of $\frac{\rho^{\gamma}}{P}$ at $t = 0.5$ from relaxation cell average method using 1000 cells.

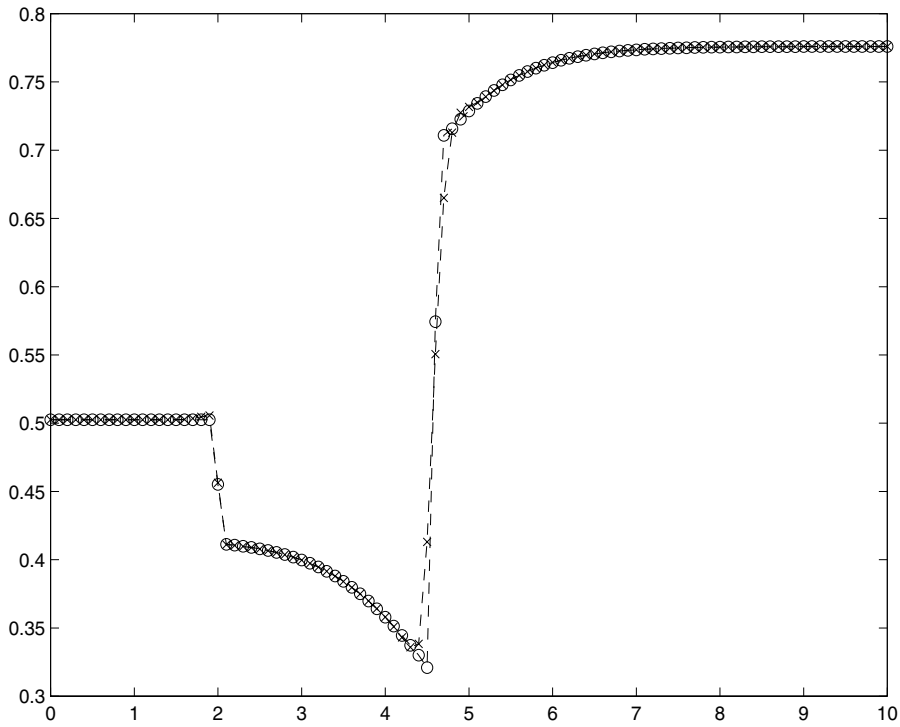

Fig. 48. Example 4.1, steady and unsteady calculation. Density in steady state; "○": solution of Roe solver using 100 cells; "×": solution of relaxation scheme using 100 cells.

The density and the quantity $\frac{\rho^{\gamma}}{P}$ at $t = 0.5$ from our slope selecting method based on Roe solver and relaxation scheme using 100 cells and that based on relaxation scheme using 4000 cells, which are used to be the reference solution, are plotted in Figs. 45 and 46, respectively. The reference solution matches with that given

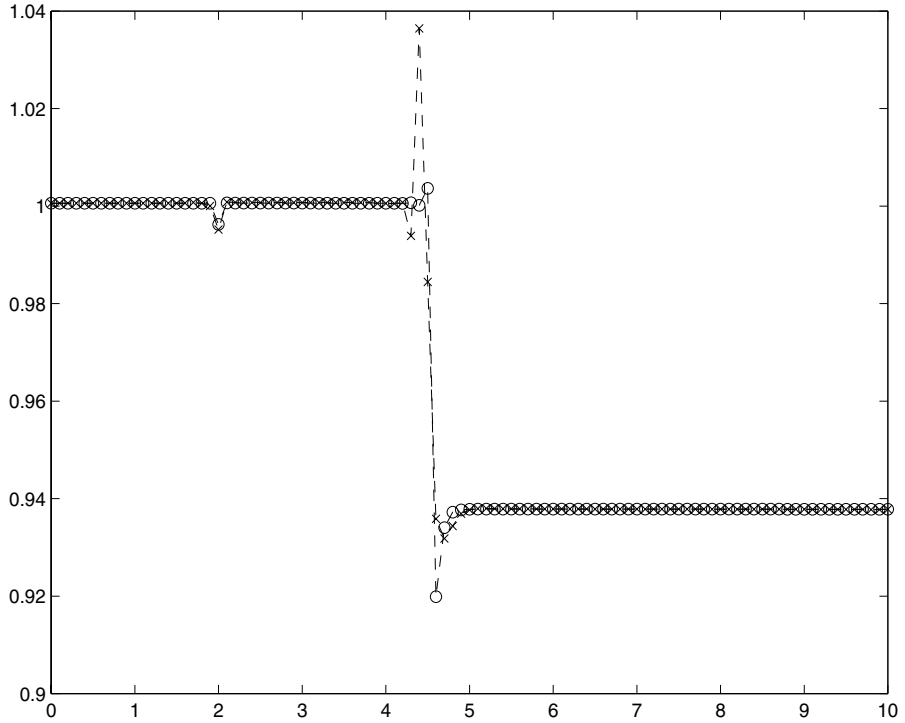

Fig. 49. Example 4.1, steady and unsteady calculation. Solutions of $\frac{\rho^\gamma}{P}$ at steady state; "○": solution of Roe solver using 100 cells; "×": solution of relaxation scheme using 100 cells.

by our method in [23]. The solution already reaches steady state across the cross-sectional discontinuity with $\frac{\rho^\gamma}{P}$ being the same constant at two sides at $t = 0.5$. We also plot the quantity $\frac{\rho^\gamma}{P}$ at $t = 0.5$ from *relaxation cell average method* using 1000 cells in Fig. 47. The result in Fig. 47 do not reaches the same constant at two sides of cross-sectional discontinuity and this gap do not decrease when more space points are used. Thus the relaxation cell average method cannot capture the energy conservation solution across the cross-sectional discontinuity. This exhibit the conventional cell average method fails in steady state capturing for this example.

Figs. 48 and 49 plot, respectively, the density and the quantity $\frac{\rho^\gamma}{P}$ in the steady state solution from our method based on Roe solver and relaxation scheme using 100 cells. These results match with that of our method in [23]. It can be seen that the steady state expression $\frac{\rho^\gamma}{P}$ reach the same constant at two sides of the cross-sectional discontinuity and a transonic shock stands in the steady state solution.

Example 4.2. A quasi-steady calculation.

We calculate in this example the disturbance propagation in a stationary steady state solution of non-isothermal nozzle flow equations using our slope selecting method. We use the zeroth order extrapolation as numerical boundary condition. We use Roe scheme to solve the homogeneous part of non-isothermal nozzle flow equations, namely Euler equations and obtain the reference solution by our method using 1000 grid points. The cross-sectional area is chosen to be

$$a(x) = \begin{cases} 1, & x < -2 \\ 0.6 + 0.1\cos\left(\frac{\pi x}{8} + 1\right), & -2 < x < 2, \\ 1, & x > 2 \end{cases}$$

on $-5 < x < 5$, as shown in Fig. 50.

We choose the steady state solution ρ_0, v_0, E_0 on $[-5, 5]$ to be $\rho_0 = 1, v_0 = 0, E_0 = 3$, choose initial density value, velocity value and total energy value as

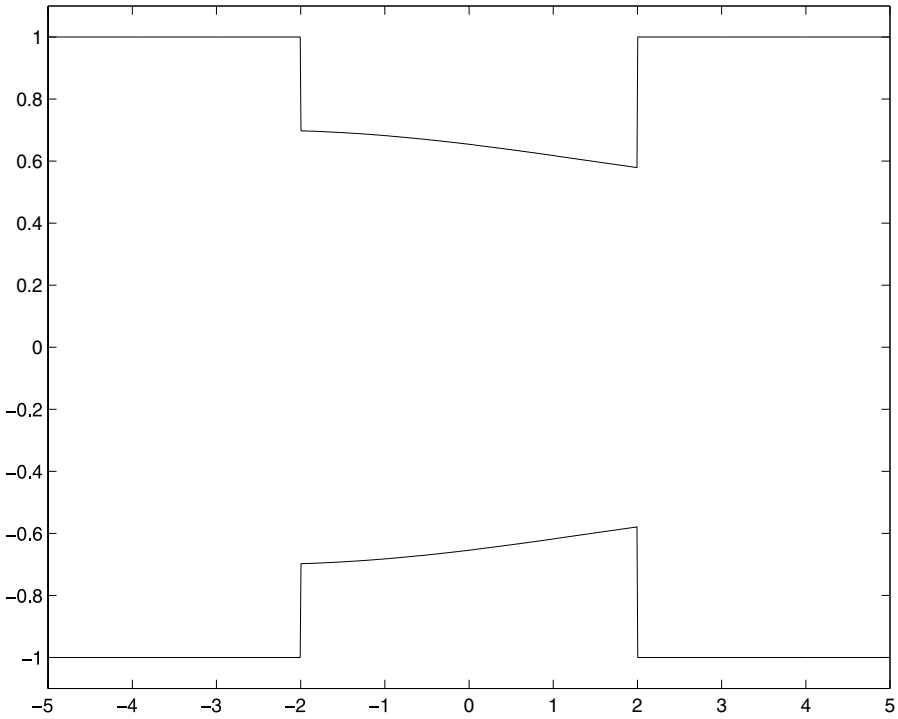

Fig. 50. Example 4.2, quasi-steady calculation. Nozzle cross-sectional area.

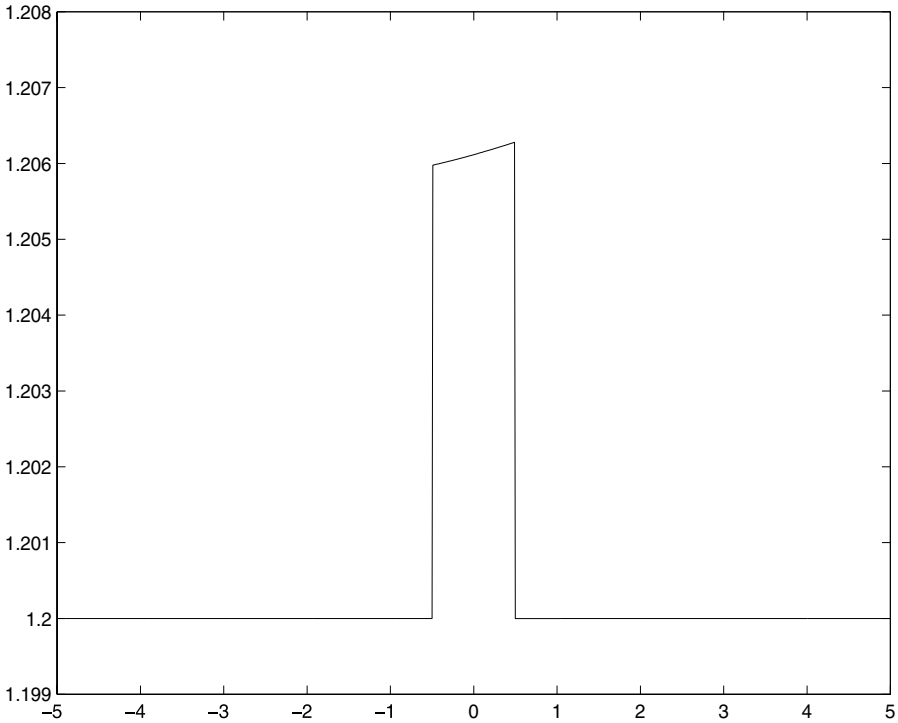

Fig. 51. Example 4.2, quasi-steady calculation. Pressure at initial time.

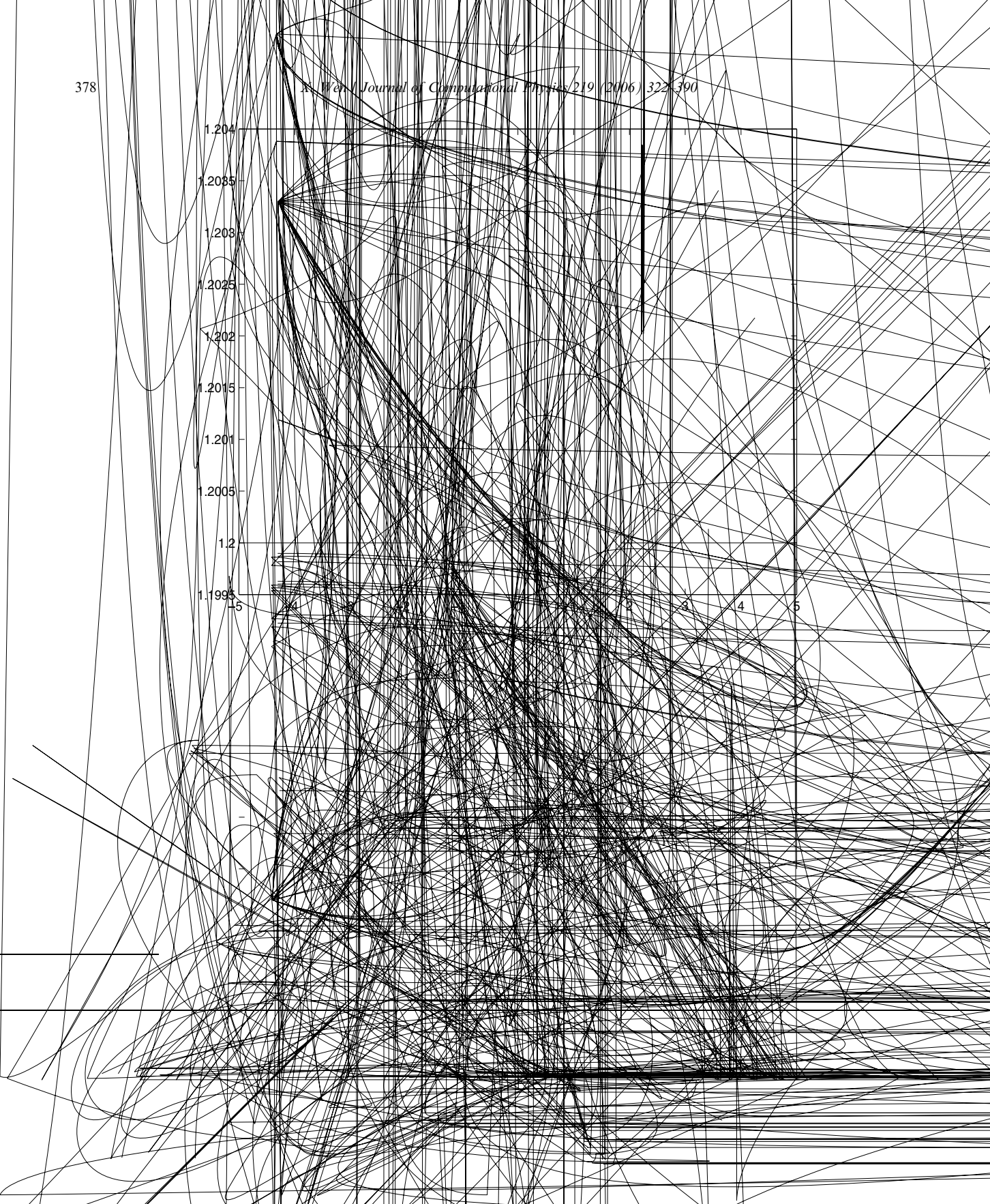

Fig. 53. Example 4.2, quasi-steady calculation. Pressure at $t = 1.8$; solid line: the reference solution; "○": solution of the slope selecting method using 200 cells

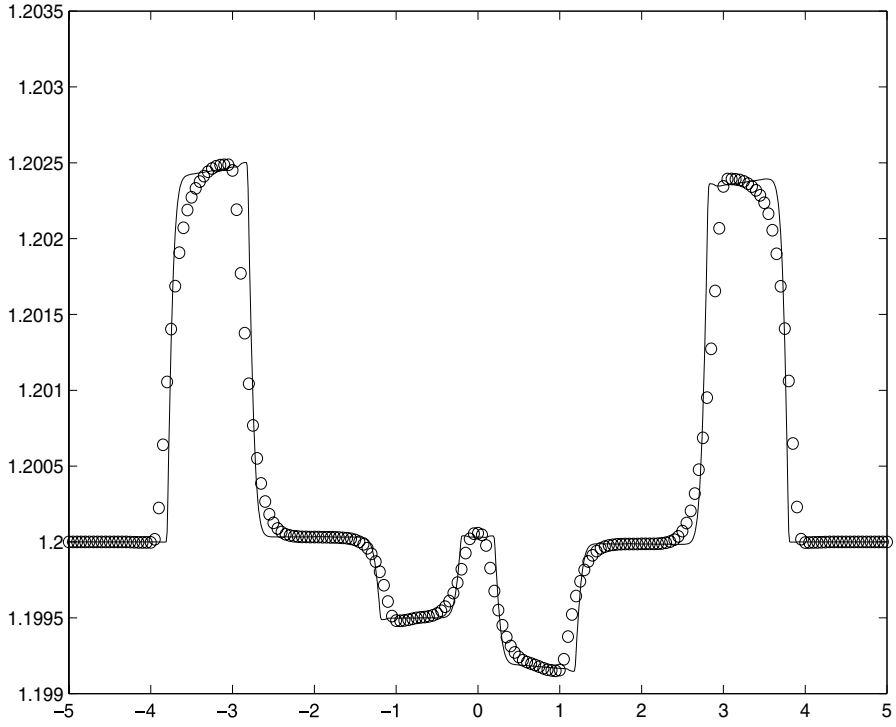

Fig. 54. Example 4.2, quasi-steady calculation. Pressure at $t = 2.5$; solid line: the reference solution; "○": solution of the slope selecting method using 200 cells.

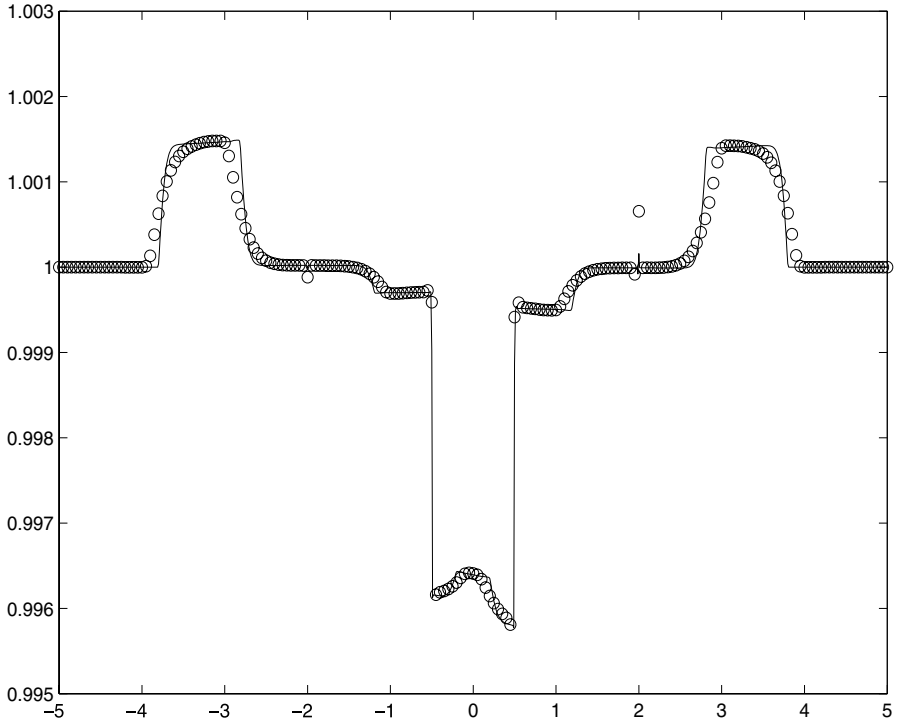

Fig. 55. Example 4.2, quasi-steady calculation. Density at $t = 2.5$; solid line: the reference solution; "○": solution of the slope selecting method using 200 cells.

$$E(x,0)=\begin{cases} E_0+10^{-2}, & -\frac{1}{2}\leqslant x\leqslant\frac{1}{2},\\ E_0, & \text{else}\end{cases}$$

and $\rho(x,0)=\rho_0, v(x,0)=v_0$. We use 200 cells and take $\frac{\Delta t}{\Delta x}=1/2$. The initial pressure is plotted in Fig. 51. Figs. 52–55 show, respectively, solutions of pressure at $t=1$, 1.8, 2.5 and density at $t=2.5$. The initial disturbance in the pressure splits into two and propagate in different direction, as shown in Fig. 52. When the initially split disturbances encounter the cross-sectional discontinuities, each further splits into two disturbances, as shown in Fig. 53. Among these disturbances, two smaller ones move back to the central part of the domain, another two larger ones continue moving outwards, as shown in Fig. 54. Fig. 55 shows the density at the same time. In these results, compared with reference solutions, the solutions by our slope selecting scheme using 200 cells can efficiently preserve the steady state solution and correctly predict the positions of propagating disturbances.

5. Conclusions

A simple well-balanced method named *the slope selecting method* is proposed for hyperbolic system with geometrical source terms having concentrations. We use two physical problems, the shallow water equations with discontinuous topography, and the quasi-one-dimensional nozzle flows with discontinuous cross-sectional area, to illustrate our method. This method is extended from the interface type method developed in [23]. Two improvements of the this method from the previous method are that this method is efficient in steady state preserving and can be designed based on any conservative scheme for the homogeneous hyperbolic system. Furthermore, the efficiency in steady state capturing of the previous method is inherited in this method. Similar to the previous method, this slope selecting method solves well the sub- or super-critical flows, and with a transonic fix, also handles well the transonic flows over the concentration. In summary, the slope selecting method is efficient in both steady state capturing and preserving, and can be easily applied to different hyperbolic system with geometrical source terms having concentrations with the knowledge of any conservative scheme for the homogeneous system.

The design principle of the slope selecting method is to start from a scheme which is efficient in steady state preserving when the source terms for the hyperbolic system do not have concentration, and then incorporate into this scheme a slope selecting strategy and the interface type source term approximation developed in [23] near or in the cell containing the source term concentration. For shallow water equations, we choose the surface gradient method (SGM) [40] as the basis of our method which is efficient in steady state preserving when the bottom is continuously variable. For nozzle flow equations, in the same principle of SGM, we design the density gradient method (DGM) for isothermal nozzle flow equations and the energy gradient method (EGM) for non-isothermal nozzle flow equations which are efficient steady state preserving schemes when the cross-sectional area is continuously variable. We base on DGM or EGM to design the slope selecting method for nozzle flow equations with discontinuous cross-sectional area.

Extensive numerical experiments demonstrate that the slope selecting method, being widely applicable to conservative schemes for the homogeneous hyperbolic system, is generally effective in steady, unsteady and quasi-steady state solutions calculation of the considered hyperbolic systems with geometrical source terms having concentrations.

Acknowledgment

This research was supported in part by the Knowledge Innovation Project of the Chinese Academy of Sciences Nos. K3502012D1 and K5502212F1.

Appendix A

This appendix gives the numerical fluxes expressions of the *HLLE* and the *relaxation* scheme for 1D homogeneous shallow water equations and homogeneous isothermal nozzle flow equations. These numerical fluxes

at an interface are calculated from the values of conserved variables on the left and right sides of the interface. These two sides values of conserved variables are the cell average values in the first order method and are obtained from the cell average values with slope limiter adjustment in the second order method.

The HLLE scheme uses the approximate Riemann solver proposed by Einfeldt [9] on the basis of the HLL solver [18] by Harten, Lax and Van Leer. For 1D homogeneous shallow water Riemann problem, the approximate solution consists three states, the two initial states connected by an intermediate states, which is determined by the conservative property of the system. The speeds of the two discontinuities separating the three states in the solution are appropriately chosen to ensure the positivity preservation and entropy inequality of the solver.

Assume the two sides values of conserved variables h, m are provided at an interface for 1D shallow water equations denoted as $h^{\mathrm{L}}_{j+\frac{1}{2}}$, $m^{\mathrm{L}}_{j+\frac{1}{2}}$, $h^{\mathrm{R}}_{j+\frac{1}{2}}$, $m^{\mathrm{R}}_{j+\frac{1}{2}}$, and the numerical fluxes for the conserved variables to be calculated are denoted as $m_{j+\frac{1}{2}}$, $e_{j+\frac{1}{2}}$, in consistence with the notations used in Section 2.3. Then these numerical fluxes are calculated as follows in HLLE scheme.

Define

$$F^{\mathrm{L}}_{j+\frac{1}{2}} = \begin{pmatrix} m^{\mathrm{L}}_{j+\frac{1}{2}} \\ \dfrac{\left(m^{\mathrm{L}}_{j+\frac{1}{2}}\right)^2}{h^{\mathrm{L}}_{j+\frac{1}{2}}} + \frac{1}{2}g\left(h^{\mathrm{L}}_{j+\frac{1}{2}}\right)^2 \end{pmatrix}, \quad F^{\mathrm{R}}_{j+\frac{1}{2}} = \begin{pmatrix} m^{\mathrm{R}}_{j+\frac{1}{2}} \\ \dfrac{\left(m^{\mathrm{R}}_{j+\frac{1}{2}}\right)^2}{h^{\mathrm{R}}_{j+\frac{1}{2}}} + \frac{1}{2}g\left(h^{\mathrm{R}}_{j+\frac{1}{2}}\right)^2 \end{pmatrix}. \tag{A.1}$$

The next involves defining the averaged water height and velocity. The choice for such values are not unique. For simplicity, in our computation we use the following averaged values

$$\bar{h} = \frac{h^{\mathrm{L}}_{j+\frac{1}{2}} + h^{\mathrm{R}}_{j+\frac{1}{2}}}{2}, \quad \bar{v} = \frac{m^{\mathrm{L}}_{j+\frac{1}{2}} + m^{\mathrm{R}}_{j+\frac{1}{2}}}{h^{\mathrm{L}}_{j+\frac{1}{2}} + h^{\mathrm{R}}_{j+\frac{1}{2}}}.$$

Define

$$\begin{aligned} c^- &= \bar{v} - \sqrt{g\bar{h}}, \quad c^+ = \bar{v} + \sqrt{g\bar{h}}, \\ b^l &= \min\left(\frac{m^{\mathrm{L}}_{j+\frac{1}{2}}}{h^{\mathrm{L}}_{j+\frac{1}{2}}} - \sqrt{gh^{\mathrm{L}}_{j+\frac{1}{2}}}, c^-\right), \\ b^r &= \max\left(\frac{m^{\mathrm{R}}_{j+\frac{1}{2}}}{h^{\mathrm{R}}_{j+\frac{1}{2}}} + \sqrt{gh^{\mathrm{R}}_{j+\frac{1}{2}}}, c^+\right), \\ b^+ &= \max(b^r, 0), \quad b^- = \min(b^l, 0). \end{aligned}$$

Then the numerical fluxes $m_{j+\frac{1}{2}}$, $e_{j+\frac{1}{2}}$ are given by

$$\begin{pmatrix} m_{j+\frac{1}{2}} \\ e_{j+\frac{1}{2}} \end{pmatrix} = \frac{b^+}{b^+ - b^-}F^{\mathrm{L}}_{j+\frac{1}{2}} - \frac{b^-}{b^+ - b^-}F^{\mathrm{R}}_{j+\frac{1}{2}} + \frac{b^+b^-}{b^+ - b^-}\begin{pmatrix} h^{\mathrm{R}}_{j+\frac{1}{2}} - h^{\mathrm{L}}_{j+\frac{1}{2}} \\ m^{\mathrm{R}}_{j+\frac{1}{2}} - m^{\mathrm{L}}_{j+\frac{1}{2}} \end{pmatrix}. \tag{A.2}$$

Similarly, for isothermal nozzle flow equations, denote the values of conserved variables at two sides of an interface to be $(a\rho)^{\mathrm{L}}_{j+\frac{1}{2}}$, $(a\rho v)^{\mathrm{L}}_{j+\frac{1}{2}}$, $(a\rho)^{\mathrm{R}}_{j+\frac{1}{2}}$, $(a\rho v)^{\mathrm{R}}_{j+\frac{1}{2}}$. The numerical fluxes at the interface, denoted by $m_{j+\frac{1}{2}}$, $e_{j+\frac{1}{2}}$, are calculated as follows in the HLLE scheme.

Since the cross-sectional discontinuities are set at the center of cells, the cross-sectional area is continuous at the interface. Denote the value of cross-sectional area at the interface to be $a_{j+\frac{1}{2}}$. Denote $\hat{k} = k(a_{j+\frac{1}{2}})^{1-\gamma}$. Define

$$F^{\mathrm{L}}_{j+\frac{1}{2}} = \begin{pmatrix} (a\rho v)^{\mathrm{L}}_{j+\frac{1}{2}} \\ \dfrac{\left((a\rho v)^{\mathrm{L}}_{j+\frac{1}{2}}\right)^2}{(a\rho)^{\mathrm{L}}_{j+\frac{1}{2}}} + \hat{k}\left((a\rho)^{\mathrm{L}}_{j+\frac{1}{2}}\right)^{\gamma} \end{pmatrix}, \quad F^{\mathrm{R}}_{j+\frac{1}{2}} = \begin{pmatrix} (a\rho v)^{\mathrm{R}}_{j+\frac{1}{2}} \\ \dfrac{\left((a\rho v)^{\mathrm{R}}_{j+\frac{1}{2}}\right)^2}{(a\rho)^{\mathrm{R}}_{j+\frac{1}{2}}} + \hat{k}\left((a\rho)^{\mathrm{R}}_{j+\frac{1}{2}}\right)^{\gamma} \end{pmatrix}. \tag{A.3}$$

Define the averaged $a\rho$ and v

$$\overline{a\rho} = \frac{(a\rho)^{\mathrm{L}}_{j+\frac{1}{2}} + (a\rho)^{\mathrm{R}}_{j+\frac{1}{2}}}{2}, \quad \bar{v} = \frac{(a\rho v)^{\mathrm{L}}_{j+\frac{1}{2}} + (a\rho v)^{\mathrm{R}}_{j+\frac{1}{2}}}{(a\rho)^{\mathrm{L}}_{j+\frac{1}{2}} + (a\rho)^{\mathrm{R}}_{j+\frac{1}{2}}}.$$

Define

$$\begin{aligned}
&c^- = \bar{v} - \sqrt{\hat{k}\gamma(\overline{a\rho})^{\gamma-1}}, \quad c^+ = \bar{v} + \sqrt{\hat{k}\gamma(\overline{a\rho})^{\gamma-1}},\\
&b^l = \min\left(\frac{(a\rho v)^{\mathrm{L}}_{j+\frac{1}{2}}}{(a\rho)^{\mathrm{L}}_{j+\frac{1}{2}}} - \sqrt{\hat{k}\gamma\left((a\rho)^{\mathrm{L}}_{j+\frac{1}{2}}\right)^{\gamma-1}}, c^-\right),\\
&b^r = \max\left(\frac{(a\rho v)^{\mathrm{R}}_{j+\frac{1}{2}}}{(a\rho)^{\mathrm{R}}_{j+\frac{1}{2}}} + \sqrt{\hat{k}\gamma\left((a\rho)^{\mathrm{R}}_{j+\frac{1}{2}}\right)^{\gamma-1}}, c^+\right),\\
&b^+ = \max(b^r, 0), \quad b^- = \min(b^l, 0).
\end{aligned}$$

Then the numerical fluxes $m_{j+\frac{1}{2}}$, $e_{j+\frac{1}{2}}$ are given by

$$\begin{pmatrix} m_{j+\frac{1}{2}} \\ e_{j+\frac{1}{2}} \end{pmatrix} = \frac{b^+}{b^+ - b^-} F^{\mathrm{L}}_{j+\frac{1}{2}} - \frac{b^-}{b^+ - b^-} F^{\mathrm{R}}_{j+\frac{1}{2}} + \frac{b^+ b^-}{b^+ - b^-} \begin{pmatrix} (a\rho)^{\mathrm{R}}_{j+\frac{1}{2}} - (a\rho)^{\mathrm{L}}_{j+\frac{1}{2}} \\ (a\rho v)^{\mathrm{R}}_{j+\frac{1}{2}} - (a\rho v)^{\mathrm{L}}_{j+\frac{1}{2}} \end{pmatrix}. \tag{A.4}$$

It can be seen that if one obtains the numerical fluxes for the isentropic equations, which is the homogeneous isothermal nozzle flow equations with cross-sectional area a dropping, with left and right hand sides conserved variables values to be $\frac{(a\rho)^{\mathrm{L}}_{j+\frac{1}{2}}}{a_{j+\frac{1}{2}}}$, $\frac{(a\rho v)^{\mathrm{L}}_{j+\frac{1}{2}}}{a_{j+\frac{1}{2}}}$, $\frac{(a\rho)^{\mathrm{R}}_{j+\frac{1}{2}}}{a_{j+\frac{1}{2}}}$, $\frac{(a\rho v)^{\mathrm{R}}_{j+\frac{1}{2}}}{a_{j+\frac{1}{2}}}$ by the HLLE scheme, and then multiplies those numerical fluxes by $a_{j+\frac{1}{2}}$, the results are the same as (A.4).

The relaxation scheme proposed by Jin and Xin [25] obtains the numerical fluxes for a nonlinear hyperbolic conservation system from a linear hyperbolic system with double variable number. Consider a 1D two equations nonlinear conservation system

$$\begin{pmatrix} u_1 \\ u_2 \end{pmatrix}_t + \begin{pmatrix} f_1(u_1, u_2) \\ f_2(u_1, u_2) \end{pmatrix}_x = 0.$$

Assume at an interface the two sides values of conserved variables are given as u_1^{L}, u_2^{L}, u_1^{R}, u_2^{R}. Denote the numerical fluxes at the interface to be calculated as $\hat{f}_1$, $\hat{f}_2$. Then in relaxation scheme these numerical fluxes are obtained by introducing a four variables linear Riemann problem

$$\begin{pmatrix} U_1 \\ U_2 \\ U_3 \\ U_4 \end{pmatrix}_t + \begin{pmatrix} 0 & 0 & 1 & 0 \\ 0 & 0 & 0 & 1 \\ \widehat{C} & 0 & 0 & 0 \\ 0 & \widehat{C} & 0 & 0 \end{pmatrix} \begin{pmatrix} U_1 \\ U_2 \\ U_3 \\ U_4 \end{pmatrix}_x = 0$$

with initial data

$$\begin{pmatrix} U_1 \\ U_2 \\ U_3 \\ U_4 \end{pmatrix}_{t=0} = \begin{cases} UL & x < 0, \\ UR & x > 0, \end{cases}$$

where

$$UL = \begin{pmatrix} UL_1 \\ UL_2 \\ UL_3 \\ UL_4 \end{pmatrix} = \begin{pmatrix} u_1^{\mathrm{L}} \\ u_2^{\mathrm{L}} \\ f_1(u_1^{\mathrm{L}}, u_2^{\mathrm{L}}) \\ f_2(u_1^{\mathrm{L}}, u_2^{\mathrm{L}}) \end{pmatrix}, \quad UR = \begin{pmatrix} UR_1 \\ UR_2 \\ UR_3 \\ UR_4 \end{pmatrix} = \begin{pmatrix} u_1^{\mathrm{R}} \\ u_2^{\mathrm{R}} \\ f_1(u_1^{\mathrm{R}}, u_2^{\mathrm{R}}) \\ f_2(u_1^{\mathrm{R}}, u_2^{\mathrm{R}}) \end{pmatrix}.$$

The constant $\widehat{C}$ in the linear system is positive and satisfies subcharacteristic condition which requires $\sqrt{\widehat{C}}$ to be greater than the absolute value of the characteristic speeds in the solution of the nonlinear system. This condition means that the characteristic speeds for the linear system are greater than those for original nonlinear equations.

The numerical fluxes $\hat{f}_1$, $\hat{f}_2$ are set to be values of U_3, U_4 at $x = 0$ in the linear Riemann problem. These values can be calculated to be given as

$$\begin{pmatrix} \hat{f}_1 \\ \hat{f}_2 \end{pmatrix} = \begin{pmatrix} \frac{UL_3+UR_3}{2} + \frac{\sqrt{\widehat{C}}}{2}(UL_1 - UR_1) \\ \frac{UL_4+UR_4}{2} + \frac{\sqrt{\widehat{C}}}{2}(UL_2 - UR_2) \end{pmatrix}. \tag{A.5}$$

For 1D shallow water equations, denote the conserved variables values at two sides of an interface to be $h^{\mathrm{L}}_{j+\frac{1}{2}}$, $m^{\mathrm{L}}_{j+\frac{1}{2}}$, $h^{\mathrm{R}}_{j+\frac{1}{2}}$, $m^{\mathrm{R}}_{j+\frac{1}{2}}$, and define the corresponding fluxes $F^{\mathrm{L}}_{j+\frac{1}{2}}$, $F^{\mathrm{R}}_{j+\frac{1}{2}}$ as in (A.1). Then from (A.5) the numerical fluxes given by the relaxation scheme are written as

$$\begin{pmatrix} m_{j+\frac{1}{2}} \\ e_{j+\frac{1}{2}} \end{pmatrix} = \frac{F^{\mathrm{L}}_{j+\frac{1}{2}} + F^{\mathrm{R}}_{j+\frac{1}{2}}}{2} + \frac{\sqrt{\widehat{C}}}{2} \begin{pmatrix} h^{\mathrm{L}}_{j+\frac{1}{2}} - h^{\mathrm{R}}_{j+\frac{1}{2}} \\ m^{\mathrm{L}}_{j+\frac{1}{2}} - m^{\mathrm{R}}_{j+\frac{1}{2}} \end{pmatrix}. \tag{A.6}$$

For homogeneous isothermal nozzle flow equations, denote the conserved variables values at two sides of an interface to be $(a\rho)^{\mathrm{L}}_{j+\frac{1}{2}}$, $(a\rho v)^{\mathrm{L}}_{j+\frac{1}{2}}$, $(a\rho)^{\mathrm{R}}_{j+\frac{1}{2}}$, $(a\rho v)^{\mathrm{R}}_{j+\frac{1}{2}}$, and define the corresponding fluxes $F^{\mathrm{L}}_{j+\frac{1}{2}}$, $F^{\mathrm{R}}_{j+\frac{1}{2}}$ as in (A.3). Then from (A.5) the numerical fluxes given by the relaxation scheme are written as

$$\begin{pmatrix} m_{j+\frac{1}{2}} \\ e_{j+\frac{1}{2}} \end{pmatrix} = \frac{F^{\mathrm{L}}_{j+\frac{1}{2}} + F^{\mathrm{R}}_{j+\frac{1}{2}}}{2} + \frac{\sqrt{\widehat{C}}}{2} \begin{pmatrix} (a\rho)^{\mathrm{L}}_{j+\frac{1}{2}} - (a\rho)^{\mathrm{R}}_{j+\frac{1}{2}} \\ (a\rho v)^{\mathrm{L}}_{j+\frac{1}{2}} - (a\rho v)^{\mathrm{R}}_{j+\frac{1}{2}} \end{pmatrix}. \tag{A.7}$$

Appendix B

This appendix gives the exact solutions with 6 effective number for Examples 2.1, 2.2, 3.1, and 3.2. Examples 2.1 and 2.2 are Riemann problems for shallow water equations with bottom step. The method for constructing the exact solutions is provided in [1].

Example 2.1

$$h(x,t) = \begin{cases} 4, & \frac{x}{t} < \xi_1, \\ \left(-\frac{1}{3\sqrt{g}}\left(\frac{x}{t} - \xi_1\right) + 2\right)^2, & \xi_1 < \frac{x}{t} < \xi_2, \\ 1.566049, & \xi_2 < \frac{x}{t} < s \\ 0.774464, & s < \frac{x}{t} < 0, \\ 1, & \frac{x}{t} > 0, \end{cases}$$

$$m(x,t)=\begin{cases}-40, & \frac{x}{t}<\xi_1,\\ \left(\frac{2}{3}\left(\frac{x}{t}-\xi_1\right)-10\right)h(x,t), & \xi_1<\frac{x}{t}<\xi_2,\\ -8.320635, & \xi_2<\frac{x}{t}<s,\\ -6, & \frac{x}{t}>s,\end{cases}$$

with $\xi_1=-16.260990$, $\xi_2=-9.230700$, $s=-2.931634$.

Example 2.2

$$h(x,t)=\begin{cases}4, & \frac{x}{t}<\xi_1,\\ \left(-\frac{1}{3\sqrt{g}}\left(\frac{x}{t}-\xi_1\right)+2\right)^2, & \xi_1<\frac{x}{t}<\xi_2,\\ 1.009629, & \xi_2<\frac{x}{t}<s,\\ 0.429476, & s<\frac{x}{t}<0,\\ \left(\frac{1}{3\sqrt{g}}\frac{x}{t}+0.942809\right)^2, & 0<\frac{x}{t}<\xi_3,\\ 2, & \frac{x}{t}>\xi_3,\end{cases}$$

$$m(x,t)=\begin{cases}-40, & x<0.5\xi_1,\\ \left(\frac{2}{3}\left(\frac{x}{t}-\xi_1\right)-10\right)h(x,t), & \xi_1<\frac{x}{t}<\xi_2,\\ -3.805371, & \xi_2<\frac{x}{t}<s,\\ -2.623519, & s<\frac{x}{t}<0,\\ \left(\frac{2}{3}\frac{x}{t}-2.951459\right)h(x,t), & 0<\frac{x}{t}<\xi_3,\\ 0, & \frac{x}{t}>\xi_3,\end{cases}$$

with $\xi_1=-16.260990$, $\xi_2=-6.914610$, $\xi_3=4.427189$, $s=-2.037139$.

Examples 3.1 and 3.2 are Riemann problems for isothermal nozzle flow equations with cross-sectional area step. The method for constructing the exact solutions is provided in [28].

Example 3.1

$$\rho(x,t)=\begin{cases}4, & \frac{x}{t}<\xi_1,\\ \left(-\frac{\gamma-1}{\gamma+1}\frac{1}{\sqrt{k\gamma}}\left(\frac{x}{t}-\xi_1\right)+2^{\gamma-1}\right)^{\frac{2}{\gamma-1}}, & \xi_1<\frac{x}{t}<0,\\ 0.144489, & 0<\frac{x}{t}<s,\\ 0.334984, & s<\frac{x}{t}<\xi_2,\\ \left(\frac{\gamma-1}{\gamma+1}\frac{1}{\sqrt{k\gamma}}\left(\frac{x}{t}-\xi_2\right)+(0.334984)^{\frac{\gamma-1}{2}}\right)^{\frac{2}{\gamma-1}}, & \xi_2<\frac{x}{t}<\xi_3,\\ 1, & \frac{x}{t}>\xi_3,\end{cases}$$

$$m(x,t)=\begin{cases}-7.2, & \frac{x}{t}<\xi_1,\\ \left(\frac{2}{\gamma+1}\left(\frac{x}{t}-\xi_1\right)-1.8\right)\rho(x,t), & \xi_1<\frac{x}{t}<0,\\ 0.235688, & 0<\frac{x}{t}<s,\\ 0.283244, & s<\frac{x}{t}<\xi_2,\\ \left(\frac{2}{\gamma+1}\left(\frac{x}{t}-\xi_2\right)+0.845545\right)\rho(x,t), & \xi_2<\frac{x}{t}<\xi_3,\\ 2, & \frac{x}{t}>\xi_3,\end{cases}$$

with $\xi_1=-3.254832$, $\xi_2=1.807837$, $\xi_3=3.154701$, $s=0.249642$.

Example 3.2

$$\rho(x,t)=\begin{cases}4, & \frac{x}{t}<\xi_1,\\ \left(-\frac{\gamma-1}{\gamma+1}\frac{1}{\sqrt{k\gamma}}\left(\frac{x}{t}-\xi_1\right)+2^{\gamma-1}\right)^{\frac{2}{\gamma-1}}, & \xi_1<\frac{x}{t}<\xi_2,\\ 2.081147, & \xi_2<\frac{x}{t}<0,\\ 2.299140, & 0<\frac{x}{t}<\xi_3,\\ \left(\frac{\gamma-1}{\gamma+1}\frac{1}{\sqrt{k\gamma}}\left(\frac{x}{t}-\xi_3\right)+(2.299140)^{\frac{\gamma-1}{2}}\right)^{\frac{2}{\gamma-1}}, & \xi_3<\frac{x}{t}<\xi_4,\\ 6, & \frac{x}{t}>\xi_4,\end{cases}$$

$$m(x,t)=\begin{cases}-6.4, & \frac{x}{t}<\xi_1,\\ \left(\frac{2}{\gamma+1}\left(\frac{x}{t}-\xi_1\right)-1.6\right)\rho(x,t), & \xi_1<\frac{x}{t}<\xi_2,\\ -1.455504, & \xi_2<\frac{x}{t}<0,\\ -0.873302, & 0<\frac{x}{t}<\xi_3,\\ \left(\frac{2}{\gamma+1}\left(\frac{x}{t}-\xi_3\right)-0.379839\right)\rho(x,t), & \xi_3<\frac{x}{t}<\xi_4,\\ 6, & \frac{x}{t}>\xi_4,\end{cases}$$

with $\xi_1=-3.054832$, $\xi_2=-2.004104$, $\xi_3=0.946732$, $\xi_4=2.556543$.

Appendix C

In this appendix, we prove the *S*-property of our slope selecting method described in Section 3.2 for isothermal nozzle flow equations with discontinuous cross-sectional area. Namely, the following theorem holds for our slope selecting method.

Theorem C.1. *When the cross-sectional area is a step function, if the interface type source term approximation in the slope selecting method can be exactly computed, the slope selecting scheme described in Section 3.2 can preserve exactly any steady state solution belonging to Definition 3.1 in which the steady state conditions (3.5), (3.6) are hold anywhere including across the cross-sectional discontinuity.*

Proof. Assume the cross-sectional area is a step function with left and right side values a_l and a_r. We only need to prove our slope selecting scheme preserve the steady state solution exactly in the cell $[x_{j-\frac{1}{2}},x_{j+\frac{1}{2}}]$ which contains the cross-sectional discontinuity in the center. The density and velocity in the steady state solution are step functions. Denote their left and right values to be ρ_l,v_l and ρ_r,v_r, which satisfy

$$a_l\rho_l v_l=a_r\rho_r v_r, \tag{C.1}$$

$$\frac{1}{2}v_l^2+k\frac{\gamma}{\gamma-1}(\rho_l)^{\gamma-1}=\frac{1}{2}v_r^2+k\frac{\gamma}{\gamma-1}(\rho_r)^{\gamma-1}. \tag{C.2}$$

It can be similarly checked as for shallow water equations that the numerical fluxes in our slope selecting method at interfaces $j\pm\frac{1}{2}$ preserve the exact values due to the slope selecting strategy implemented in the method.

$$m_{j-\frac{1}{2}}=a_l\rho_l v_l,\quad e_{j-\frac{1}{2}}=a_l\rho_l(v_l)^2+ka_l(\rho_l)^\gamma,$$
$$m_{j+\frac{1}{2}}=a_r\rho_r v_r,\quad e_{j+\frac{1}{2}}=a_r\rho_r(v_r)^2+ka_r(\rho_r)^\gamma,$$

and the interface values of ρ,v defined for interface type source term approximation (3.13), (3.17) are

$$\rho^*_{j-\frac{1}{2}}=\rho_l,\quad \rho^*_{j+\frac{1}{2}}=\rho_r,\quad v^*_{j-\frac{1}{2}}=v_l,\quad v^*_{j+\frac{1}{2}}=v_r. \tag{C.3}$$

Our slope selecting scheme for isothermal nozzle flow equations in the cell $[x_{j-\frac{1}{2}}, x_{j+\frac{1}{2}}]$ thus can be written as

$$\partial_t(a\rho)_j + \frac{a_r\rho_r v_r - a_l\rho_l v_l}{\Delta x} = 0, \tag{C.4}$$

$$\partial_t(a\rho v)_j + \frac{\left(a_r\rho_r v_r^2 + k a_r(\rho_r)^\gamma\right) - \left(a_l\rho_l v_l^2 + k a_l(\rho_l)^\gamma\right)}{\Delta x} = \frac{k}{\Delta x}\int_{x_{j-\frac{1}{2}}}^{x_{j+\frac{1}{2}}} (\hat{\rho})^\gamma \hat{a}_x \, dx, \tag{C.5}$$

where $\hat{\rho}$, $\hat{a}$ are smooth functions on $[x_{j-\frac{1}{2}}, x_{j+\frac{1}{2}}]$ defined in Section 3.2.

The flux difference for $a\rho$ in scheme (C.4) is zero due to (C.1). Recall $\hat{v}$ defined in Section 3.2. For steady state solutions satisfying one of conditions (3.9)–(3.11) described in Definition 3.1, the transonic fix in our source term approximation does not apply. So the endpoint values for functions $\hat{\rho}$, $\hat{v}$ are given by (3.22), which are given by (C.3). Recall the identities (3.19), (3.20), the flux difference for $a\rho v$ in scheme (C.5) can be calculated as

$$\begin{aligned}
&\frac{\left(a_r\rho_r v_r^2 + k a_r(\rho_r)^\gamma\right) - \left(a_l\rho_l v_l^2 + k a_l(\rho_l)^\gamma\right)}{\Delta x} - \frac{k}{\Delta x}\int_{x_{j-\frac{1}{2}}}^{x_{j+\frac{1}{2}}} (\hat{\rho})^\gamma \hat{a}_x \, dx \\
&= \frac{1}{\Delta x}\int_{x_{j-\frac{1}{2}}}^{x_{j+\frac{1}{2}}} \left[(\hat{a}\hat{\rho}(\hat{v})^2)_x + (k\hat{a}(\hat{\rho})^\gamma)_x - k(\hat{\rho})^\gamma \hat{a}_x\right] dx = \frac{1}{\Delta x}\int_{x_{j-\frac{1}{2}}}^{x_{j+\frac{1}{2}}} \left[(\hat{a}\hat{\rho}\hat{v})_x\hat{v} + (\hat{a}\hat{\rho}\hat{v})\hat{v}_x + k\hat{a}\gamma(\hat{\rho})^{\gamma-1}\hat{\rho}_x\right] dx \\
&= \frac{1}{\Delta x}\int_{x_{j-\frac{1}{2}}}^{x_{j+\frac{1}{2}}} \left[H_x\hat{v} + \hat{a}\hat{\rho}(\hat{v}\hat{v}_x + k\gamma(\hat{\rho})^{\gamma-2}\hat{\rho}_x)\right] dx = \frac{1}{\Delta x}\int_{x_{j-\frac{1}{2}}}^{x_{j+\frac{1}{2}}} \left[H_x\hat{v} + \hat{a}\hat{\rho}G_x\right] dx.
\end{aligned} \tag{C.6}$$

Finally, recall the definitions of H, G (3.18) and the facts (C.1), (C.2), one knows H, G indeed are constants in the cell $[x_{j-1/2}, x_{j+1/2}]$. So the function in the integration (C.6) is identically zero and the flux difference for $a\rho v$ in scheme (C.5) is zero. Thus this steady state solution is exactly preserved by our slope selecting scheme described in Section 3.2. □

Appendix D

In this appendix, we prove the *S*-property of our slope selecting method described in Section 4.2 for non-isothermal nozzle flow equations with discontinuous cross-sectional area. Namely, the following theorem holds for our slope selecting method.

Theorem D.1. *When the cross-sectional area is a step function, the slope selecting scheme described in Section 4.2 can preserve exactly any stationary steady state solution belonging to Definition 4.1 if the Euler equations solver used by the slope selecting method has the property in Definition 4.3, and can preserve exactly any non-stationary steady state solution belonging to Definition 4.2 in which the steady state conditions 4.10, 4.11, 4.12 are hold anywhere including across the cross-sectional discontinuity if the interface type source term approximation in the slope selecting method can be exactly computed.*

Proof. Assume the cross-sectional area is a step function with left and right side values a_l and a_r. We only need to prove our slope selecting scheme preserve the steady state solution exactly in the cell $[x_{j-\frac{1}{2}}, x_{j+\frac{1}{2}}]$ which contains the cross-sectional discontinuity in the center. We discuss the stationary and non-stationary steady state solution, respectively.

For stationary steady state solution case, the velocity, total energy are constants on the entire domain. Denote them by $\tilde{v} = 0$ and $\widetilde{E}$. It can be checked that the conserved variables values at two sides of interface $j+\frac{1}{2}$ in our slope selecting method take the following form due to the slope selecting strategy implemented in the method.

$$(a\rho)^{\mathrm{L}}_{j+\frac{1}{2}} = (a\rho)_{\mathrm{L}}, \quad (a\rho v)^{\mathrm{L}}_{j+\frac{1}{2}} = 0, \quad (aE)^{\mathrm{L}}_{j+\frac{1}{2}} = a_{\mathrm{r}}\widetilde{E},$$
$$(a\rho)^{\mathrm{R}}_{j+\frac{1}{2}} = (a\rho)_{\mathrm{R}}, \quad (a\rho v)^{\mathrm{R}}_{j+\frac{1}{2}} = 0, \quad (aE)^{\mathrm{R}}_{j+\frac{1}{2}} = a_{\mathrm{r}}\widetilde{E},$$

where $(a\rho)_{\mathrm{L}}$, $(a\rho)_{\mathrm{R}}$ are certain values which may not be equal.

Since the Euler equations solver used by the slope selecting method has the property in Definition 4.3, the numerical fluxes at interface $j+\frac{1}{2}$ in the slope selecting method are given by

$$m_{j+\frac{1}{2}} = 0, \quad e_{j+\frac{1}{2}} = (\gamma-1)\widetilde{E}a_{\mathrm{r}}, \quad f_{j+\frac{1}{2}} = 0.$$

In the same way, the numerical fluxes at interface $j-\frac{1}{2}$ are given by

$$m_{j-\frac{1}{2}} = 0, \quad e_{j-\frac{1}{2}} = (\gamma-1)\widetilde{E}a_{\mathrm{l}}, \quad f_{j-\frac{1}{2}} = 0.$$

Also notice the quantities $E^*_{j\pm\frac{1}{2}}$ in (4.21), $v^*_{j\pm\frac{1}{2}}$ and $P^*_{j\pm\frac{1}{2}}$ in (4.28) can be checked to be

$$E^*_{j\pm\frac{1}{2}} = \widetilde{E}, \quad v^*_{j\pm\frac{1}{2}} = 0, \quad P^*_{j\pm\frac{1}{2}} = (\gamma-1)\widetilde{E}.$$

Thus in this stationary steady state solution case, our slope selecting scheme for non-isothermal nozzle flow equations in the cell $[x_{j-\frac{1}{2}}, x_{j+\frac{1}{2}}]$ can be written as

$$\partial_t(a\rho)_j + \frac{0-0}{\Delta x} = 0, \tag{D.1}$$
$$\partial_t(a\rho v)_j + \frac{(\gamma-1)\widetilde{E}a_{\mathrm{r}} - (\gamma-1)\widetilde{E}a_{\mathrm{l}}}{\Delta x} = \frac{P^*_{j-\frac{1}{2}} + P^*_{j+\frac{1}{2}}}{2}\frac{a_{\mathrm{r}} - a_{\mathrm{l}}}{\Delta x}, \tag{D.2}$$
$$\partial_t(aE)_j + \frac{0-0}{\Delta x} = 0. \tag{D.3}$$

The flux difference in (D.2) is also zero since $P^*_{j\pm\frac{1}{2}} = (\gamma-1)\widetilde{E}$. Thus this stationary steady state solution is exactly preserved by our slope selecting scheme described in Section 4.2.

For non-stationary steady state solution case, the density, velocity and total energy in the steady state solution are step functions. Denote their left and right values to be $\rho_{\mathrm{l}}, v_{\mathrm{l}}, E_{\mathrm{l}}$ and $\rho_{\mathrm{r}}, v_{\mathrm{r}}, E_{\mathrm{r}}$. The two sides pressures are

$$P_{\mathrm{l}} = (\gamma-1)\left(E_{\mathrm{l}} - \frac{1}{2}\rho_{\mathrm{l}}(v_{\mathrm{l}})^2\right), \quad P_{\mathrm{r}} = (\gamma-1)\left(E_{\mathrm{r}} - \frac{1}{2}\rho_{\mathrm{r}}(v_{\mathrm{r}})^2\right).$$

It holds that $v_{\mathrm{l}} \neq 0$, $v_{\mathrm{r}} \neq 0$, $\rho_{\mathrm{l}} \neq 0$, $\rho_{\mathrm{r}} \neq 0$, and

$$a_{\mathrm{l}}\rho_{\mathrm{l}}v_{\mathrm{l}} = a_{\mathrm{r}}\rho_{\mathrm{r}}v_{\mathrm{r}}, \tag{D.4}$$
$$a_{\mathrm{l}}v_{\mathrm{l}}\left(\gamma E_{\mathrm{l}} - \frac{\gamma-1}{2}\rho_{\mathrm{l}}(v_{\mathrm{l}})^2\right) = a_{\mathrm{r}}v_{\mathrm{r}}\left(\gamma E_{\mathrm{r}} - \frac{\gamma-1}{2}\rho_{\mathrm{r}}(v_{\mathrm{r}})^2\right), \tag{D.5}$$
$$\frac{\rho_{\mathrm{l}}^{\gamma}}{E_{\mathrm{l}} - \frac{1}{2}\rho_{\mathrm{l}}(v_{\mathrm{l}})^2} = \frac{\rho_{\mathrm{r}}^{\gamma}}{E_{\mathrm{r}} - \frac{1}{2}\rho_{\mathrm{r}}(v_{\mathrm{r}})^2}. \tag{D.6}$$

It can be checked that the numerical fluxes in our slope selecting method at interfaces $j\pm\frac{1}{2}$ preserve the exact values due to the slope selecting strategy implemented in the method.

$$m_{j-\frac{1}{2}} = a_{\mathrm{l}}\rho_{\mathrm{l}}v_{\mathrm{l}}, \quad e_{j-\frac{1}{2}} = a_{\mathrm{l}}\rho_{\mathrm{l}}(v_{\mathrm{l}})^2 + P_{\mathrm{l}}a_{\mathrm{l}}, \quad f_{j-\frac{1}{2}} = v_{\mathrm{l}}(E_{\mathrm{l}} + P_{\mathrm{l}})a_{\mathrm{l}},$$
$$m_{j+\frac{1}{2}} = a_{\mathrm{r}}\rho_{\mathrm{r}}v_{\mathrm{r}}, \quad e_{j+\frac{1}{2}} = a_{\mathrm{r}}\rho_{\mathrm{r}}(v_{\mathrm{r}})^2 + P_{\mathrm{r}}a_{\mathrm{r}}, \quad f_{j+\frac{1}{2}} = v_{\mathrm{r}}(E_{\mathrm{r}} + P_{\mathrm{r}})a_{\mathrm{r}},$$

and the interface values of ρ, v, E, P defined for interface type source term approximation (4.21), (4.28) are

$$\rho^*_{j-\frac{1}{2}} = \rho_{\mathrm{l}}, \quad \rho^*_{j+\frac{1}{2}} = \rho_{\mathrm{r}}, \quad v^*_{j-\frac{1}{2}} = v_{\mathrm{l}}, \quad v^*_{j+\frac{1}{2}} = v_{\mathrm{r}}, \tag{D.7}$$
$$E^*_{j-\frac{1}{2}} = E_{\mathrm{l}}, \quad E^*_{j+\frac{1}{2}} = E_{\mathrm{r}}, \quad P^*_{j-\frac{1}{2}} = P_{\mathrm{l}}, \quad P^*_{j+\frac{1}{2}} = P_{\mathrm{r}}. \tag{D.8}$$

Thus in this non-stationary steady state solution case, our slope selecting scheme for non-isothermal nozzle flow equations in the cell $[x_{j-\frac{1}{2}}, x_{j+\frac{1}{2}}]$ can be written as

$$\partial_t(a\rho)_j + \frac{a_r\rho_r v_r - a_l\rho_l v_l}{\Delta x} = 0, \tag{D.9}$$

$$\partial_t(a\rho v)_j + \frac{(a_r\rho_r v_r^2 + P_r a_r) - (a_l\rho_l v_l^2 + P_l a_l)}{\Delta x} = \frac{1}{\Delta x}\int_{x_{j-\frac{1}{2}}}^{x_{j+\frac{1}{2}}} \widehat{P}\hat{a}_x \,\mathrm{d}x, \tag{D.10}$$

$$\partial_t(aE)_j + \frac{v_r(E_r + P_r)a_r - v_l(E_l + P_l)a_l}{\Delta x} = 0, \tag{D.11}$$

where $\widehat{P}$, $\hat{a}$ are smooth functions on $[x_{j-\frac{1}{2}}, x_{j+\frac{1}{2}}]$ defined in Section 4.2.

The flux differences for $a\rho$ and aE in schemes (D.9), (D.11) are zero due to (D.4), (D.6). Recall $\hat{\rho}$, $\hat{v}$, $\widehat{E}$ defined in Section 4.2. For steady state solutions satisfying one of conditions (4.16)–(4.18) described in Definition 4.2, the transonic fix in our source term approximation does not apply. So the endpoint values for functions $\hat{\rho}$, $\hat{v}$, $\widehat{E}$ are given by (4.34), which are given by (D.7), (D.8). According to (4.35), the endpoint values of $\widehat{P}$ are $P^*_{j\pm\frac{1}{2}}$ in (4.28), which are given by (D.8). Recall the identities (4.31), (4.32) and (4.33), the flux difference for $a\rho v$ in scheme (D.10) can be calculated as

$$\begin{aligned}
&\frac{(a_r\rho_r v_r^2 + P_r a_r) - (a_l\rho_l v_l^2 + P_l a_l)}{\Delta x} - \frac{1}{\Delta x}\int_{x_{j-\frac{1}{2}}}^{x_{j+\frac{1}{2}}} \widehat{P}\hat{a}_x \,\mathrm{d}x = \frac{1}{\Delta x}\int_{x_{j-\frac{1}{2}}}^{x_{j+\frac{1}{2}}} [(\hat{a}\hat{\rho}(\hat{v})^2)_x + (\widehat{P}\hat{a})_x - \widehat{P}\hat{a}_x]\,\mathrm{d}x \\
&= \frac{1}{\Delta x}\int_{x_{j-\frac{1}{2}}}^{x_{j+\frac{1}{2}}} [(\hat{a}\hat{\rho}\hat{v})_x\hat{v} + (\hat{a}\hat{\rho}\hat{v})\hat{v}_x + \widehat{P}_x\hat{a}]\,\mathrm{d}x = \frac{1}{\Delta x}\int_{x_{j-\frac{1}{2}}}^{x_{j+\frac{1}{2}}} \left[H_x\hat{v} + \hat{a}\hat{\rho}\left(\hat{v}\hat{v}_x + \frac{\widehat{P}_x}{\hat{\rho}}\right)\right]\mathrm{d}x \\
&= \frac{1}{\Delta x}\int_{x_{j-\frac{1}{2}}}^{x_{j+\frac{1}{2}}} [H_x\hat{v} + \hat{a}\hat{\rho}(T_1 + T_2)]\,\mathrm{d}x,
\end{aligned} \tag{D.12}$$

where T_1, T_2 are defined as

$$T_1 = \hat{v}\hat{v}_x + \frac{\gamma}{\gamma-1}\left(\frac{\widehat{P}}{\hat{\rho}}\right)_x, \quad T_2 = \frac{\widehat{P}_x}{\hat{\rho}} - \frac{\gamma}{\gamma-1}\left(\frac{\widehat{P}}{\hat{\rho}}\right)_x.$$

T_1 can be evaluated as

$$T_1 = \hat{v}\hat{v}_x + \frac{\gamma}{\gamma-1}\left(\frac{\widehat{P}}{\hat{\rho}}\right)_x = \left(\frac{1}{2}(\hat{v})^2 + \frac{\gamma}{\gamma-1}\frac{\widehat{P}}{\hat{\rho}}\right)_x = \left(\frac{\frac{1}{2}\hat{\rho}(\hat{v})^2 + \gamma(\widehat{E} - \frac{1}{2}\hat{\rho}(\hat{v})^2)}{\hat{\rho}}\right)_x = \left(\frac{G}{H}\right)_x. \tag{D.13}$$

T_2 can be evaluated as

$$\begin{aligned}
T_2 &= \frac{\widehat{P}_x}{\hat{\rho}} - \frac{\gamma}{\gamma-1}\left(\frac{\widehat{P}}{\hat{\rho}}\right)_x = \frac{-1}{\gamma-1}\frac{\widehat{P}_x}{\hat{\rho}} + \frac{\gamma}{\gamma-1}\frac{\widehat{P}}{(\hat{\rho})^2}\hat{\rho}_x = \frac{1}{\gamma-1}\frac{(\widehat{P})^2}{(\hat{\rho})^{\gamma+1}}\left(-\frac{\widehat{P}_x(\hat{\rho})^\gamma}{(\widehat{P})^2} + \gamma\frac{(\hat{\rho})^{\gamma-1}\hat{\rho}_x}{\widehat{P}}\right) \\
&= \frac{1}{\gamma-1}\frac{(\widehat{P})^2}{(\hat{\rho})^{\gamma+1}}\left(\frac{(\hat{\rho})^\gamma}{\widehat{P}}\right)_x = \frac{1}{(\gamma-1)^2}\frac{(\widehat{P})^2}{(\hat{\rho})^{\gamma+1}}F_x.
\end{aligned} \tag{D.14}$$

Together with (D.12), (D.13) and (D.14), the flux difference for $a\rho v$ in scheme (D.10) is calculated to be

$$\frac{1}{\Delta x}\int_{x_{j-\frac{1}{2}}}^{x_{j+\frac{1}{2}}} \left[H_x\hat{v} + \hat{a}\hat{\rho}\left(\left(\frac{G}{H}\right)_x + \frac{1}{(\gamma-1)^2}\frac{(\widehat{P})^2}{(\hat{\rho})^{\gamma+1}}F_x\right)\right]\mathrm{d}x. \tag{D.15}$$

Finally, recall the definitions of H, G, F (4.30) and the facts (D.4), (D.5) and (D.6), one knows H, G, F indeed are constants in the cell $[x_{j-1/2}, x_{j+1/2}]$. So the function in the integration (D.15) is identically zero and the flux difference for $a\rho v$ in scheme (D.10) is zero. Thus this non-stationary steady state solution is exactly preserved by our slope selecting scheme described in Section 4.2. □

References

[1] F. Alcrudo, F. Benkhaldoun, Exact solutions to the Riemann problem of the shallow water equations with a bottom step, Comput. Fluids 30 (2001) 643–671.
[2] E. Audusse, F. Bouchut, M.-O. Bristeau, R. Klein, B. Perthame, A fast and stable well-balanced scheme with hydrostatic reconstruction for shallow water flows, SIAM J. Sci. Comp. 25 (2004) 2050–2065.
[3] A. Bernudez, M.E. Vazquez, Upwind methods for hyperbolic conservation laws with source terms, Comput. Fluids 23 (1994) 1049–1071.
[4] R. Botchorishvili, B. Perthame, A. Vasseur, Equilibrium schemes for scalar conservation laws with stiff sources, Math. Comp. 72 (241) (2003) 131–157.
[5] A. Chinnayya, A.Y. Le Roux, A new general Riemann solver for the shallow-water equations with friction and topography, 1999, preprint.
[6] A. Chinnayya, A.Y. Le Roux, N. Seguin, A well-balanced numerical scheme for the approximation of the shallow-water equations with topography: the resonance phenomenon, 2003, preprint.
[7] A.I. Delis, Improved application of the HLLE Riemann solver for the shallow water equations with source terms, Commun. Numer. Meth. Eng. 19 (2003) 59–83.
[8] A.I. Delis, Th. Katsaounis, Relaxation schemes for the shallow water equations, Int. J. Numer. Meth. Fluids 41 (2003) 695–719.
[9] B. Einfeldt, C.D. Munz, P.L. Roe, B. Sjogreen, On Godunov-type methods near low densities, J. Comput. Phys. 92 (1991) 273–295.
[10] T. Gallouët, J.-M. Hérard, N. Seguin, Some approximate Godunov schemes to compute shallow-water equations with topography, Comput. Fluids 32 (2003) 479–513.
[11] H.M. Glaz, T.P. Liu, The asymptotic analysis of wave interactions and numerical calculations of transonic nozzle flow, Adv. Appl. Math. 5 (1984) 111–146.
[12] S.K. Godunov, Finite difference schemes for numerical computation of solutions of the equations of fluid dynamics, Math. USSR Sbornik 47 (1959) 271–306.
[13] L. Gosse, A well-balanced flux-vector splitting scheme designed for hyperbolic systems of conservation laws with source terms, Comput. Math. Appl. 39 (2000) 135–159.
[14] L. Gosse, A well-balanced scheme using non-conservative products designed for hyperbolic systems of conservation laws with source terms, Math. Models Methods Appl. Sci. 11 (2) (2001) 339–365.
[15] L. Gosse, A.-Y. Le Roux, A well-balanced scheme designed for inhomogeneous scalar conservation laws, C. R. Acad. Sci., Paris. Sér I 323 (1996) 543–546.
[16] J.M. Greenberg, A.-Y. Le Roux, A well-balanced scheme for the numerical processing of source terms in hyperbolic equations, SIAM J. Numer. Anal. 33 (1996) 1–16.
[17] J.M. Greenberg, A.-Y. Le Roux, R. Baraille, A. Noussair, Analysis and approximation of conservation laws with source terms, SIAM J. Numer. Anal. 34 (1997) 1980–2007.
[18] A. Harten, P.D. Lax, B. Van Leer, On upstream differencing and Godunov-type schemes for hyperbolic conservation laws, SIAM Rev. 25 (1983) 35–61.
[19] M.E. Hubbard, P. Garcia-Navarro, Flux difference splitting and the balancing of source terms and flux gradients, J. Comput. Phys. 165 (2000) 89–125.
[20] H. Nessyahu, E. Tadmor, Non-oscillatory central differencing for hyperbolic conservation laws, J. Comput. Phys. 87 (1990) 408–463.
[21] S. Jin, A steady-state capturing method for hyperbolic system with geometrical source terms, Math. Model. Numer. Anal. 35 (2001) 631–646.
[22] S. Jin, J.-G. Liu, The effects of numerical viscosities I. Slowly moving shocks, J. Comput. Phys. 126 (1996) 373–389.
[23] S. Jin, X. Wen, An efficient method for computing hyperbolic systems with geometrical source terms having concentrations, J. Comput. Math. 22 (2004) 230–249.
[24] S. Jin, X. Wen, Two interface type numerical methods for computing hyperbolic systems with geometrical source terms having concentrations, SIAM J. Sci. Comp. 26 (2005) 2079–2101.
[25] S. Jin, Z.-P. Xin, The relaxation schemes for systems of conservation laws in arbitrary space dimensions, Commun. Pure Appl. Math. XLVIII (1995) 235–276.
[26] A. Kurganov, D. Levy, Central-upwind schemes for the Saint–Venant system, Math. Model. Numer. Anal. 36 (3) (2002) 397–425.
[27] A. Kurganov, S. Noelle, G. Petrova, Semidiscrete central-upwind schemes for hyperbolic conservation laws and Hamilton–Jacobi equations, SIAM J. Sci. Comput. 23 (3) (2001) 707–740.
[28] P.G. LeFloch, M.D. Thanh, The riemann problem for fluid flows in a nozzle with discontinuous cross-section, Commun. Math. Sci. 1 (2003) 763–797.
[29] R.J. LeVeque, Numerical Methods for Conservation Laws, Birkhäuser, Basel, 1990.
[30] R.J. LeVeque, Balancing source terms and flux gradients in high-resolution Godunov methods: the quasi-steady wave-propagation algorithm, J. Comput. Phys. 146 (1998) 346–365.
[31] B. Perthame, C. Simeoni, A kinetic scheme for the Saint–Venant system with a source term, CALCOLO 38 (4) (2001) 201–231.
[32] Ch. Makridakis, Th. Katsaounis, Relaxation models and finite element schemes for the shallow water equations, in: Thomas Y. Hou, Eitan Tadmor (Eds.), Hyperbolic Problems: Theory, Numerics, Applications, Proceedings of the Ninth International Conference on Hyperbolic Problems held in CalTech, Pasadena, March 25–29, 2002.
[33] P.L. Roe, Approximate Riemann solvers, parameter vectors, and difference schemes, J. Comput. Phys. 43 (1981) 357–372.

[34] P.L. Roe, Upwinding differenced schemes for hyperbolic conservation laws with source terms, in: Nonlinear Hyperbolic Problems, Proc. Adv. Res. Workshop, St. Étienne, 1986Lect. Notes Math., vol. 1270, Springer, Berlin, 1987, pp. 41–45.
[35] C.W. Shu, S. Osher, Efficient implementation of essentially non-oscillatory shock capturing scheme, J. Comput. Phys. 77 (1988) 439–471.
[36] M.E. Vazquez-Cendon, Improved treatment of source terms in upwind schemes for shallow water equations in channels with irregular geometry, J. Comput. Phys. 148 (1999) 497–526.
[37] J.W. Wang, R.X. Liu, A comparative study of finite volume methods on unstructured meshes for simulation of 2D shallow water wave problems, Math. Comput. Simul. 53 (2000) 171–184.
[38] K. Xu, A well-balanced gas-kinetic scheme for the shallow water equations with source terms, J. Comput. Phys. 178 (2) (2002) 533–562.
[39] J.G. Zhou, D.M. Causon, D.M. Ingram, C.G. Mingham, Numerical solutions of the shallow water equations with discontinuous bed topography, Int. J. Numer. Meth. Fluids 38 (2002) 769–788.
[40] J.G. Zhou, D.M. Causon, C.G. Mingham, D.M. Ingram, The surface gradient method for the treatment of source terms in the shallow water equations, J. Comput. Phys. 168 (2001) 1–25.